UNLIMITED DISTRIBUTION

National Defence Research and Development Branch
Défense Nationale Bureau de Recherche et Développment

CR/89/445
Volume I

PARAMETERIZATION OF DIRECTIONAL SPECTRA – PART 2
Volume 1: FINAL REPORT

by
Barbara–Ann Juszko

JUSZKO SCIENTIFIC SERVICES
483 Sue Mar Place
Victoria, British Columbia, Canada
V9C 3E1

Scientific Authority Contract Number
Ross Graham W7707–9–0214/01–OCS

31 December 1989

CONTRACTOR REPORT

Prepared for

Defence Research Establishment Atlantic
Centre de Recherches pour la Défense Atlantique

Canada

ABSTRACT

The objectives of this work were to assess the ability of the 10–parameter model, examined in Part 1 of the study, to represent hindcast directional wave spectra and to provide an appraisal of how well the ODGP hindcast model predicted existing WAVEC observations. The parametric model acceptably reproduced the hindcast spectra over 90% of the time, with nearly 70% of the records having residual errors of less than 10%. There was little loss of information as indicated by the behavior of selected spectral statistics. A comparison of the hindcast spectra with field observations showed a significant correlation between energy levels, peak wave direction and vector mean direction. The hindcast directional peaks appeared to be generally sharper than the field data. No definite conclusions could be formed on specific frequency–direction features due to intrinsic limitations in directional spectral techniques. A coherence analysis between hindcast and measured winds indicated that the man–machine mix of hindcast input winds did provide an improvement over a purely geostrophic estimate. The coherence–squared dropped below acceptable levels at frequencies above 0.75 cycles per day (cpd). This behavior was reflected in the coherences of the vector mean wave field (ie. significant waveheight at the vector mean direction). Limiting the analysis to selected wave frequency bands, indicated that the hindcast model did not reproduce the observed swell signature with any statistical confidence while the ”sea” showed acceptable coherences to frequencies between 0.75 and 1.0 cpd.

RÉSUMÉ

Ces travaux visaient à évaluer l’adéquation de modèle à 10 paramètres, analysé dans la partie 1 de l’étude, en vue de la représentation des spectres directionnelles post–analyses d’ondes et d’évaluer la corrélation entre le modèle post–analyse ODGP et les mesures WAVEC actuelles. Le modèle parametrique reproduisait correctement le spectre post–analyse 90% du temps, près de 70% des fichiers comportant des erreurs résiduelles inférieures à 10%. Le comportement de certaines statistiques spectrales indiquait une faible perte d’information. La comparaison entre le spectre post–analyse et les mesures sur le terrain a révéle une corrélation significative entre les niveaux d’énergie, la direction principals des ondes et la direction vectorielle moyenne. Il semble qu’en general, les pointes directionnelles rétrospectives sont plus prononcées que les données sur le terrain. On ne peut tirer aucune conclusion nette à propos des caractéristiques fréquence–direction, en raison des limites inhérentes aux techniques spectrales directionnelles. Une analyse de coherence entre les données post–analyses et les vents mesurés à indiqué que la combinaison homme–machine de vents d’entrée post–analyses constituait une amelioration par rapport à une estimation uniquement

géostrophique. Le carré de la cohérence passait au–dessous du niveau acceptable dans les fréquences supérieures a 0.75 cycle, par jour. Ce comportement se retrouvait dans la cohérence du vecteur moyen champ ondulatoire (c’est–a–dire la hauteur significative d’ondes dans la direction vectorielle moyenne). Si on limite l’analyse à des bandes de fréquences ondulatoires choisies, on constate que le modèle post–analyse ne reproduit pas avec une confiance statistique suffisante la signature de houle observée, tandis que la ”mer” présente une coherence suffisante pour les fréquences de 0.75 à 1.0 cycle par jour.

TABLE OF CONTENTS

LIST OF FIGURES

LIST OF TABLES

1. INTRODUCTION

The description of complex directional wave spectra, using a limited number of parameters, serves not only to reduce data storage requirements, but allows for the characterization of the spectra, which is useful in both theoretical and practical applications. In Part 1 of this study (Juszko, 1989), data handling techniques and software were developed to perform and assess the parameterization of directional wave spectra collected in the winter of 1984 by a Datawell WAVEC buoy moored near the Hibernia C–96 drill site. The results indicated that a 10–parameter directional model could be fitted to the data by means of a non–linear, least–squares fit and would adequately represent the data spectrum approximately 90% of the time.

This parameterization is not limited to field measured spectrum and could equally represent directional wave spectra predicted by a hindcast numerical model. Using the offshore Data Gathering Program (ODGP) model, directional wave spectra have been produced and archived for numerous locations off Canada's East Coast. In Part 2 of this study, hindcast spectra, for a grid point and time period corresponding to the data of Part 1, will be examined. The ability of the 10–parameter model to reproduce the hindcast spectra will be assessed. Further, this report will provide an appraisal of how well the hindcast model spectra reproduces the directly measured wave directional spectra under actual field conditions.

2. STUDY BACKGROUND

2.1 Study Objectives

There were two primary objectives in this study. The first objective was to determine whether or not the parameterization of Part 1, performed on field directional wave spectra, could equally represent directional spectra produced by a numerical hindcast model. Any developed software of Part 1 would be modified to specifically and efficiently handle the hindcast spectra in order to allow for future routine operational processing.

The second objective was to assess how well the hindcast directional wave spectra reproduced the directly measured spectra. The usefulness of hindcasts models have generally been judged according to their ability to predict selected statistical properties of the heave spectrum. As the hindcast spectra were available for a time period and location corresponding to the WAVEC data analyzed in Part 1, this provided an ideal opportunity to assess the full two–dimensional behavior of the model.

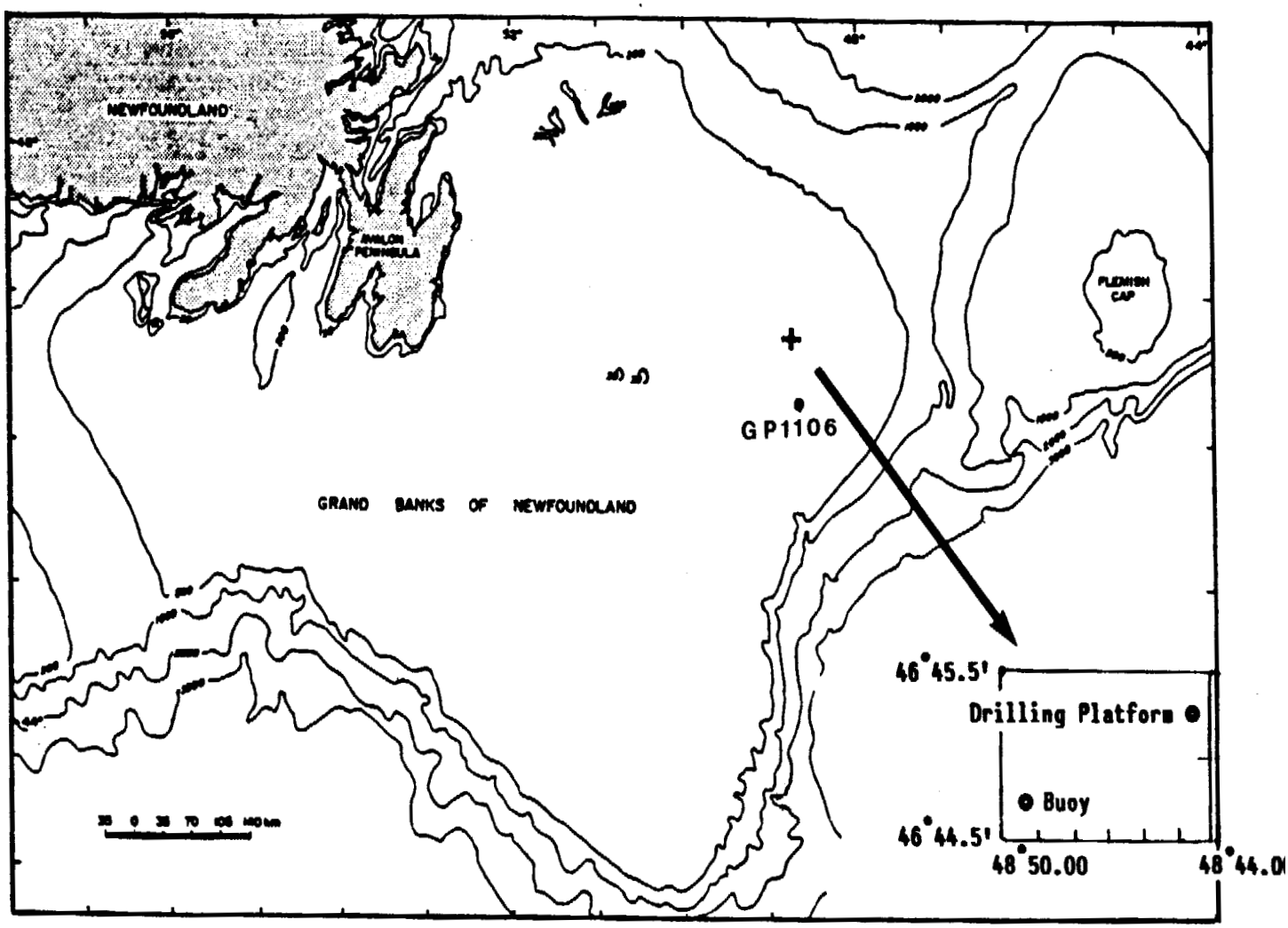

Fig. 1 Study location

2.2 Data Sources

The hindcast wave spectra were produced by MacLaren Plansearch Ltd., using the ODGP Spectral Ocean Wave Model, in order to provide a wave climate data base for the East Coast of Canada. The selected spectra were calculated at grid point identification number 1106 (46 degrees 15 min. North, 48 deg. 45 min. West) chosen as a representative Grand Banks/Hibernia site (see Figure 1). The time period extended from February 27 to April 91 1984. The spectra were produced every six hours and archived as 15 frequency by 24 direction (15 degree resolution) energy estimates. The frequency resolution was variable with nominal frequencies at: 0.2545, 0.2792, 0.3142, 0.3491,

0.3840, 0.4189, 0.4538, 0.5062, 0.5760, 0.6458, 0.7331, 0.8377, 0.9948, 1.309 and 1.9373 radians/sec. The hindcast model input winds, associated with grid point 1106, also formed part of the stored information as well as selected statistical spectral properties. For further details on the model, grid information, etc. the reader is referred to a report by MacLaren Plansearch (1988).

The field data were collected using a Datawell slope–following WAVEC buoy (Marine Environmental Data Service Station No. 249) moored at 46 deg. 44.83 min. North, 48 deg. 49.75 min. West, approximately 55 kms North of grid point 1106. This data set covers the period from February 28 to April 3, 1984 with the buoy sampling for 34 minutes, at a rate of once every 0.78125 seconds, every three hours except during storms when a continuous sampling regime was implemented. Meteorological information was available from MANMAR records of the West Venture mobile drilling unit, operated by Mobil Oil Canada Ltd., stationed at 46 deg, 45.17 min. North, 48. deg. 44,59 min. West, approximately 5 kms East of the buoy. The directional data spectrum consisted of 16 frequencies (from 0.314 to 3.14 radians/sec at a uniform bandwidth of 0.188496 rps or 0.03 Hz) and 90 directions (ie. 4 degree resolution). These were produced using a high–resolution directional analysis technique and details on the processing are included in the Part 1 report (Juszko, 1989).

2.3 Methodology

The parameterization of the hindcast wave spectrum was performed by initially fitting the six–parameter Ochi and Hubble (1976) (OH) model:

$$S(\omega) = \frac{\frac{1}{4}\sum_{l=1}^{2}\left(\frac{4\lambda_l+1}{4}\,\omega m_l^4\right)^{\lambda_l}\,\delta_l^2\; e^{-\frac{(4\lambda_l+1)}{4}\left(\frac{\omega m_l}{\omega}\right)^4}}{\Gamma(\lambda_l)\,\omega^{4\lambda_l+1}} \qquad (1)$$

to the amplitude spectrum. Here $S(\omega)$ represents the OH spectrum, ωm the peak frequency, δ the significant wave height or variance parameter, and λ a spectral shape parameter. The OH model consists of two portions ideally representing the separate sea and swell components of the spectrum. This preliminary fit allowed for the initial assessment of the OH model when representing the hindcast spectra as well as providing a set of first guesses for the heave parameters when performing the full 10–parameter fit to the model given by:

$$M(\omega,\theta) = \frac{1}{4} \sum_{I=1}^{2} \frac{(4\lambda_I+1\ \ \omega m_I^4)^{\lambda_I}\ \delta_I^2\ e^{-\frac{(4\lambda_I+1)}{4}\left(\frac{\omega m_I}{\omega}\right)^4} * A(P_I)\cos^{2P_I}\left(\frac{\theta-\theta m_I}{2}\right)}{\Gamma(\lambda_I)\omega^{4\lambda_I+1}} \quad (2)$$

Here A(Pi) is a normalization factor for the area under a COS**2P curve, P is the directional spread parameter and Θm is the mean direction. A(P) is expressed as:

$$A(P) = 2^{(2P-1)}\Gamma^2(P+1)/(\pi\Gamma(2P+1)) \quad (3)$$

The fit procedure, required functions and derivatives, were discussed in Part 1 and their general features remained unaltered. Slight modifications were required to handle the variable frequency resolution and to improve program efficiency. The fit procedure consisted of an iterative technique where the model parameters are altered slightly and a fit residual is calculated in order to decide whether or not the change provides for an improved fit. A combined steepest descent and Newton method approach (Levenberg–Marquardt method) was used to supply the new parameter values while the fit residual was calculated as:

$$\sum_{I=1}^{N} [E(\omega_I) - S(\omega_I)]^2 WT_I^2 \quad OR \quad \sum_{I=1}^{N}\sum_{J=1}^{M} [D(\omega_I,\theta_J) - M(\omega_I,\theta_J)]^2 WT_I^2 \quad (4)$$

where S and M are the fit spectra, E and D the data or hindcast spectra and the sums are performed over all frequencies and, when applicable, directions. WT represents a frequency weighting given by:

$$WT1 = \frac{\text{BANDWIDTH}}{\text{TOTAL BANDWIDTH}}$$

In this application, WTi can be given as the frequency resolution divided by the total frequency range or the number of bands averaged per frequency divided by the total number of frequency bands (in this case 60.43 bands). Similarly, the model evaluation statistics RESH, where

$$RESH = \frac{\sum_{I=1}^{N} [E(\omega_I) - S(\omega_I)]^2 WT_I^2}{\sum_{I=1}^{N} [E(\omega_I)]^2 WT_I^2} \quad (5)$$

for the OH model fit and RESD for the 10-parameter directional fit,

$$RESD = \frac{\sum_{I=1}^{N}\sum_{J=1}^{M}[D(\omega_I,\theta_J) - M(\omega_I,\theta_J)]^2 WT_I^2}{\sum_{I=1}^{N}\sum_{J=1}^{M}[D(\omega_I,\theta_J)]^2 WT_I^2} \quad (6)$$

also contain this weighting factor which was not required in Part 1 as the frequency resolution was constant. New software to perform the fit was written in order to provide more efficient program operation. Further details on the fit procedure can be found in Juszko (1989) and on the software operation in the accompanying User's Manual.

To aid in the fit assessment, and later the hindcast model evaluation,selected spectral summary properties were calculated. These include:

HSIG significant wave height in meters as 4.0 sqrt (Total Variance)

TP Peak period in seconds – period associated with the heave spectral peak

VMD Vector mean direction of the record in radians (taken as FROM)

PDIR Peak direction in radians (FROM) – direction associated with the maximum $D(\omega,\Theta)$ value

TDIR Period associated with the maximum $D(\omega,\Theta)$ value in seconds

P Spread P about PDIR determined through a fit to a cosine-power expression, including isotropic noise (α), given as

$$S(\theta) = A\cos^{2P}\left(\frac{\theta-\theta m}{2}\right) + \alpha$$

To assess the distribution of these properties, of the fit parameters, and to allow for comparison between data sets, the following statistics were also calculated:

$$MEAN = \bar{X} = (1/N) * \sum_{I=1}^{N} x_I$$

$$\text{ABSOLUTE DEVIATION (ADEV)} = (1/N) * \sum_{I=1}^{N} |x_I - \bar{X}|$$

STANDARD DEVIATION (SDEV)= $\sigma = \mathrm{SQRT}\left[\, 1/(N-1) * \sum_{i=1}^{N} (x_i - \overline{X})^2 \,\right]$

SKEWNESS (SKEW) = $(1/N) * \sum_{i=1}^{N} \left[\frac{x_i - \overline{X}}{\sigma} \right]^3$

KURTOSIS (KURT) = $\left\{ (1/N) * \sum_{i=1}^{N} \left[\frac{x_i - \overline{X}}{\sigma} \right]^4 \right\} - 3$

MEAN ERROR (ME) = $(1/N) * \sum_{i=1}^{N} (x1_i - x2_i)$

ROOT MEAN SQUARE ERROR (RMSE) = $\mathrm{SQRT}\left[(1/N) * \sum_{i=1}^{N} (x1_i - x2_i)^2 \right]$

% SCATTER = $100 * \frac{\mathrm{RMSE}}{\overline{X}}$

CORRELATION COEFFICIENT (CC) = $\dfrac{\sum_{i=1}^{N} (x1_i - \overline{X1})(x2_i - \overline{X2})}{\mathrm{SQRT}\left[\sum_{i=1}^{N} (x1_i - \overline{X1})^2 \right] * \mathrm{SQRT}\left[\sum_{i=1}^{N} (x2_i - \overline{X2})^2 \right]}$

SIGNIFICANCE LEVEL = Significance level at which the null hypothesis of zero correlation is disproved.

The second objective of this study was to evaluate the hindcast model performance with respect to the existing WAVEC buoy measurements. In order to perform a proper comparison, one would like to eliminate as many factors as possible which could influence the results. These include such features as location and sampling regime of the buoy, frequency and direction resolution of the calculated spectra, geophysical factors such as wave refraction due to water depth effects or currents and intrinsic features of the model and data processing used. The buoy data were subsampled so that only the corresponding six hourly records were used in the comparison. There was approximately 55 kms separating the buoy and the model grid point hence one may expect some difference in spectral development during storms between the two records. The travel time for waves between the two sites, at expected peak sea frequencies, is less than the six-hourly sampling, thus given the time series resolution, site effects should not greatly influence the results if the wind field has a large spatial coherence. This is also true for the travel times of

swell waves, however, these may be present in the area for only a short time (ie. possibly missed by the six-hourly sampling) or, in cases of shallow water, may be measured at one site and not another when bottom refraction is significantly determining the wave travel path on small scales (ie. if the spatial scales of the wave field are smaller than the model grid). There appeared to be no consistent absence of swell energy in the data and the water depth at the study site was relatively uniform so that small scale refraction should not be a concern in this experiment. A mean rotation between the model and data wave directions may be present on a large scale if refraction of waves travelling from deep water onto the bank occurred. As the data spectra covered a wider frequency range and had a higher direction resolution than the hindcast spectra, an interpolation procedure was used to map the data spectra onto the hindcast frequency-direction array in order to eliminate effects due to the difference in spectral resolution. These "interpolated" data spectra were then processed with the identical programs used on the hindcast data and the results were compared. Geophysical factors and intrinsic features of the processing could not be controlled and their influence was addressed in Section 4 .

The comparison between the hindcast model and data spectra was extended to include the corresponding 10-parameter fit spectra. Qualitative assessment was made by examining overlayed time series of statistics, scatterplots of one statistic against the other and contour plots of selected directional spectra. Quantitative comparisons included the calculation of RESD values between the data sets, of the distribution and comparison statistics listed earlier and of the coherence of energy vectors between records.

3. PARAMETERIZATION OF THE HINDCAST SPECTRA

3.1 Fit of the Ochi and Hubble Six Parameter model

3.1.1 Fit Procedure

The Ochi and Hubble (1976) model describes the surface displacement spectrum using two additive components, low frequency "swell" and high frequency "sea", each described using three parameters: a modal frequency (ωm), a significant wave height (δ) and a shape parameter (λ). The spectrum has the functional form:

$$S(\omega) = \frac{1}{4} \sum_{l=1}^{2} \frac{\left(\frac{4\lambda_l + 1}{4}\ \omega m_l^4\right)^{\lambda_l}\ \delta_l^2\ e^{-\frac{(4\lambda_l+1)}{4}\left(\frac{\omega m_l}{\omega}\right)^4}}{\Gamma(\lambda_l)\omega^{4\lambda_l+1}}$$

The required first guesses for the non-linear fit were obtained in a manner similar to the data fit of Part 1. The heave spectrum was

scanned for the frequencies associated with the two largest peaks ($\omega m1$ and $\omega m2$, $\omega m1 < \omega m2$). The first guess for the values of $\delta 1$ and $\delta 2$ were calculated from the spectrum according to:

$$\delta_1 = 4.0 * \mathrm{SQRT} \left(\int_{\omega_1}^{\omega_2} E(\omega) d\omega \right) \qquad \omega_1 = 0.254$$

$$\delta_2 = 4.0 * \mathrm{SQRT} \left(\int_{\omega_2}^{\omega_3} E(\omega) d\omega \right) \qquad \omega_2 = (\omega m_1 + \omega m_2) * 0.5$$

$$\omega_3 = 1.937$$

The first guesses for the shape parameters, $\lambda 1$ and $\lambda 2$, were taken as constant at 2.5 and 1.0 respectively.

During the fit iterations, limits were required on the parameters to ensure convergence at geophysically realistic values. These limits were set to:

$$0 < \delta_1, \delta_2, \lambda_1, \lambda_2 < 20$$

$$\omega m_1 \leq \omega m_2$$

$$0.25 \leq \omega m_1 \quad \omega m_2 < 1.9$$

The "stop" criteria were set at 100 iterations, or 15 iterations in a row resulting in a relative change in the fit residual of less than 2.E-5, or 10 iterations in a row resulting in an increase in the fit residual. An optional second processing was performed if $\omega m2 > 1.696$ or $\omega m2 - \omega m1 < .001$. The first guesses for the frequencies were then reset to $\omega m1 - .0314$ and $\omega m1 + .094$, respectively. This allowed for better modelling of low frequency energy.

3.1.2 Fit Assessment

Figure 2 contains the time series of the six fit parameters. Fig. 3 shows the distribution of the RESH residuals calculated, in a manner similar to Eq. 5 with the summation now over all records at a given frequency as opposed to over frequency at one record, as a function of frequency (upper) and when weighting is provided by the peak spectral density value EMAX (lower). This provides an assessment of the model behavior over the frequency range, both absolutely and as a function of the relative energy contribution of the given frequency to the spectrum, Fig. 4 displays the percent occurrence of RESH values. The time series of fit parameters are smoother and the RESH results are better than those observed in Part 1 for the data spectrum (Figs, 3 , 5 and 6 , respectively), Hindcast spectra tend to be smooth, with fewer non-significant peaks which are often found in data spectra, which may allow for a better fit or simply reduce point-by-point error contributions. Figure 5 contains sample overlayed OH model fits to the hindcast spectra and it appears that

the hindcast amplitude spectrum can be represented quite well by the OH model.

3.2 Fit of the 10–Parameter Model

3.2.1 Fit Procedure

A non–linear, least–squares fit of the hindcast spectra to the model

$$M(\omega,\theta) = \frac{1}{4}\,\frac{\sum_{i=1}^{2}\left(\frac{4\lambda_i+1}{4}\,\omega m_i^4\right)^{\lambda_i}\,\delta_i^2\, e^{-\frac{(4\lambda_i+1)}{4}\left(\frac{\omega m_i}{\omega}\right)^4} * A(P_i)\cos^{2P_i}\left(\frac{\theta-\theta m_i}{2}\right)}{\Gamma(\lambda_i)\omega^{4\lambda_i+1}}$$

was performed. The A(P) term represents a variance normalization factor for the area under a COS**2P curve and is given by:

$$A(P) = 2^{(2P-1)}\Gamma^2(P+1)/(\pi\Gamma(2P+1))$$

It acts to adjust the variance explained by δi and as such can be included as a ”post–fit” correction eliminating the need to evaluate both the function and its complex derivative during the fit procedure.

The first guesses for the ten parameters use the six heave parameters from an earlier OH model fit and obtains P and Θm values from a ”quick fit” to the linear expression:

$$LN(S(\theta)) = P*LN\left(\cos^2\left(\frac{\theta-\theta m}{2}\right)\right)$$

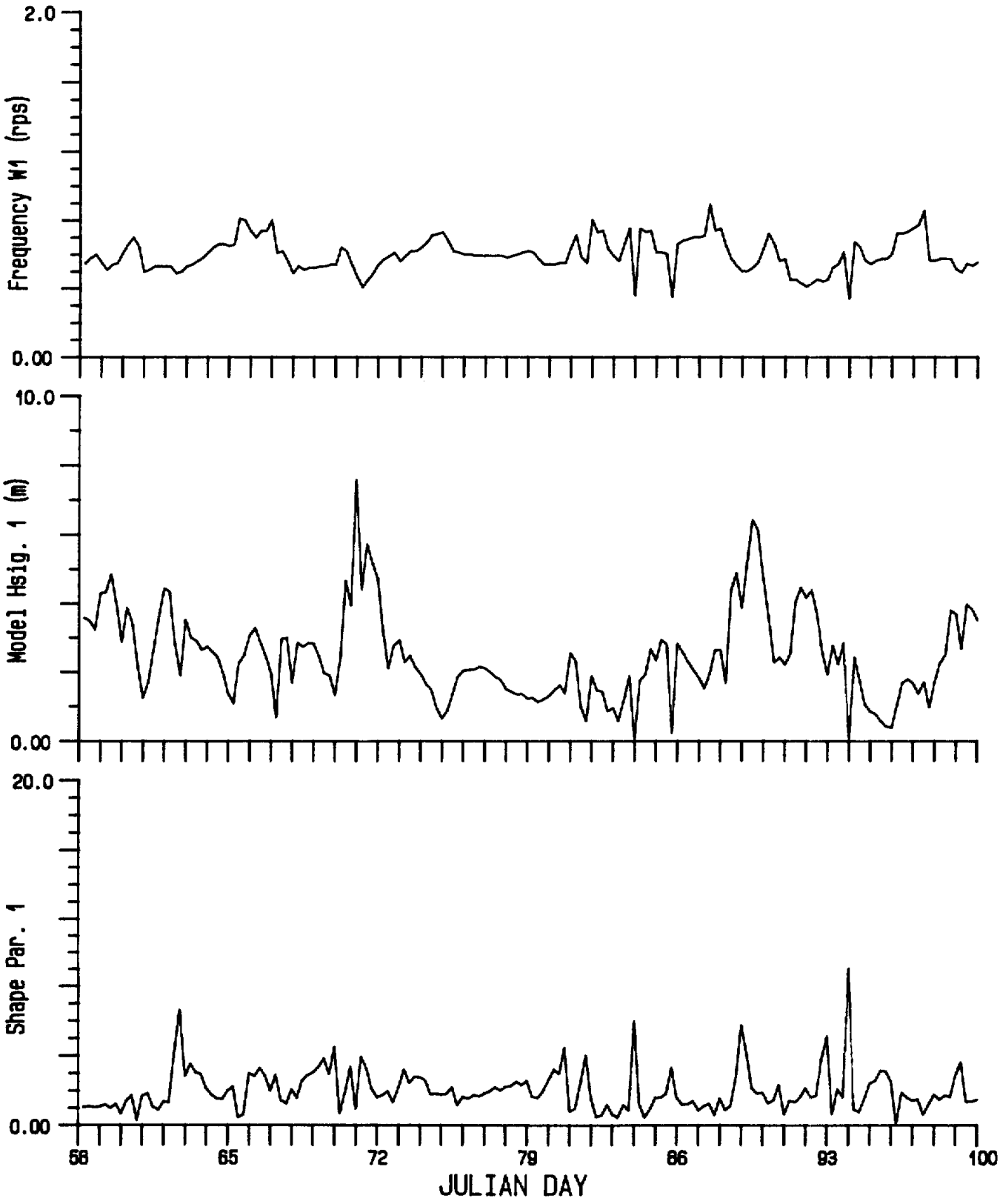

Fig. 2 Time series of OH model fit parameters.

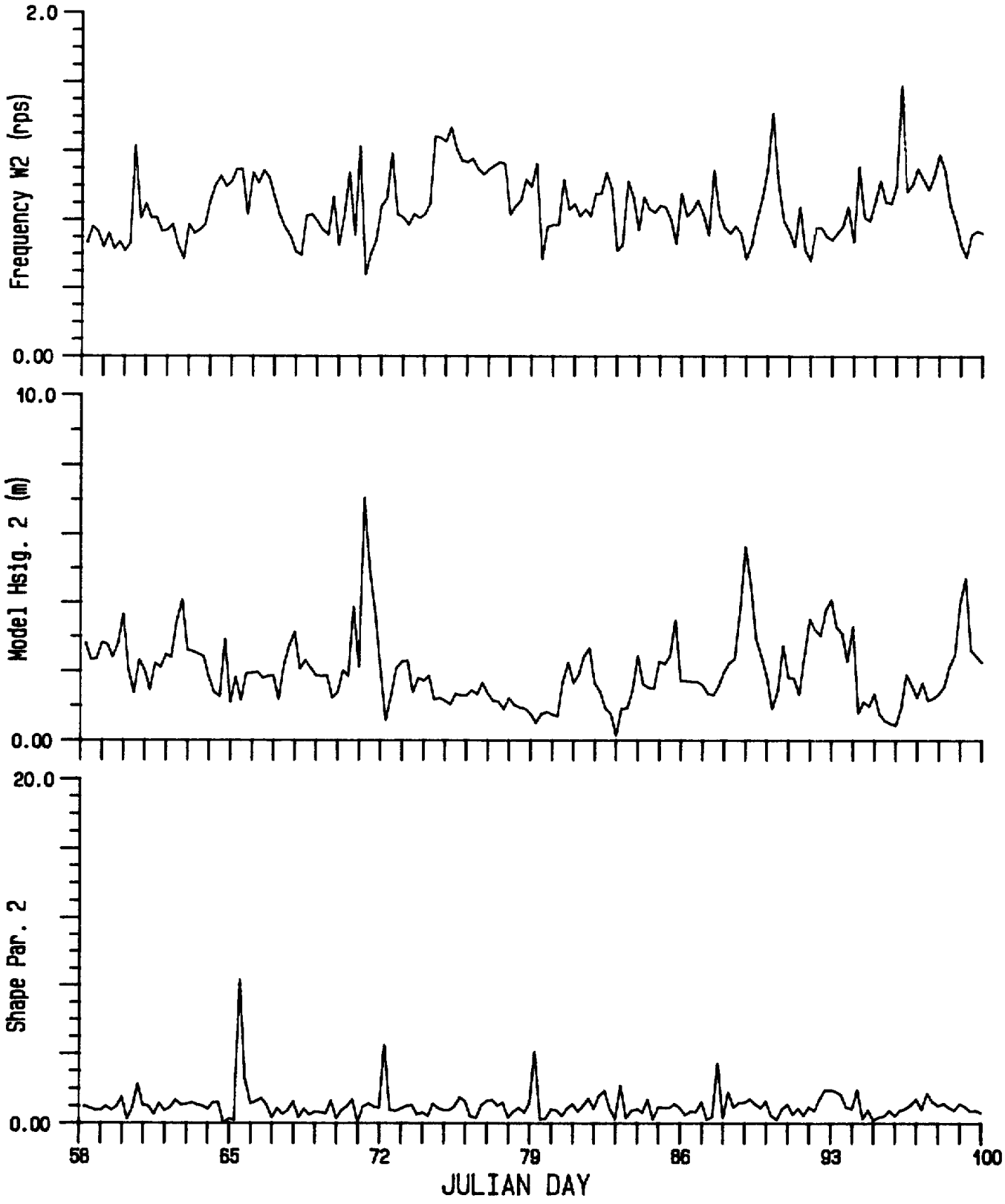

Fig. 2 (continued)

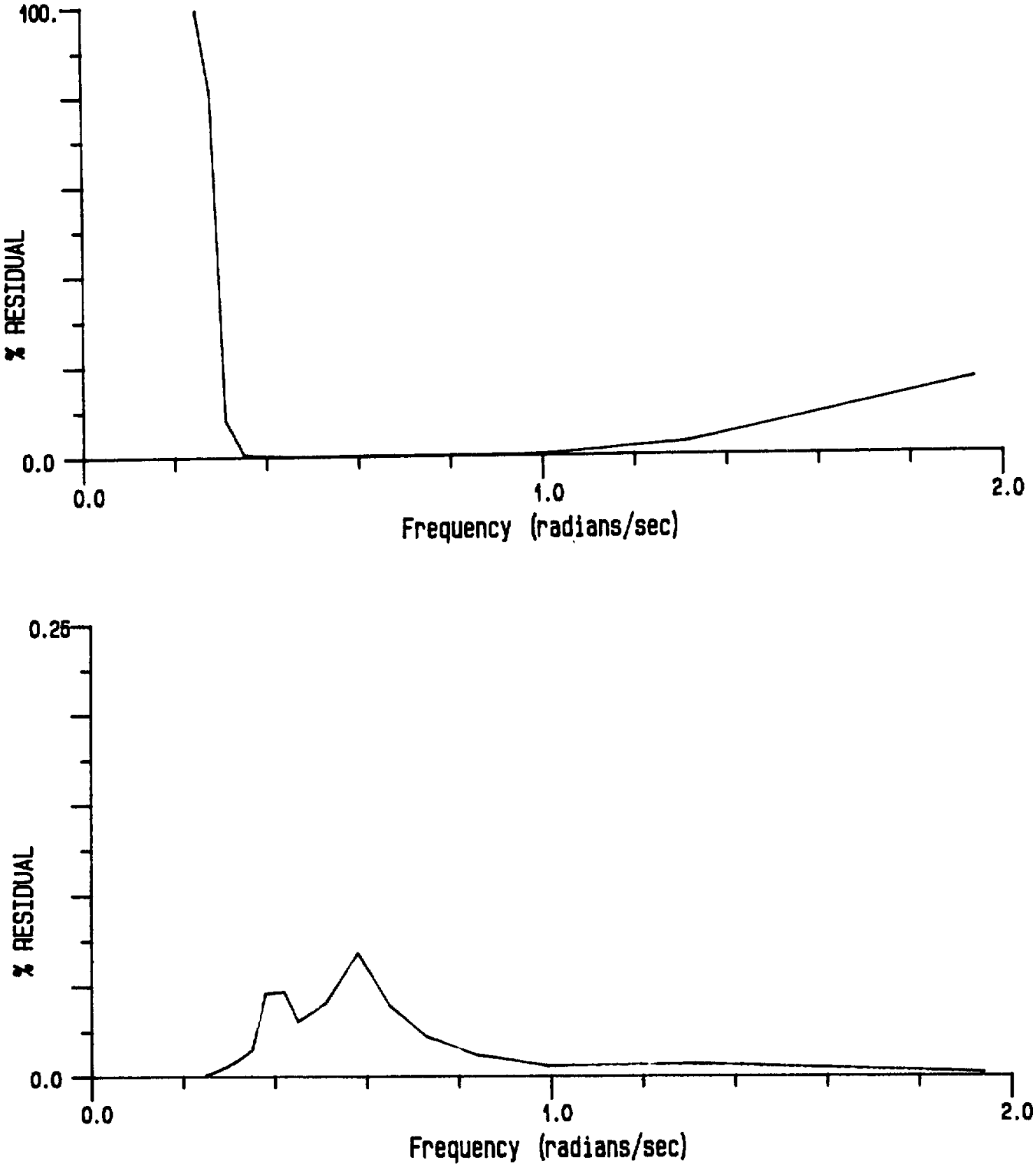

Fig. 3 RESH as a function of frequency. Upper: weighting by E(w); Lower: weighting by EMAX.

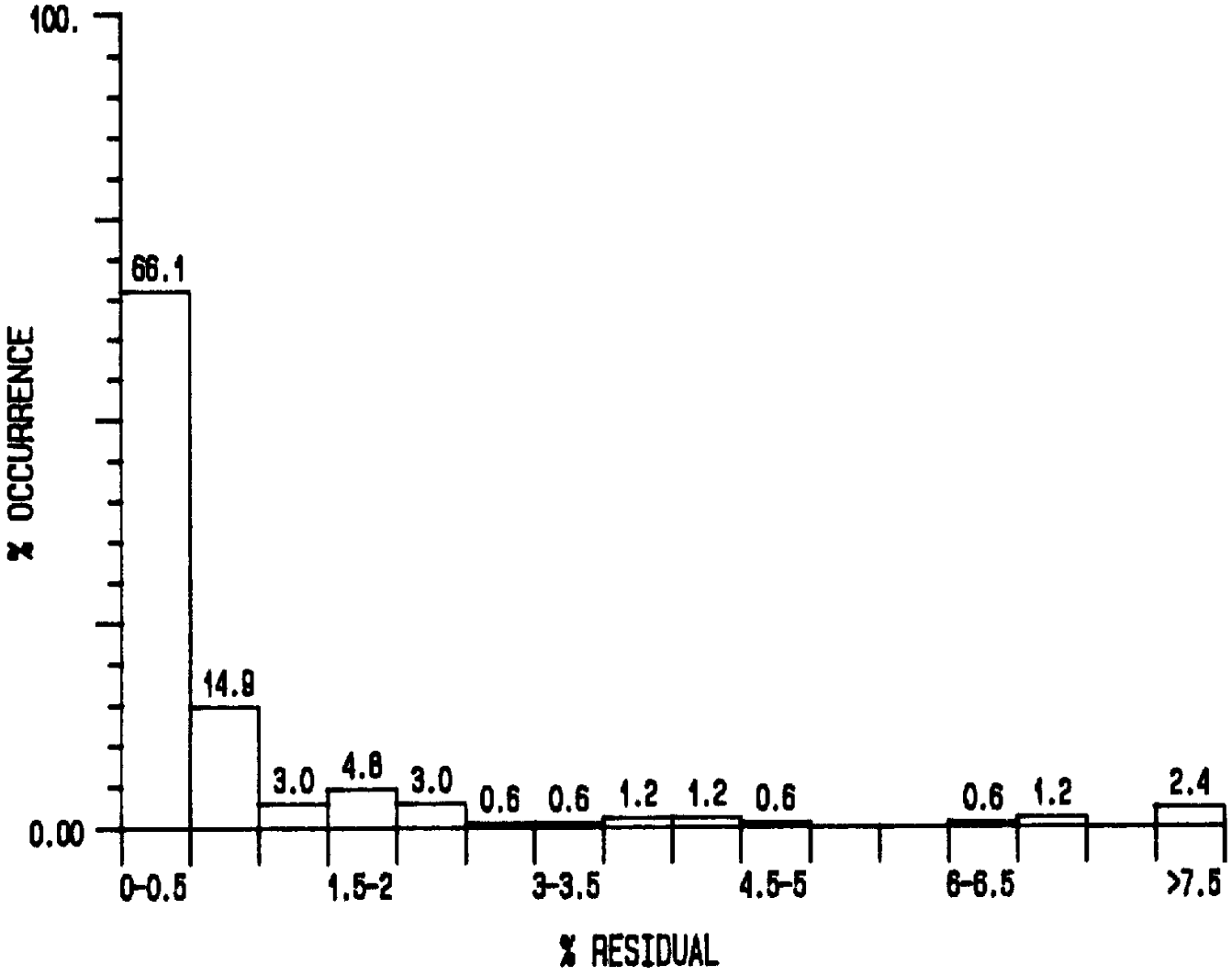

Fig. 4 Percent occurrence of RESH values.

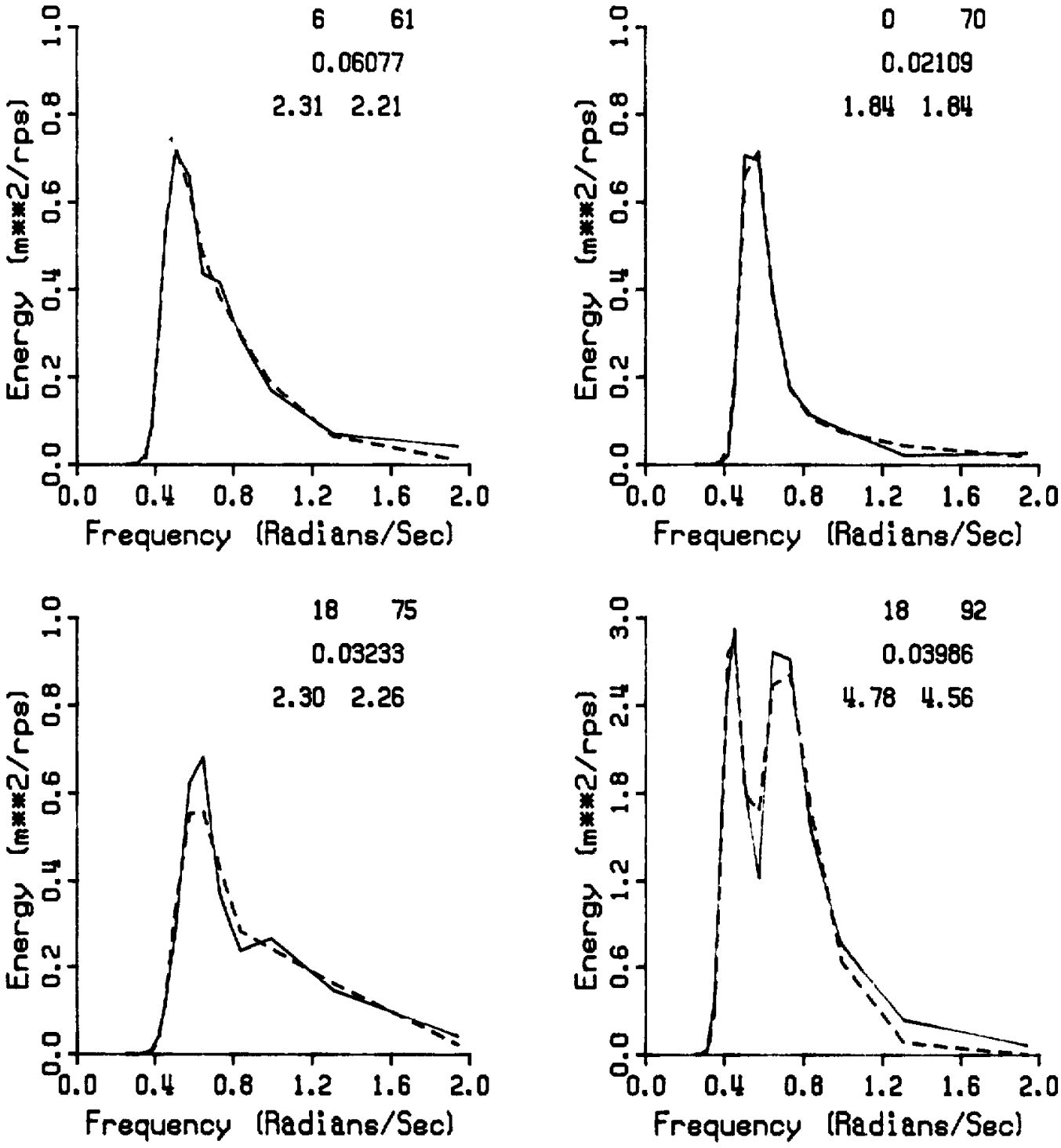

Fig. 5 Examples of the OH model fit (dashed line). Included on the plot are record time/day, RESH value and HSIG of the hindcast (left) and fit (right) spectra.

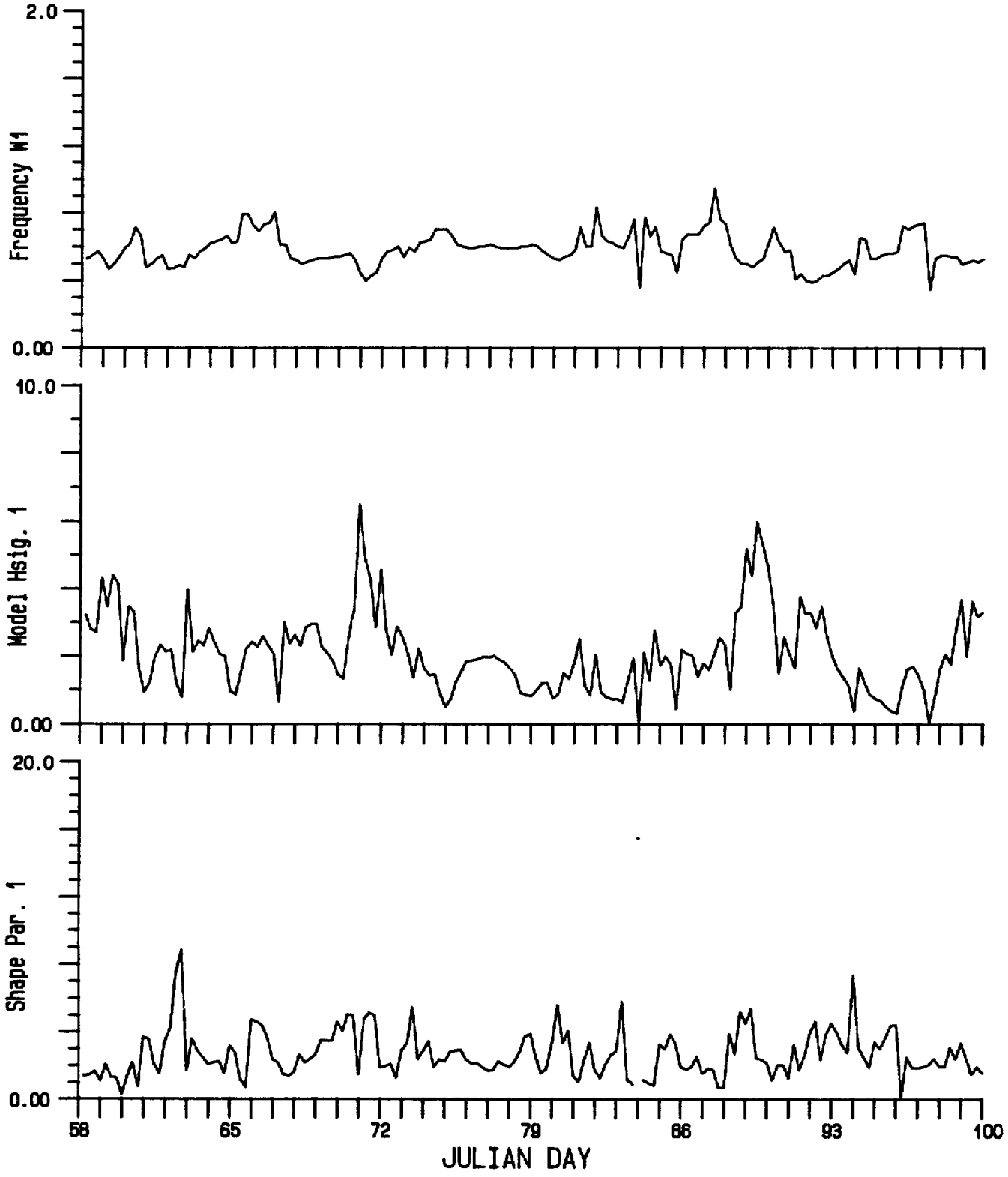

Fig. 6 Time series of fit parameters, angular half-width and RESD value for the 10-parameter fit to the hindcast spectra.

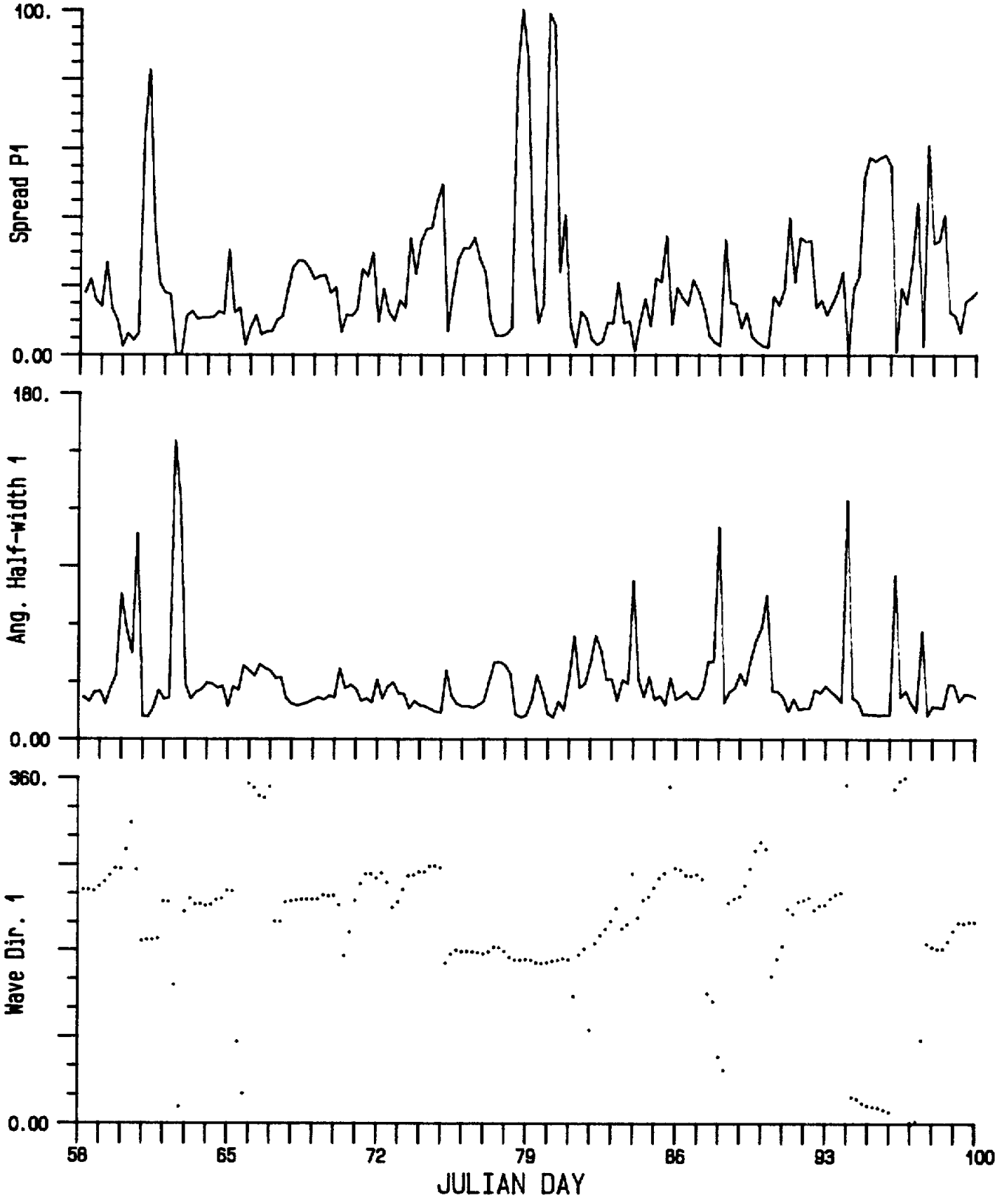

Fig. 6 (continued)

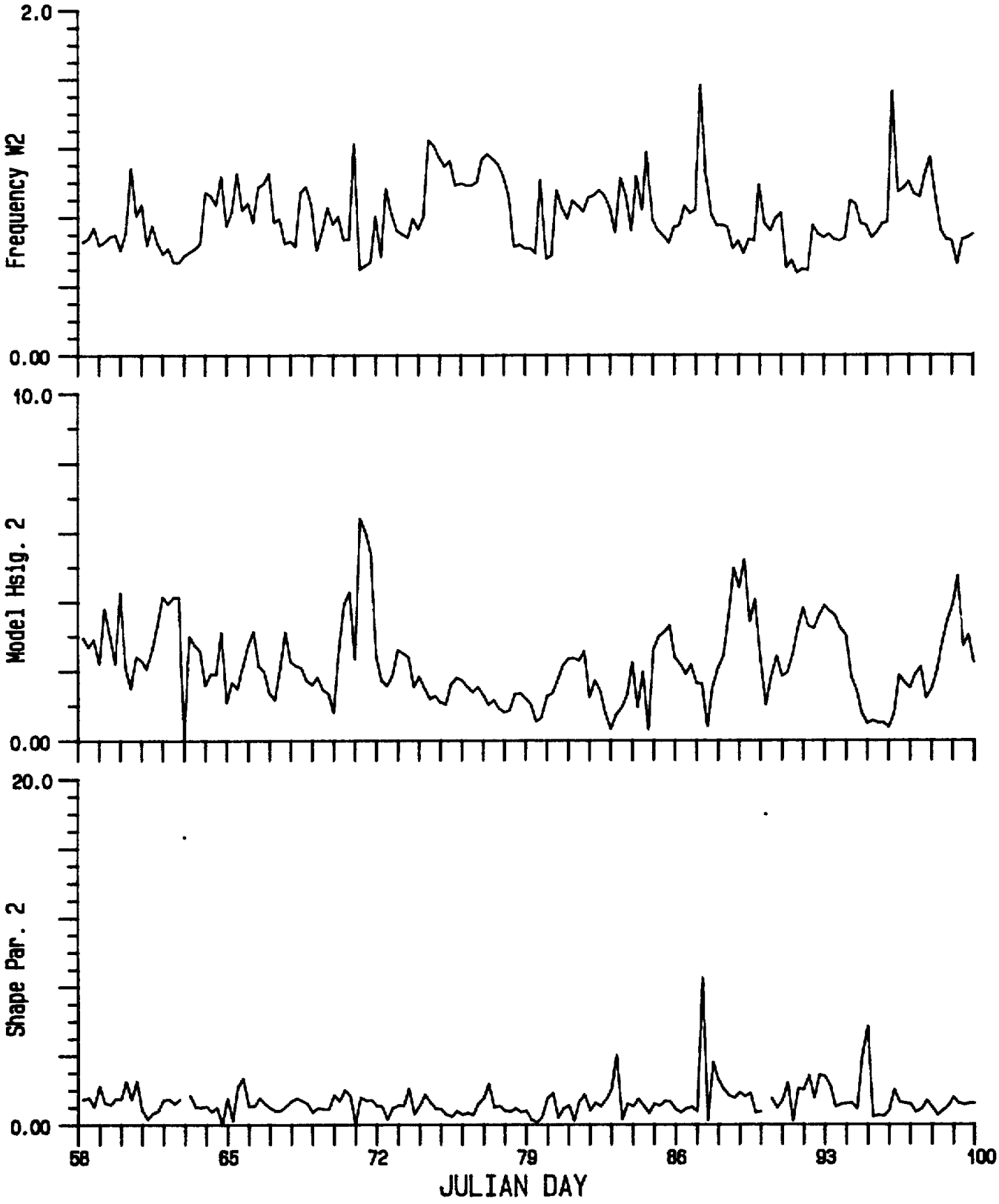

Fig. 6 (continued)

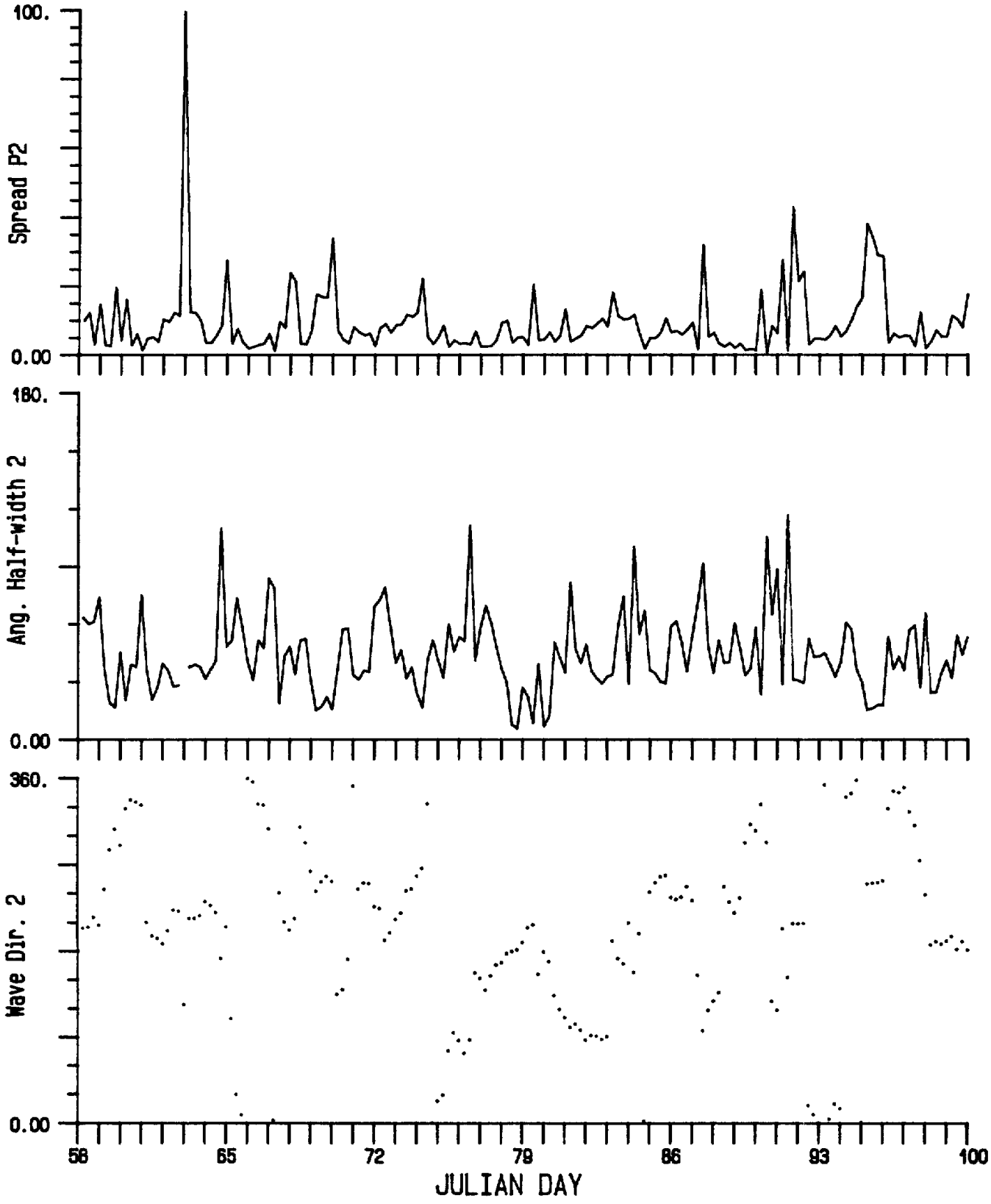

Fig. 6 (continued)

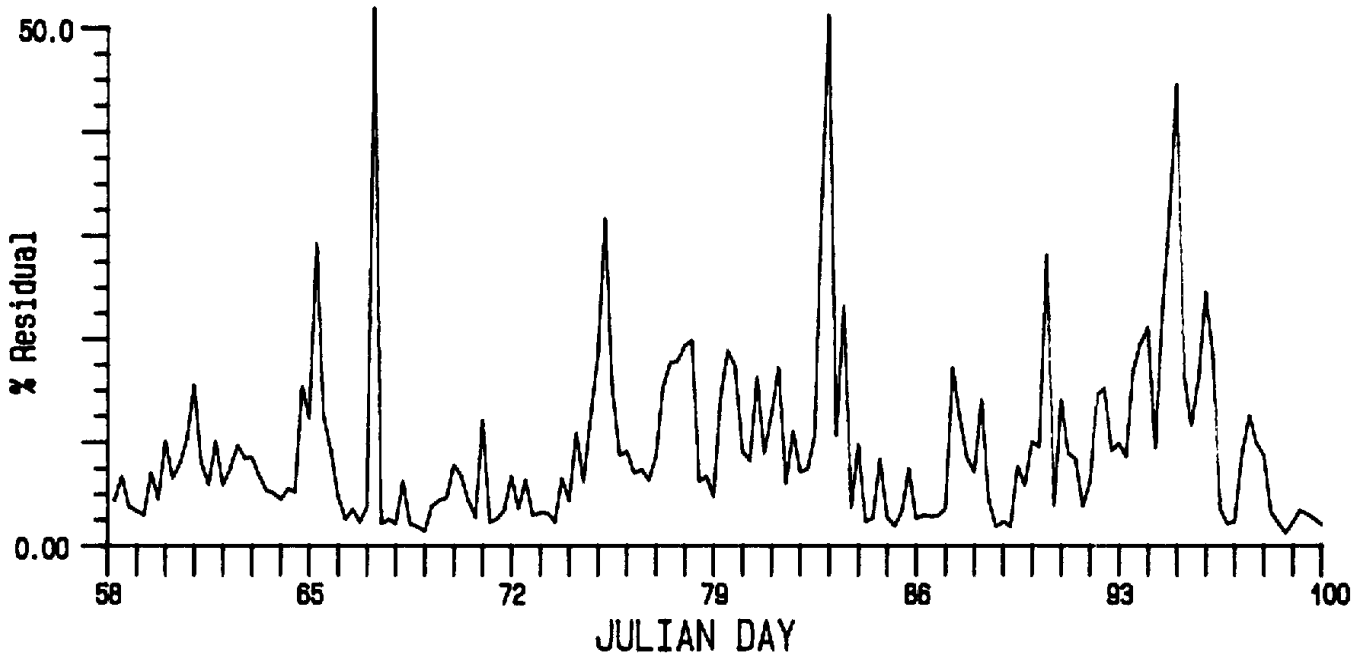

Fig. 6 (continued)

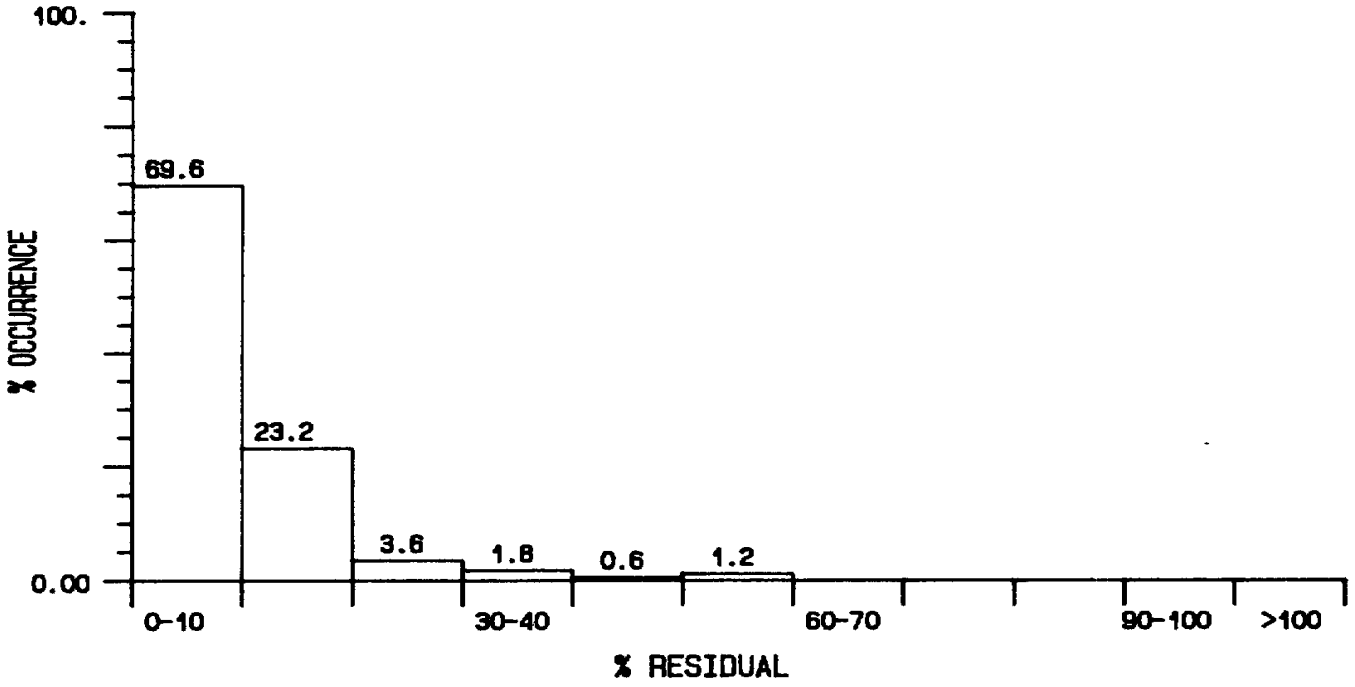

Fig. 7 Percent occurrence of RESD values.

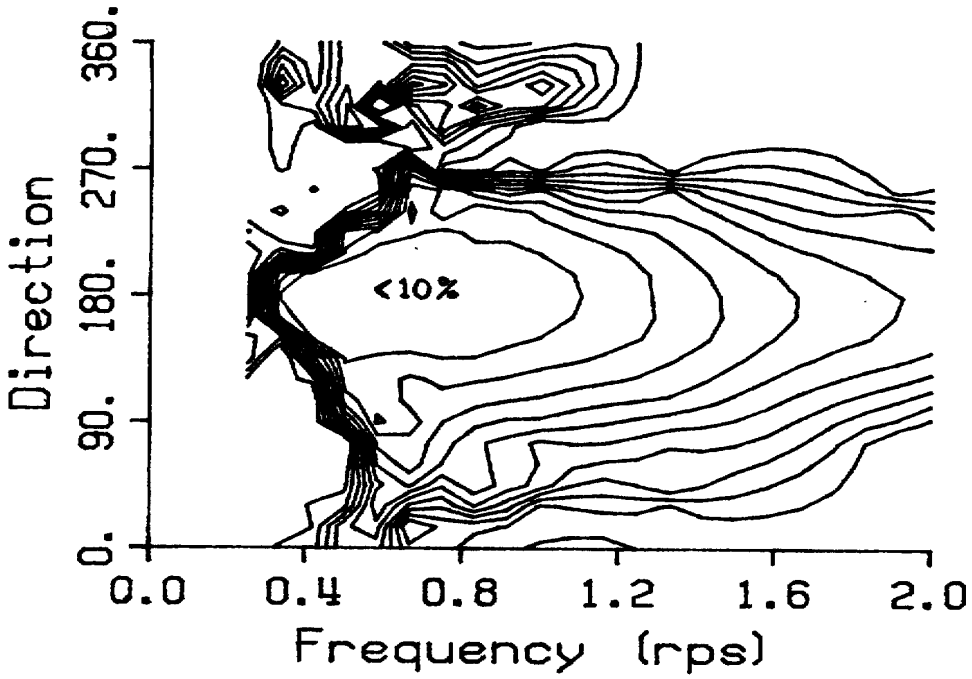

Fig. 8 Contoured % residual of the fit spectra. (10% contour intervals)

where S(Θ) is the direction energy array associated with frequencies ωm1 and ωm2. A fit to the peak is emphasized by limiting the directions to those associated with energies above 10% of the peak value. The P values are bounded by 1.0 and 100. If ωm1=ωm2 (ie. same index array position), the directional array S(Θ) is scanned to see if it is bimodal. If so, and the relative magnitude of the two peaks are comparable (ratio > 1%), the half-point direction between the two peaks is calculated and assigned to both Θm1 and Θm2 with corresponding P values of 1.0. The fit procedure would then determine the proper mean direction for the set 1 and 2 parameters. If ωm2 >1.0 and ωm2-ωm1 > 0,5, two vector mean directions are calculated (about the mid frequency) and assigned to the corresponding Θm1 and Θm2. This helps to provide the best overall fit when the two peak frequencies are widely separated. As the 10-parameter model is limited to a maximum of two direction peaks in a given frequency band, while the hindcast model often showed multiple swell peaks in addition to sea peaks, the fit would not consistently provide the best (ie. lowest RESD) representation. These ”poor” fits tend to occur in series as they represent a given geophysical condition. The best method to handle these records was found to require a second processing (if RESD>20%) using the previous records fit parameters as the first guesses.

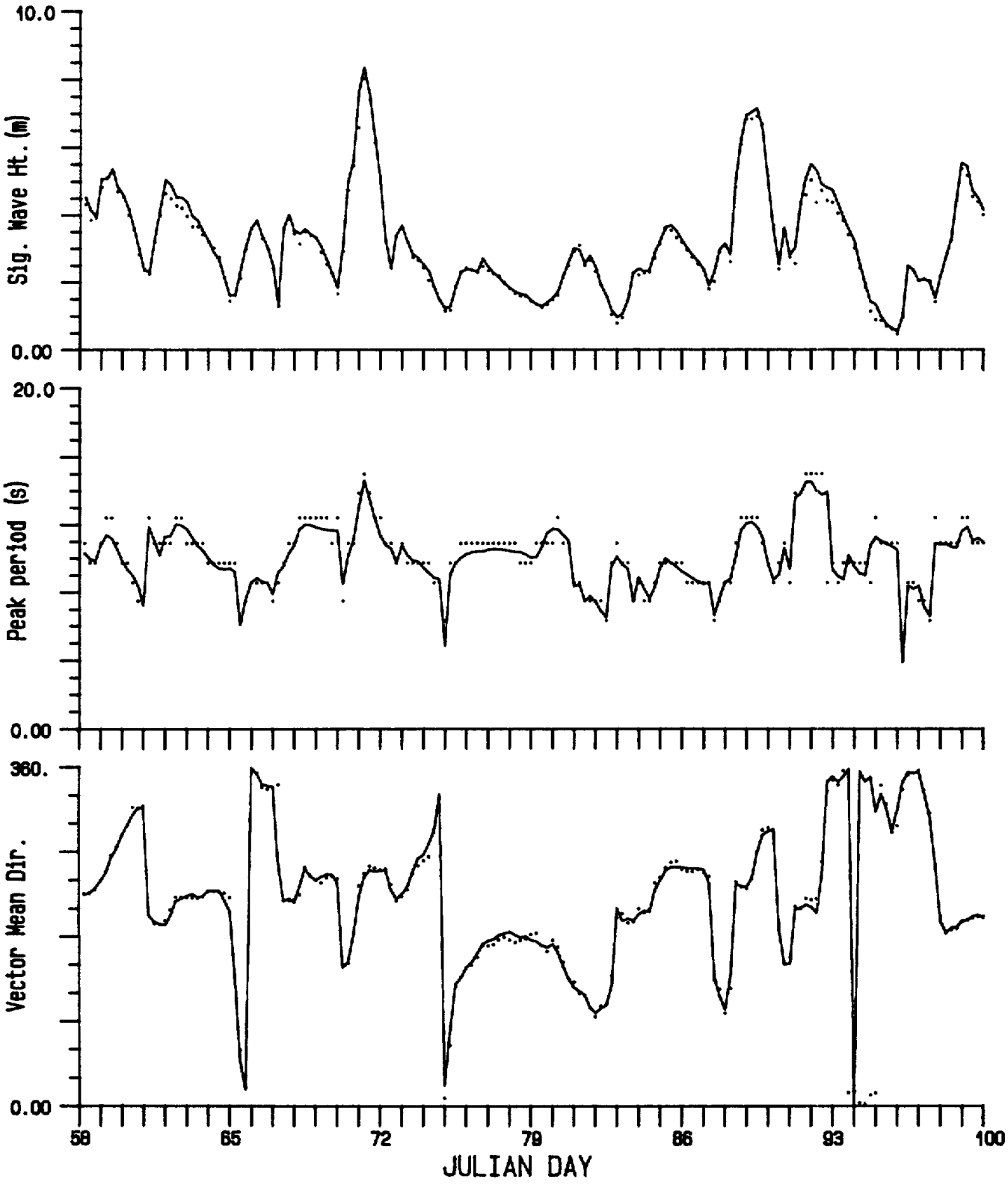

Fig. 9 Time series of HSIG, TP and VMD for the hindcast (solid) and 10-parameter fit (dots) spectra.

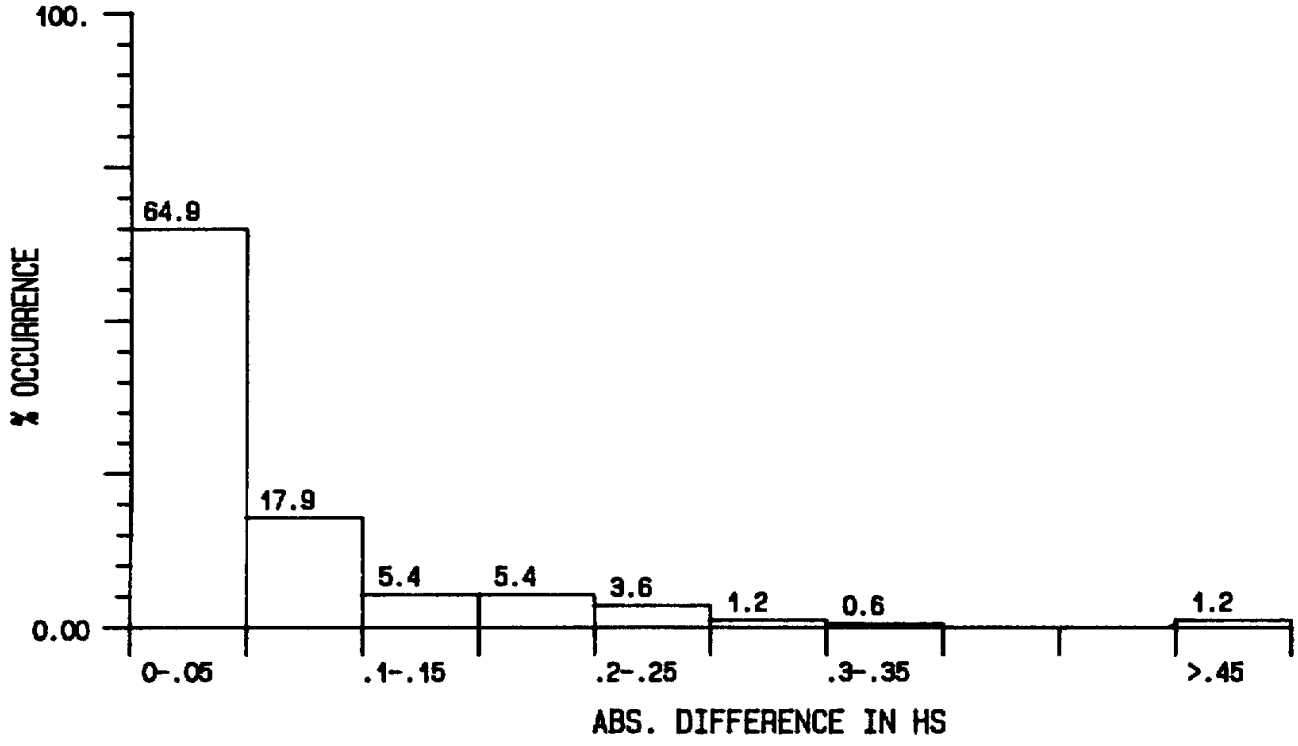

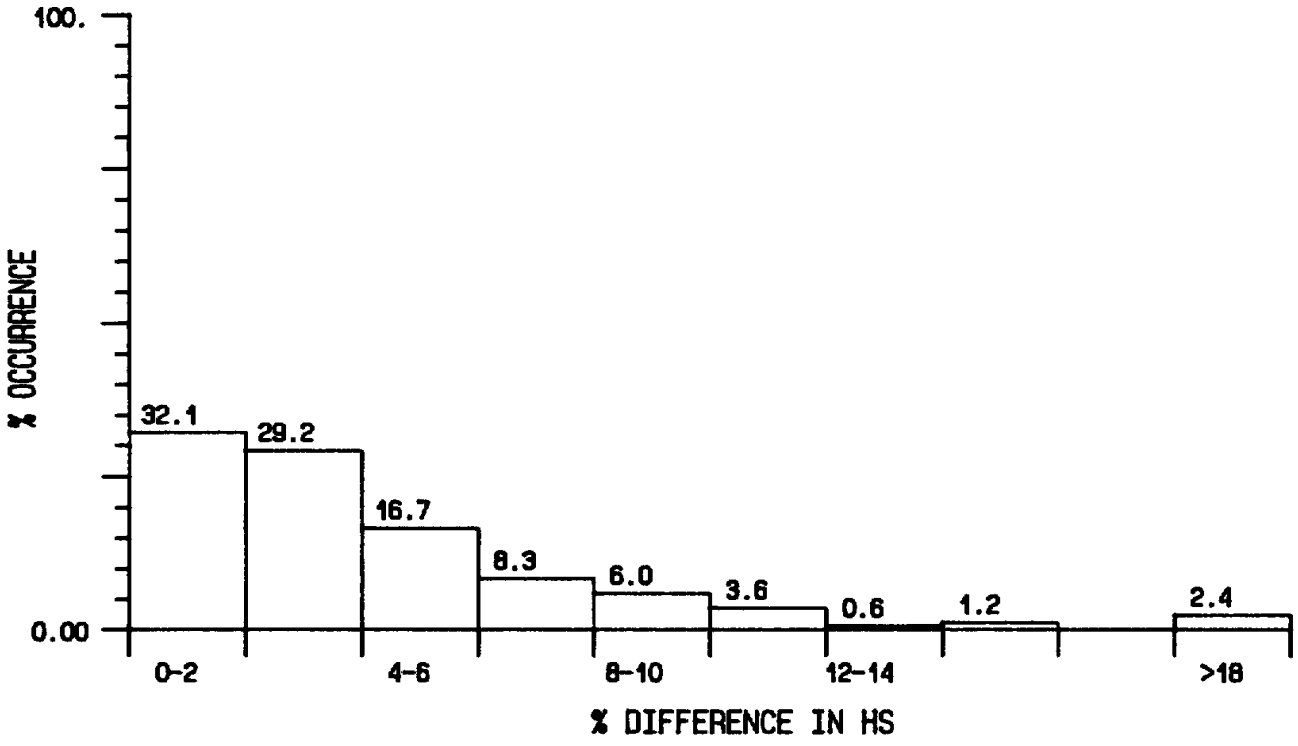

Fig. 10 Percent occurrence of the absolute and percent difference in HSIG between the hindcast and 10-parameter fit.

During the fit, bounds on the parameters were required and included those previously set on the heave parameters during the OH model fit, forcing the P value to lie between 0 and 100 and the direction parameters to lie between –pi and pi. Due to the circular nature of direction arrays, the directional spectra was centered about the mean direction (to midpoint frequencies) prior to fitting and re-centered between iterations if the modal frequencies were separated by at least O.1 radians/sec. The fit was terminated after 50 iterations, or if 7 iterations in a row resulted in a relative change in the fit residual less than or equal to .001, or if 10 iterations in a row resulted in an increase in the fit residual.

TABLE 1. Summary statistics for spectral properties of the hindcast model (M) and corresponding 10-parameter fit (F) spectra.

	HSIG (m)	TP (sec)	VMD (rad)	PDIR (rad)	TDIR (sec)	P
No. of Observ.	168	168	168	168	168	167
Mean M	3.19	10.07	3.93	3.91	10.79	11.24
F	3.07	10.20	3.94	3.92	10.52	10.58
ADEV M	1.18	1.34	0.94	0.95	1.48	8.74
F	1.13	1.49	0.96	0.92	1.51	6.60
SDEV M	1.51	1.75	1.21	1.25	1.85	12.87
F	1.45	1.89	1.24	1.23	1.95	10.04
SKEW M	0.87	-0.11	0.36	0.86	0.39	2.74
F	0.83	0.13	0.43	0.87	0.08	2.88
KURT M	0.66	0.89	-0.34	0.07	-0.002	11.05
F	0.67	0.20	-0.33	0.13	0.27	12.34
ME	0.12	-0.13	-0.03	-0.003	0.27	0.73
RMSE	0.20	0.68	0.17	0.21	0.93	9.45
% SCAT	6.28	6.70	4.43	5.46	8.75	86.36
CC	0.99	0.94	0.99	0.99	0.89	0.69
SI.LEV	0	0	0	0	0	0

3.2.2 Fit Assessment

The fit assessment was performed by examining both the behavior of the RESD values and the ability of the model fit to reproduce selected spectral properties, Figure 6 contains the time series of the fit parameters and RESD, and Fig. 7 shows the histogram distribution of the RESD values. Approximately 93% of the records have RESD values less than 20% which can be compared against the 87% acceptance for the original data spectral fits. Less accurate fits to the hindcast spectra tend to occur under low energy conditions or, as expected, when multiple directional peaks are present and the 10-parameter model is then not a suitable candidate. Fig, 8 contains the contoured % residual error calculated over all the hindcast records in order to assess the fit behavior about the direction peak centered at 180 degrees as a common reference point. The results show

similar behavior to those of the 10–parameter fit on the data spectra illustrated in Fig. 31F of the Part 1 report. The directional peaks are being fit well for frequencies between 0.4 and 1.2 rps. Errors increase away from the peak and at the highest frequencies as these regions generally contain very low energy and a small absolute error may represent a large relative % error. Examples of the fit, associated with the two storms encountered during the study, are included in Appendix 1 (along with the corresponding data and data fits which will be discussed in Section 4).

The ability of the 10–parameter model to reproduce selected spectral features is illustrated in the overlayed time series plots of HSIG, TP and VMD (Fig. 9). the histogram of the error in HSIG (Fig. 10) and the summary statistics of Table 1 (previously defined in Section 2.3). The agreement in the statistics is very good with the largest discrepancy in HSIG (>O.5m) occurring during the veering period and concurrent sea growth on days 92–93. The summary statistics in Table 1 show similar distribution properties. The skewness represents the degree of asymmetry of the distribution around its mean with a positive value signifying an asymmetric distribution extending towards more positive x values (and vice versa). The kurtosis measures the relative peakedness or flatness of the distribution with respect to a normal distribution. Positive values indicate a peaked distribution and negative values a flat distribution. These two shape statistics are included to show whether or not the overall distribution of selected properties of two data sets are similar. The largest shape difference occurs in the period statistics. The mean, ADEV and SDEV of the directional properties, VMD and PDIR, are similar, though the VMD shows a flatter distribution than the PDIR (approx. normal). The VMD statistic contains contributions from swell which may broaden the distribution. The input hindcast spectra are taken as absolute so that, when examining the direction statistics, a negative mean error indicates that the fit is rotated clockwise by this amount from the hindcast spectra. There may be fewer P estimates used in the calculation as the estimation procedure for P cannot always provide an appropriate value when the direction spectra is not unimodal. This is not a serious problem for the hindcast spectra as the directional peaks are generally very sharp but does occur more frequently in the WAVEC data statistics. With the exception of the spread parameter P, the ME, RMSE and % scatter are small. The two time series are highly correlated with a significance level less than .00001 (entered as 0 in this and subsequent tables). The spread parameter P shows considerable scatter with an RMSE of 9.5 and scatter index of 86%. The P parameter is non–linear (ie, a linear change in P is not reflected by a corresponding linear change in angular half–width) and the scatter is not surprising given both the nature of

the parameter and observations made during Part 1 of the study. As will be seen in Section 4 , due to innate features of the data analysis and the hindcast model, this scatter in P will become relatively inconsequential as a comparison of the directional spreads could not be performed with any confidence.

4. BEHAVIOR OF THE HINDCAST MODEL

4.1 Factors Influencing The Comparison

Various factors could influence the inter–comparison between the hindcast model spectra and the data spectra and their corresponding 10–parameter fits. As mentioned in Section 2.3 , the hindcast grid point and buoy location were approximately 55 kms. apart with the grid point being almost due South of the buoy. Waves of frequencies less than 1.9 rps (assuming deep water phase velocities or 0.96 rps for group velocities, which is the speed at which energy travels), would cross this distance in less than 3 hours (ie. half the sampling interval). These frequencies were generally associated with the energy containing region of the spectrum and if the wave field were spatially coherent and slowly varying, the distance separating the two sites should not affect the comparison. This may not necessarily be true for a swell signal of short duration or small scale meteorological features. However, given the six hour sampling, geophysical features having time scales less than 12 hours should not be expected to be reproduced regardless of the model accuracy.

Hindcast models are often considered to be as good as their input winds. A brief examination of the winds will be conducted in Section 4.2 . Hindcast models cannot explicitly model swell generated in a region beyond the model boundaries. As a selected space and time step are required by the numerical model, processes occurring on shorter scales, such as wave breaking, are either parameterized or assumed to have little affect on the generated wave spectra. These factors may supply a random error and influence the variance of the statistics. Hindcast models are able to predict more than two directional peaks in a given frequency band, however they include no isotropic noise in the directional distribution. Conversely, both the data spectra and the 10–parameter model are limited to a maximum of two directional peaks and, at this time, there exists no directional spectral analysis technique capable of resolving more than two peaks per frequency when applied to slope following buoys. In fact, in cases of bimodal distributions, even the high–resolution techniques (see Marsden and Juszko,1987) tend to under–resolve the two peaks resulting in spectra broader than input test simulations. The presence of isotropic noise (background noise levels of 5 to 10% at the spectral peak with higher levels away from the peak or in bimodal spectra, see Juszko, 1988) may also act to broaden the data directional distribution. It will be seen

in Section 4.4 that these factors severely limit conclusions about the directional spread features observed.

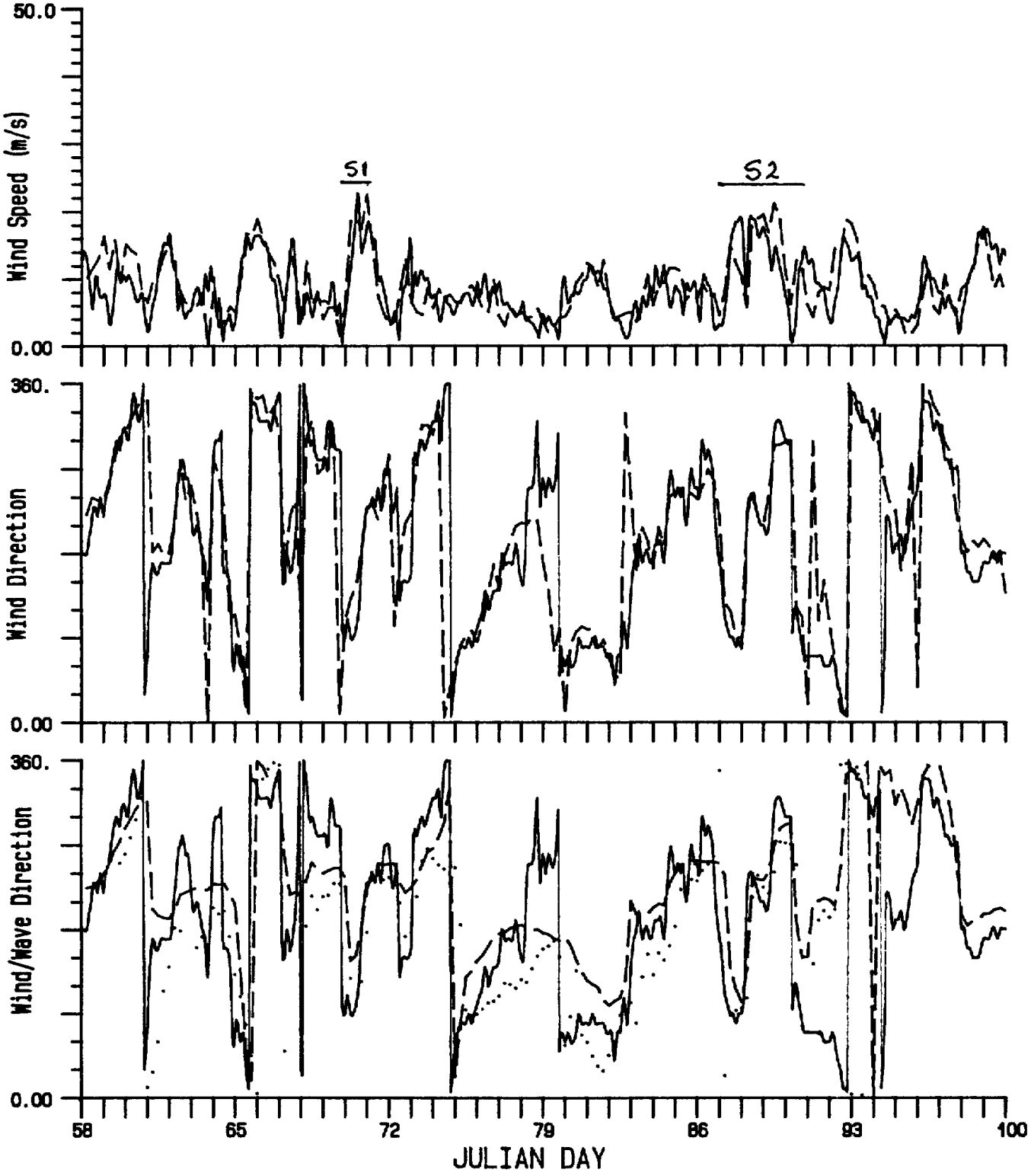

Fig. 11 Time series of MANMAR (solid) and hindcast (dashed) winds. The bottom plot shows the VMDs of the hindcast (dashed) and data (dotted) spectra.

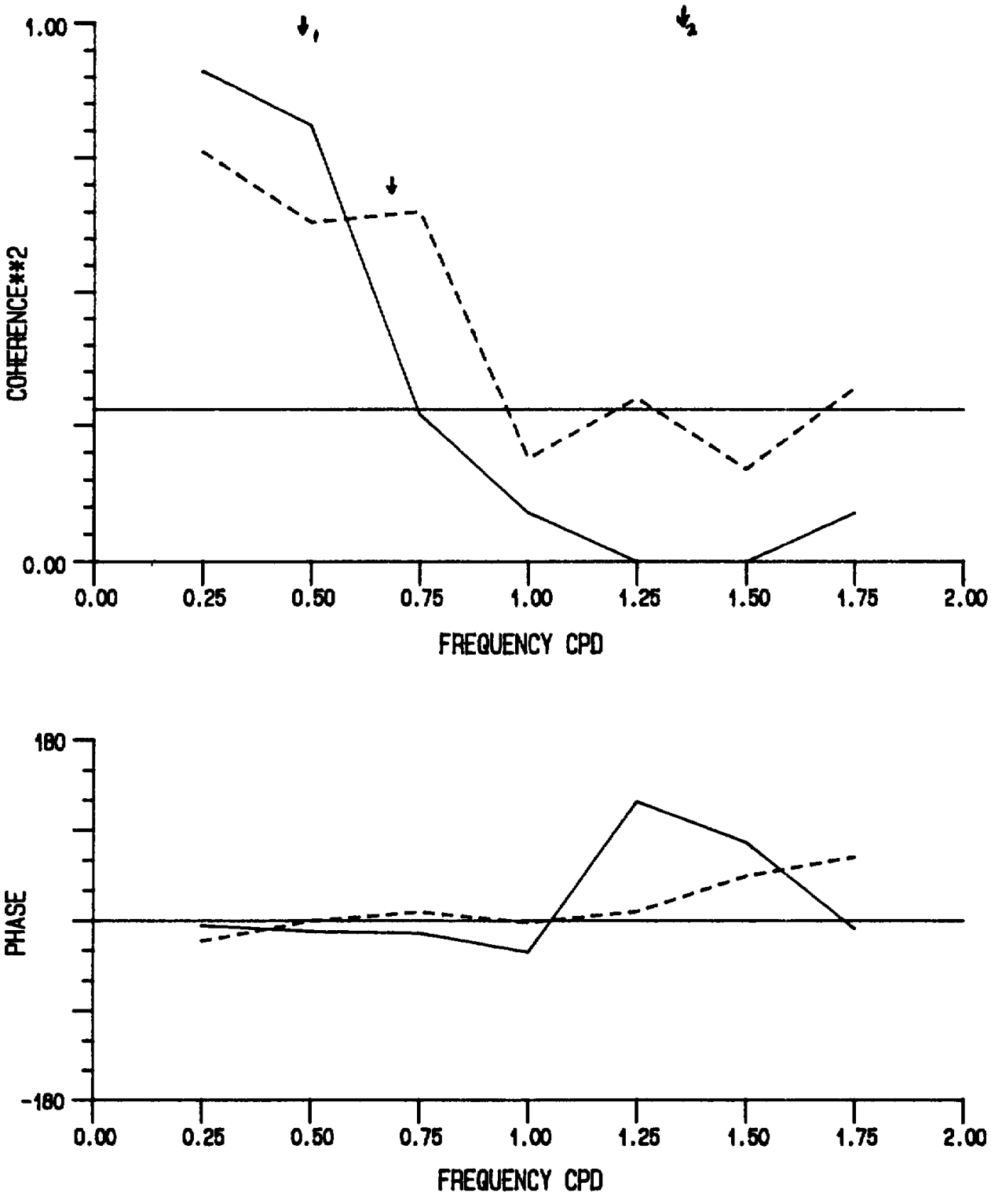

Fig. 12 Inner coherence squared and phase of the MANMAR and hindcast winds. Solid line: Counter-clockwise; Dashed line: Clockwise component.

4.2 Input Winds

A preliminary examination of the input winds to the hindcast model at grid point 1106 and the measured MANMAR winds (on the West Venture; 5 kms East of the WAVEC buoy) would indicate if there existed any large discrepancies that could influence the spectra. As hindcast model wind fields are structured to include a contribution of directly measured winds, along with geostrophic winds, the two data sets are not fully independent and one would expect generally good agreement between them, Fig. 11 contains the time series of rig winds (solid), model input winds (dashed), and shown on the lower plot, VMD of model spectra (dashed) and VMD of the WAVEC spectra (dots). The agreement in wind speeds is generally quite good with the first storm (S1;day 70–71) being reproduced quite well. This storm consisted of a low pressure center approaching the study site from the SW resulting in a rapid increase in wind speeds on day 70 to a peak of approx. 23 m/s after 13,5 hours. The wind directions then shifted by 120 degrees (from E to SW), and remained from the SW for about nine hours and during the following storm decay. The second storm (day 87–90) consisted of a low pressure centre which approached the Hibernia region from the S–SW with associated winds rising to approx. 20 m/s in 18 hrs. The center passed directly over the study region, as noted by a drop in the wind speed and concurrent veering of the direction early on day 88, then stalled north of the area for nearly 24 hours. The winds slowly decayed and shifted in direction approx. 110 degrees) as the pressure center moved off. The hindcast winds did not show as high a rise in wind speed during the first stage of the storm though the temporary drop in speed and direction shift associated with the passage of the low pressure centre were reproduced. Similar maximum winds were reached during the second part of the storm while there was a slight delay in initiation of the storm decay. The hindcast winds appeared to miss a slight rise in the local winds on day 91. It will be seen in Section 4.4 , that the time series of model HSIG reflected these slight differences in the specified winds. The two wind directions agree well except when wind speeds are low (eg. days 77–79, 83). The VMDs tend to reflect the wind direction during more energetic conditions. Contributions from the swell play a role at all times and dominate when wind speeds are low (eg. day 74 through 80, 91–92).

A coherence analysis between the hindcast winds and observed rig winds would provide some indication of the shortest time scale feature that could possibly be modelled with confidence. A discussion of coherence analysis of vector time series, as applied here, can be found in Gonella (1972). Fig. 12 shows the inner coherence squared between the counter–clockwise (solid) and clockwise (dashed) rotating wind vectors. Also shown on Fig. 12 is the phase in degrees which is approximately zero over the coherent frequency range. The outer

coherences were never significant. There were 20 degrees of freedom in the analysis and a 0.25 cycles per day (cpd) resolution. The solid line in the upper plot indicates the 95% confidence limit on the coherence squared (ie. where the coherence is significantly different from zero). Also noted are the 0.5 coherence squared cut–off levels (ie. where 50% of the variance in that frequency band is explained) when geostrophic winds (1 – Marsden, 1987 and de Young and Tang, 1989) and wave slope derived winds (2 Marsden and Juszko, 1989) are compared with directly measured winds. The hindcast winds showed a similar cut–off around 0.75 cpd (ie. time scales of 1.25 to 1.5 days) which is somewhat better than geostrophic (2.5 – 2.0 days) though poorer than inferred winds from wave slope information (0.75 days). The peak in the clockwise coherence**2 at 0.75 cpd was consistent with the veering of observed winds associated with the passage of low pressure centres through the area. This data set was obviously limited in both temporal and spatial coverage and similar coherence analyses should be conducted on the much larger archived wind files. Such an analysis would show up the weaknesses in wind field specification in a quantitative manner and on a geographic basis.

4.3 Treatment of the WAVEC Data

In order to eliminate uncertainties in the comparison due to different frequency and direction array assignments, the WAVEC directional spectra (constant frequency resolution of .03 Hz or .1885 rps, between .314 and 3.14 rps – 16 frequencies; four degree resolution in direction) were mapped onto the hindcast spectra array. The interpolation scheme used was a combination of Laplacian and spline interpolation as provided by PLOT88 library and described in Young and Van Woert (1989). The effect of the interpolation on the mean wave parameters, and later, on the 10–parameter fit, was assessed. Fig. 13 contains the time series of HSIG, TP and VMD calculated before (solid) and after (dotted) performing the interpolation. Both the overall energy and average directional properties of the wave field are conserved by the interpolation. Given the considerable difference in the frequency array assignments between the input and output, the discrepancies in peak period are acceptable.

The adjusted data spectra were processed using the hindcast model software. Figs. 14 , 15 and 16 contain the time series of OH model fit parameters, the distribution of RESH with frequency, both absolutely and weighted by the peak spectral density as in Fig. 3 , and the histogram of RESH occurrence. The results are comparable to those seen in Part 1 of the study.

Figs. 17 and 18 contain the time series of fit parameters, RESD values and the histogram of RESD occurrence for the full 10–parameter fit. The residual values are comparable to those for the

fit to the original data spectra (Fig, 22 – Part 1) though it appears that in the latter case there were a greater percentage of records with RESD <10%. This is deceptive as the fit performs better under high energy conditions, and in Part 1, there were considerably more observations during storms which biases the results. Fig. 18 indicates that approximately 90% of the records had RESD values less than 20% (compared with 93% for the hindcast spectra seen in Section 3.2.2).

Fig. 19 contains the overlayed time series of HSIG, TP and VMD of the interpolated data spectra (solid) and the corresponding 10–parameter fit spectra (dotted). The agreement is generally quite good though slightly poorer than in the fit to the hindcast spectra (Fig. 9). This is shown more quantitatively by the slightly higher ME, RMSE, and % Scatter and lower correlation values in Table 2 (when compared to Table 1). The shape of the distributions are similar. The slightly poorer agreement may be due to the flatter direction spectra of the data (eg. see contour plots in Appendix 1) which could possible hinder the directional fit compared with a sharp directional peak.

Whether or not the choice of frequency and direction resolution has a significant affect on the fit results may be determined through an examination of the summary statistics calculated on the two sets of fit parameters. These are given in Table 3 . It can be seen that the major differences occur in the shape related parameters ($\lambda 1$, $\lambda 2$, P1 and P2) and there are lower correlations (and larger errors) for all the second (”sea”) set of parameters which would be expected given the changes in array resolution and the range of frequencies covered. Performing the interpolation is necessary for any point–by–point comparison between the hindcast and data spectra and should improve the comparison for the second set of parameters (seas). However, the interpolation appears to be broadening the energy distribution of the ”swell” (as indicated by λ) perhaps reflecting the mapping from a coarse frequency grid to a finer one at low frequencies which may act to smooth the spectra.

4.4 Comparison of Hindcast Model Spectra and Field Measurements

Throughout the following comparison, the two sets of spectra (hindcast and interpolated WAVEC) and their corresponding fit spectra will be examined.

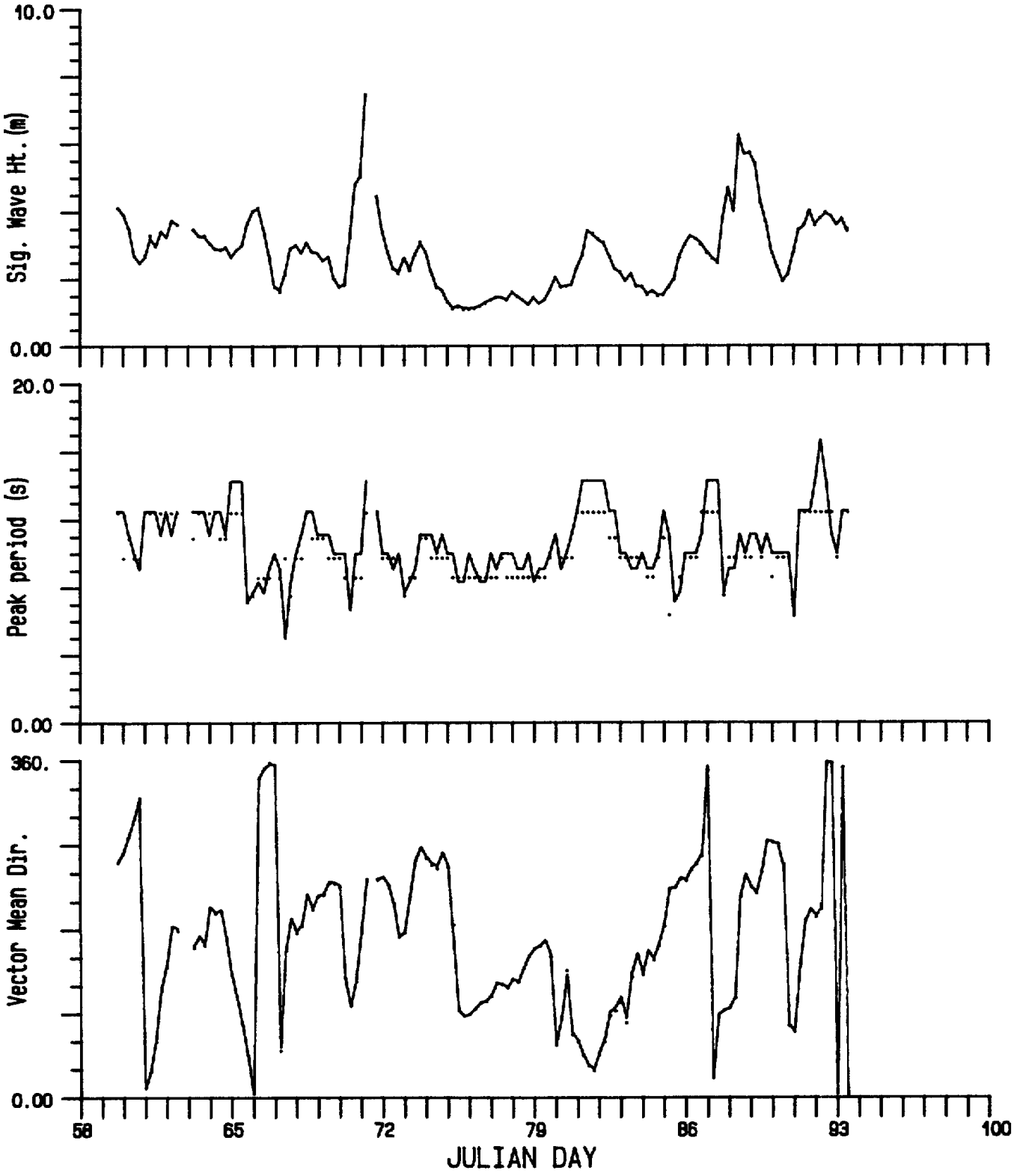

Fig. 13 Time series of HSIG, TP and VMD before (solid) and after (dotted) performing the interpolation on the data spectra.

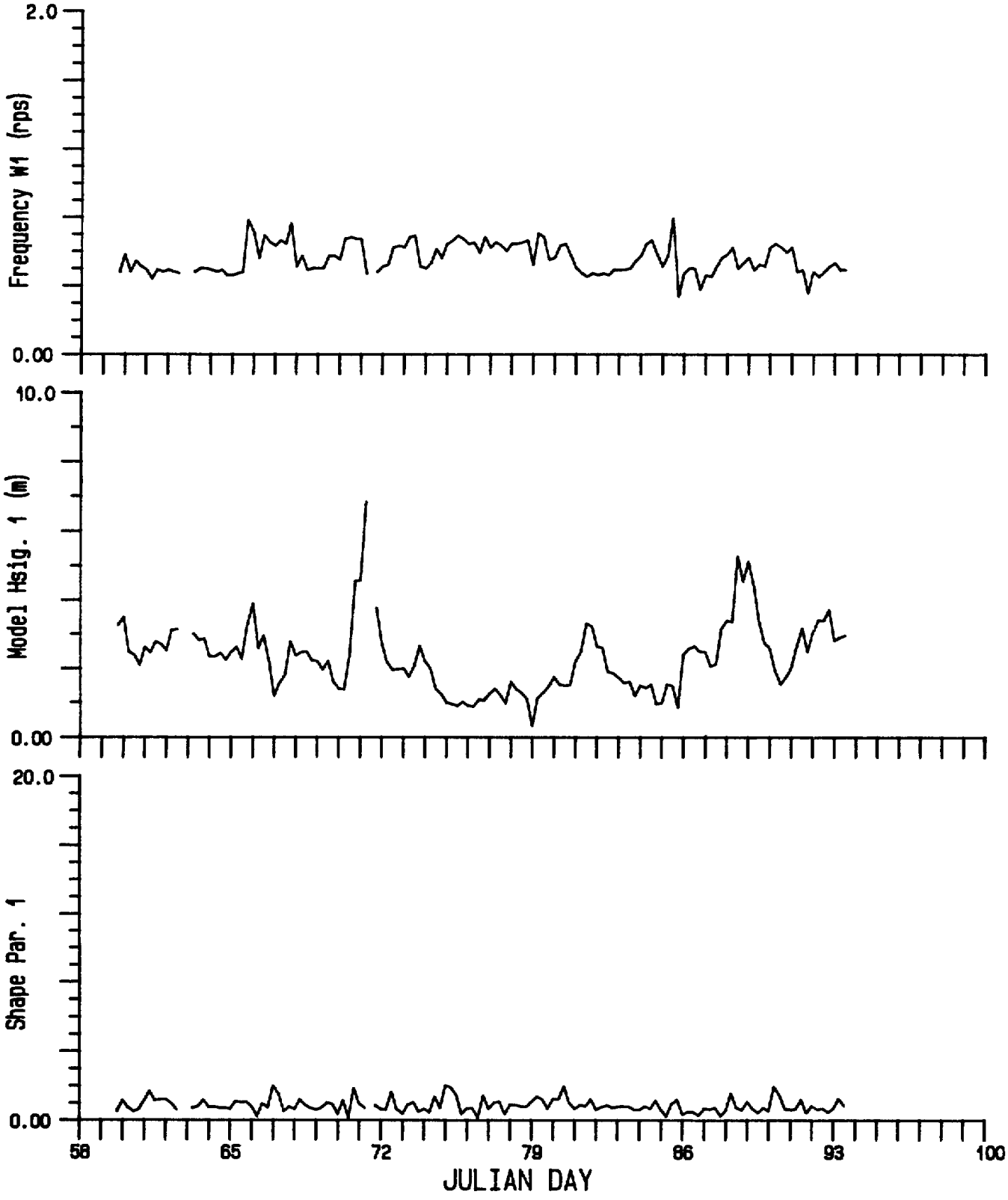

Fig. 14 Time series of OH fit parameters to the data.

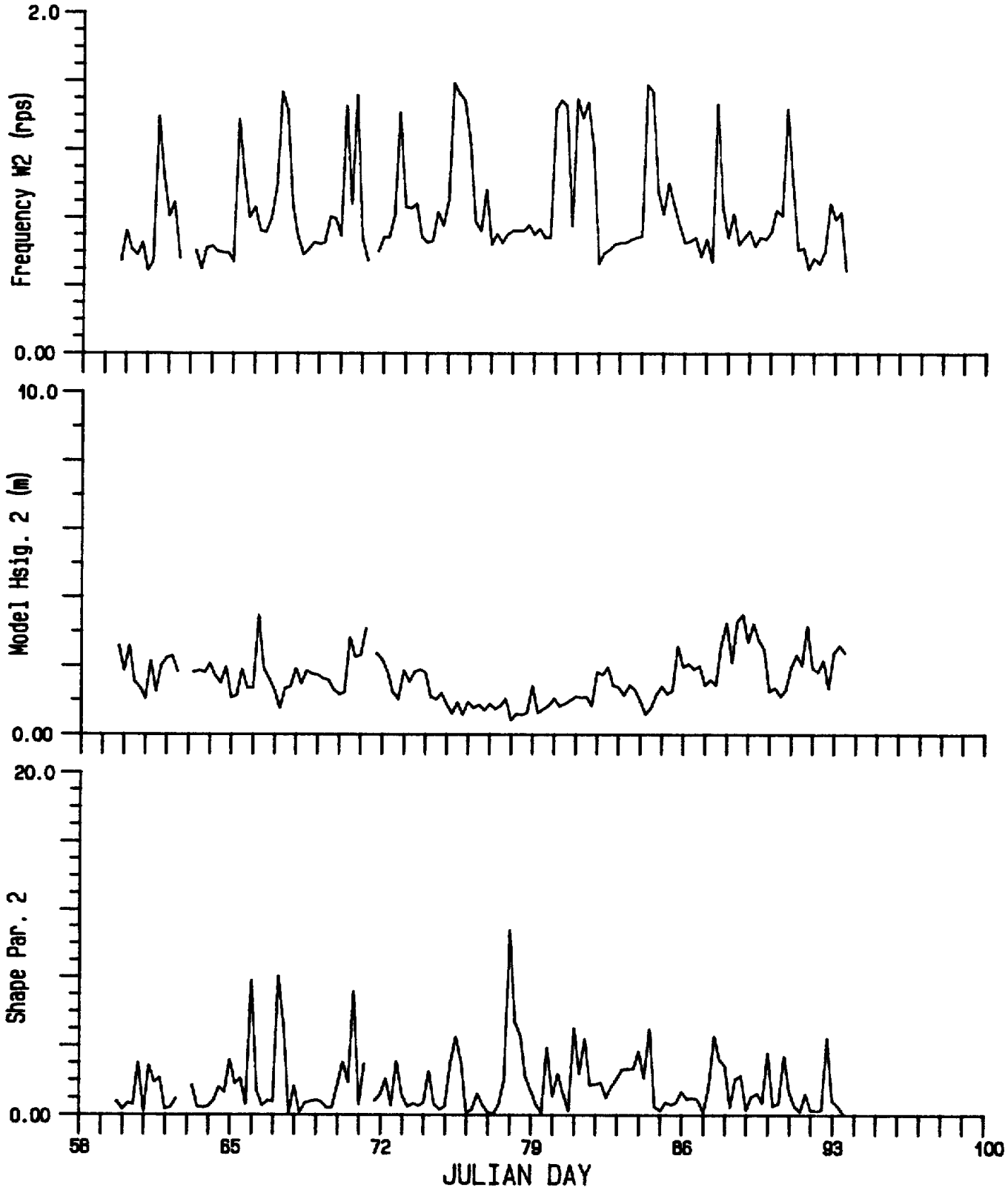

Fig. 14 (continued)

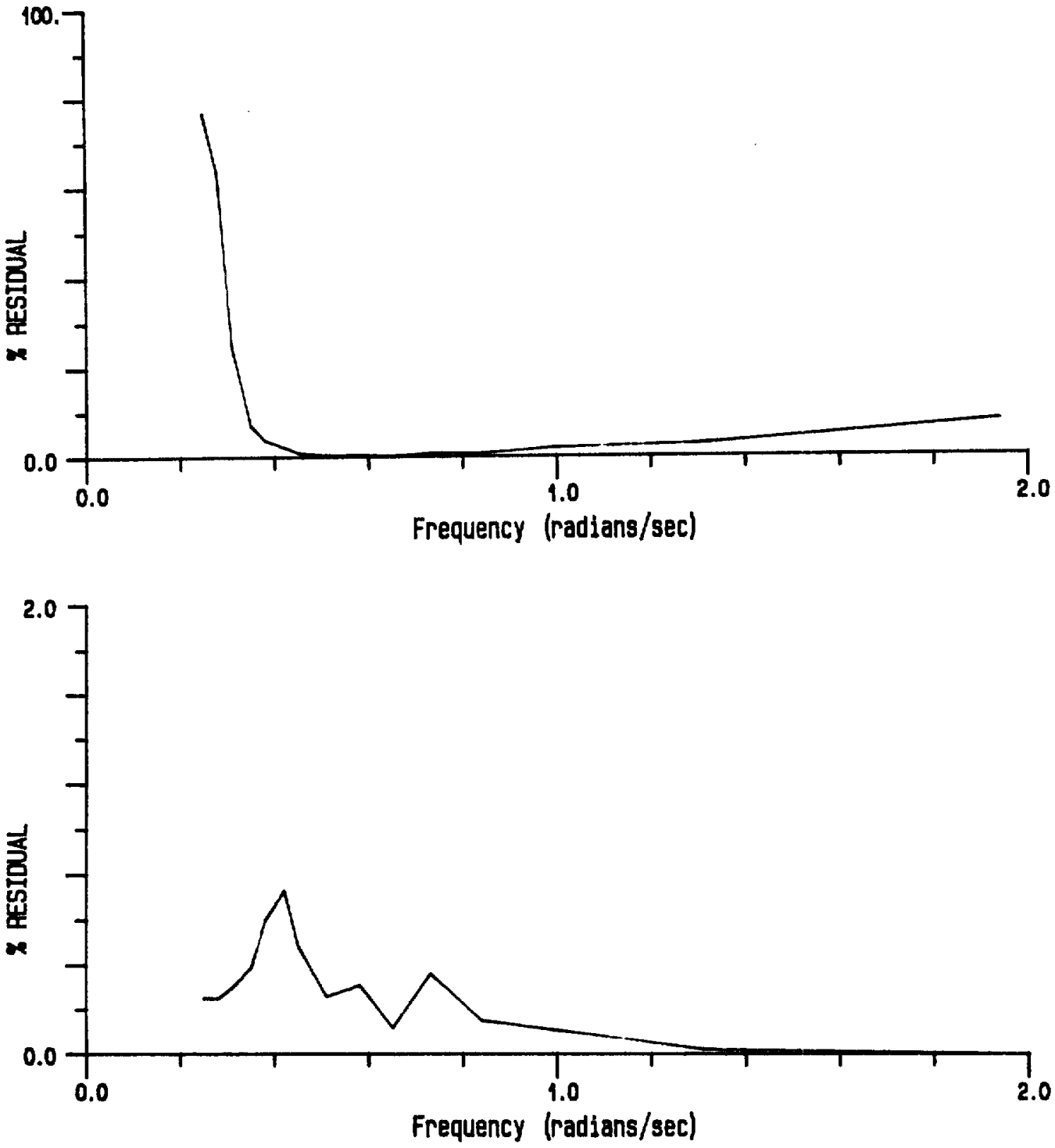

Fig. 15 RESH as a function of frequency for the fit to the data spectra. Upper: weighting by E(w); Lower: weighting by EMAX.

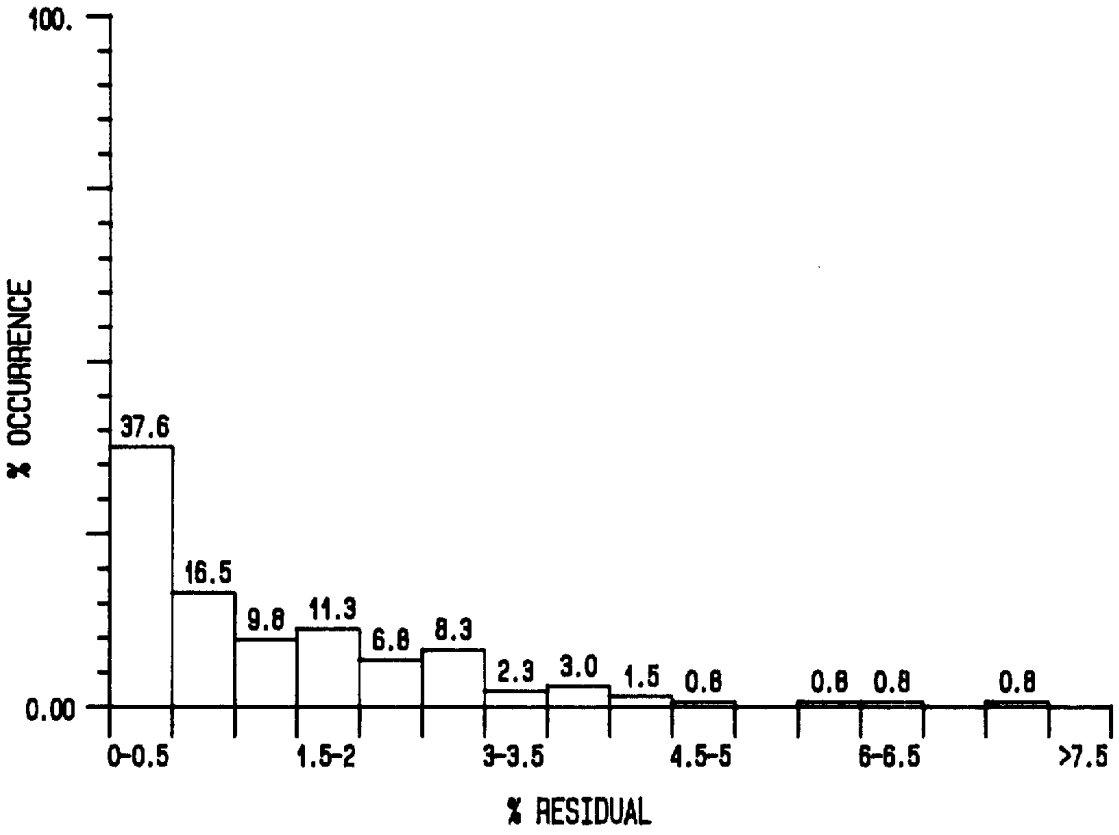

Fig. 16 Percent occurrence of RESH values for the fit to the data spectra.

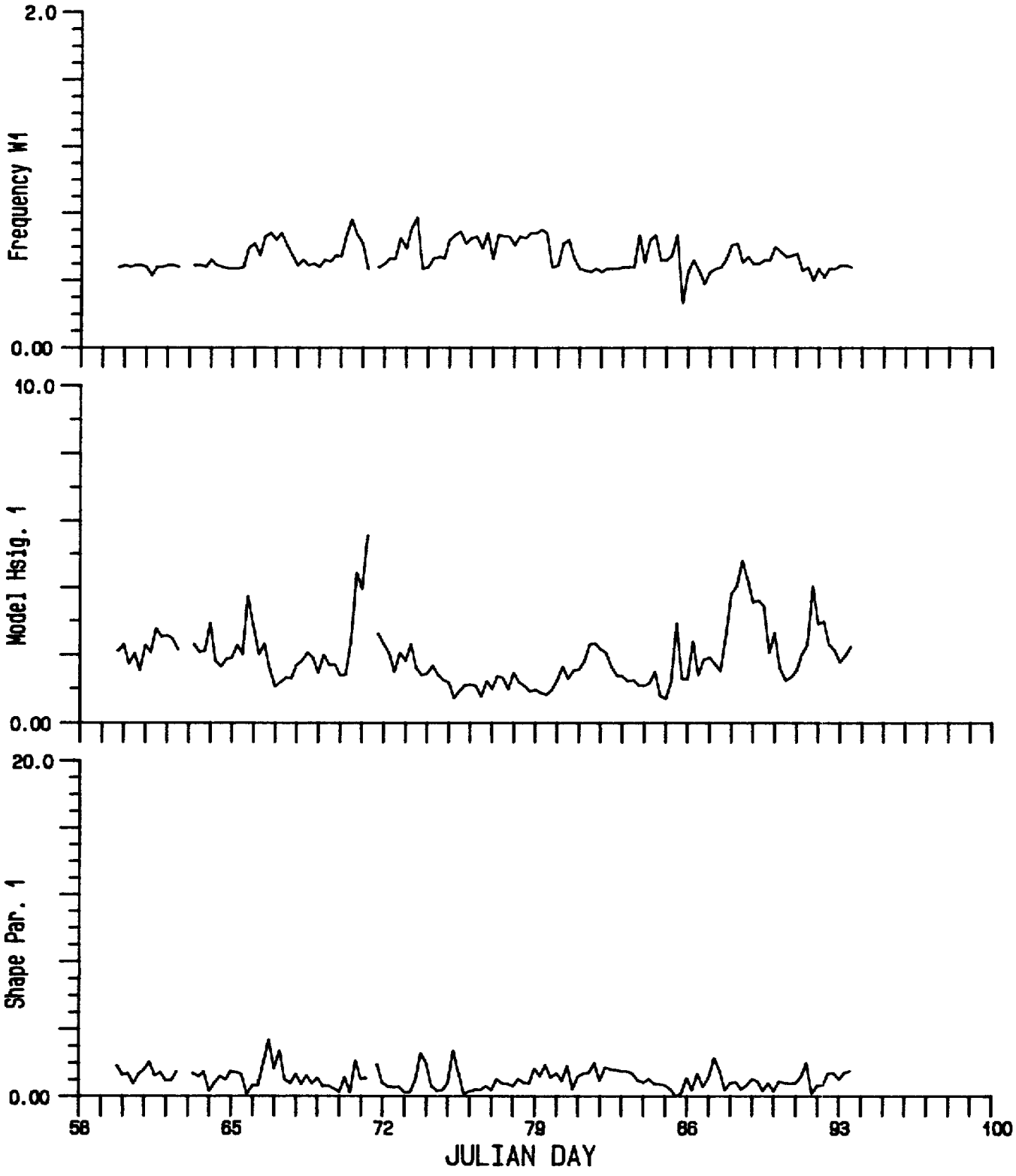

Fig. 17 Time series of fit parameters, ang. half-width and RESD values for the 10-parameter fit to the data spectra.

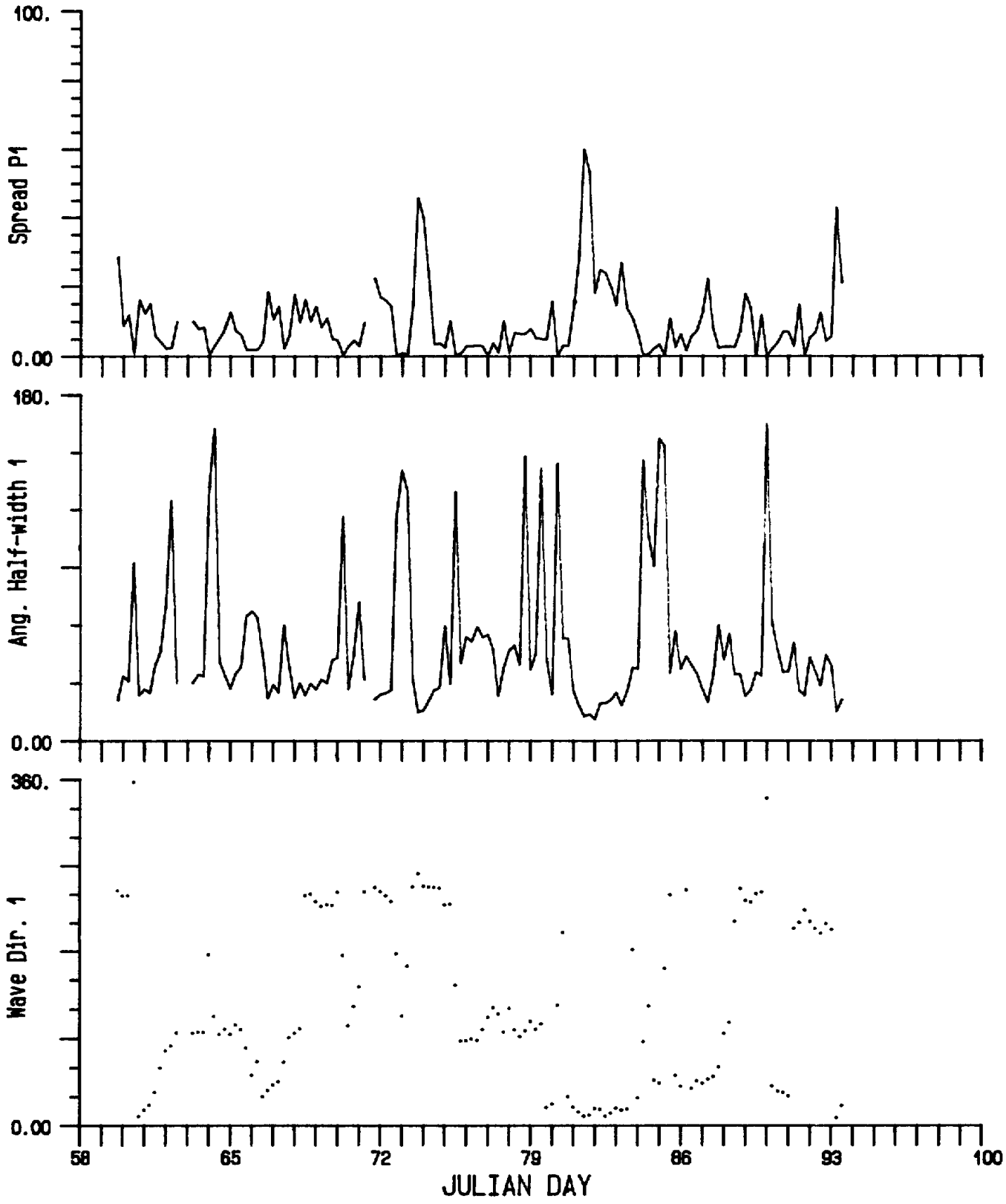

Fig. 17 (continued)

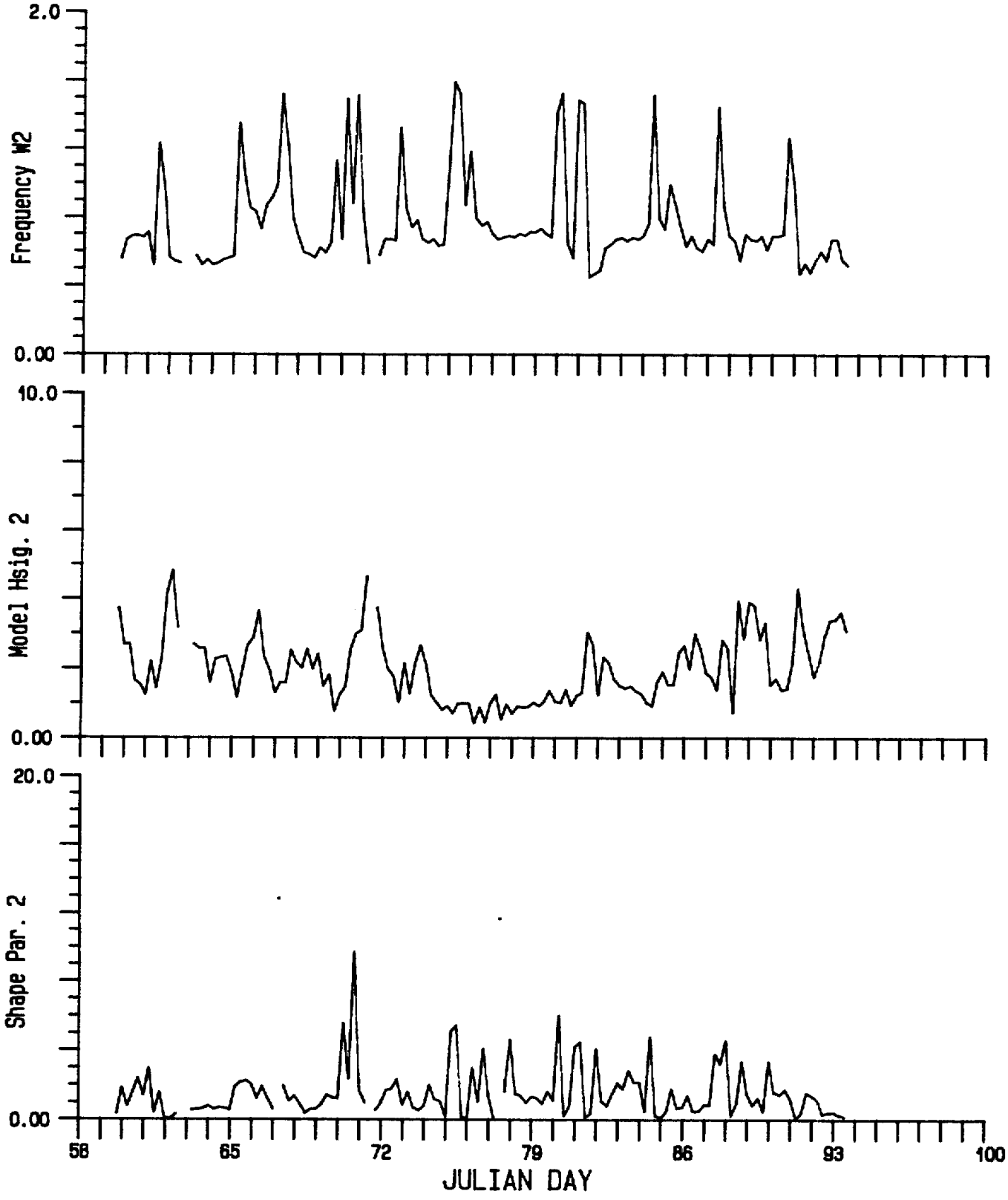

Fig. 17 (continued)

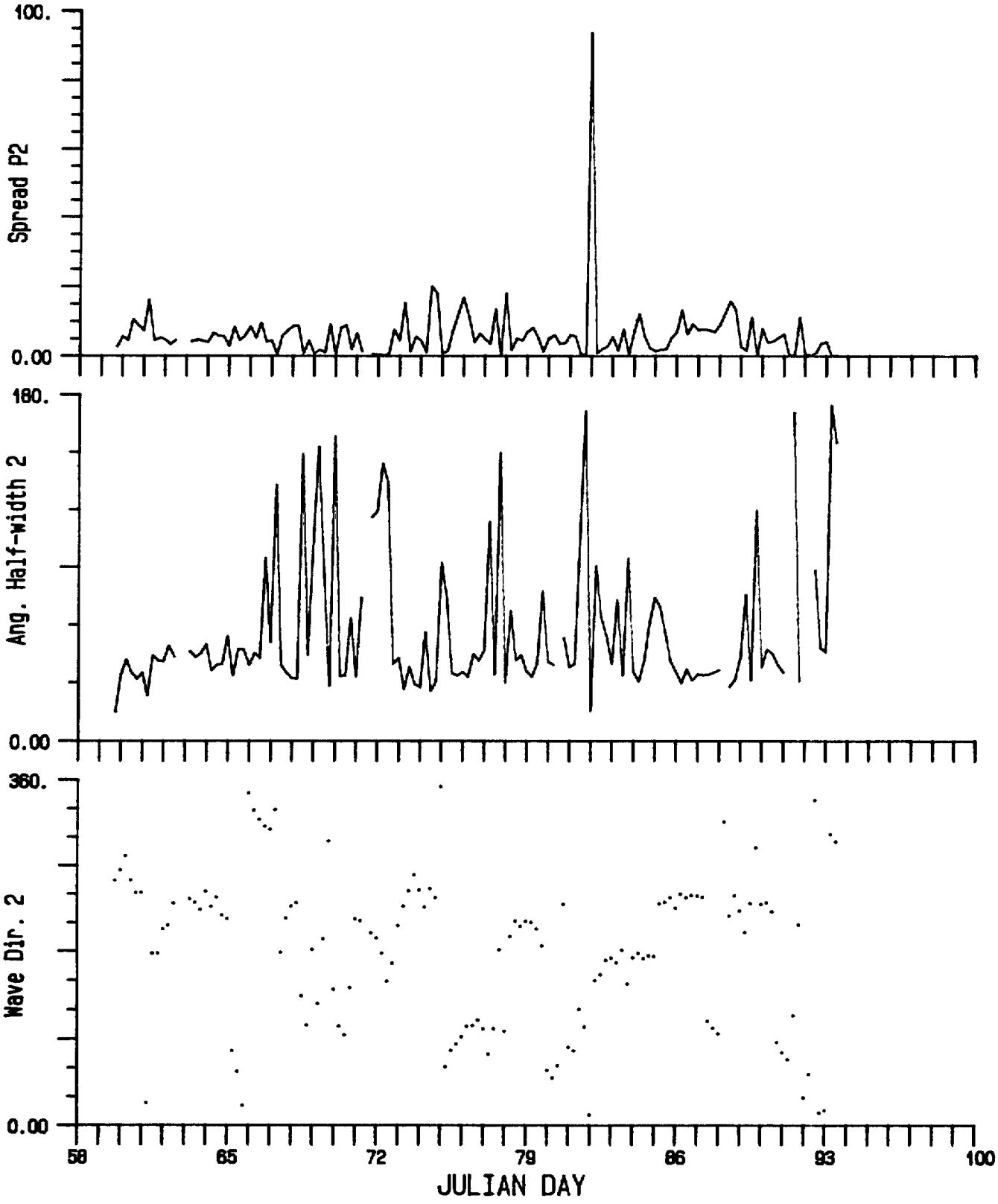

Fig. 17 (continued)

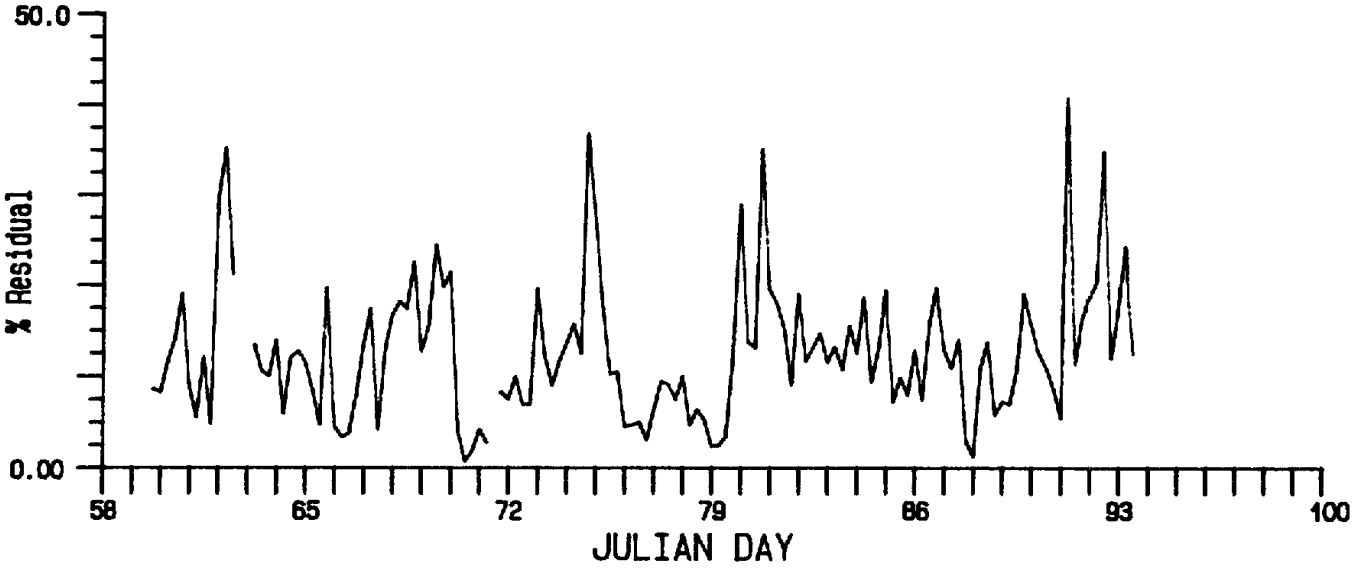

Fig. 17 (continued)

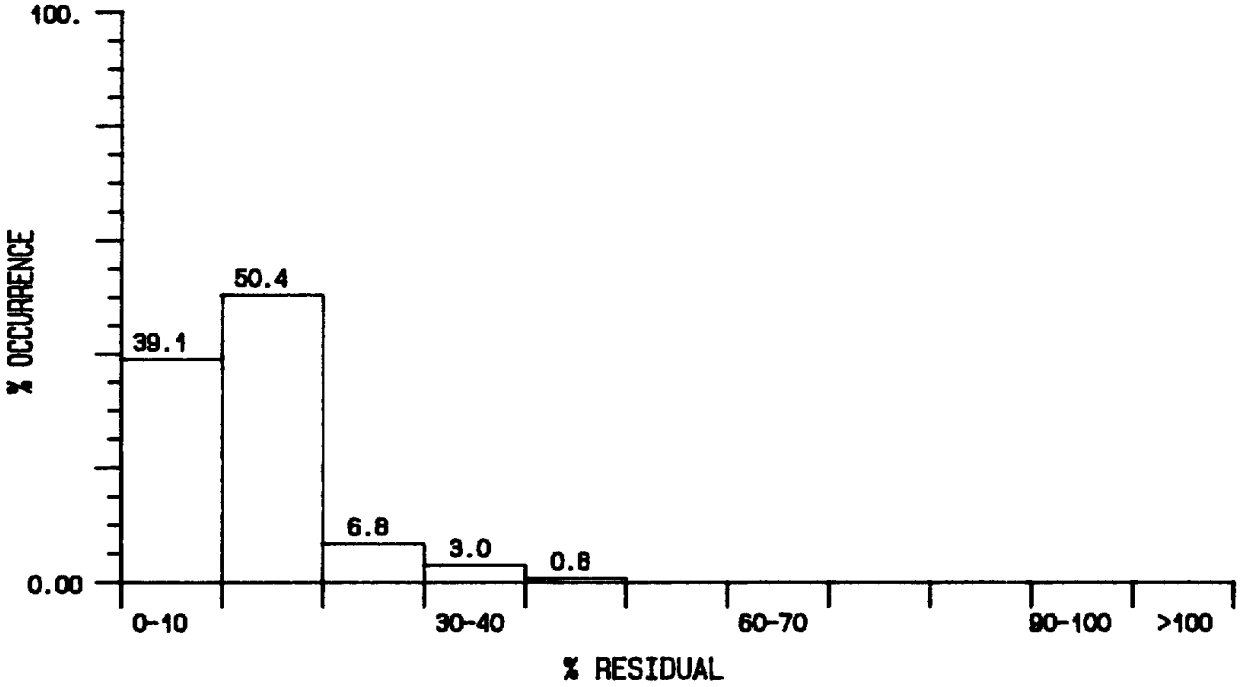

Fig. 18 Percent occurrence of RESD values for the fit to the data spectra.

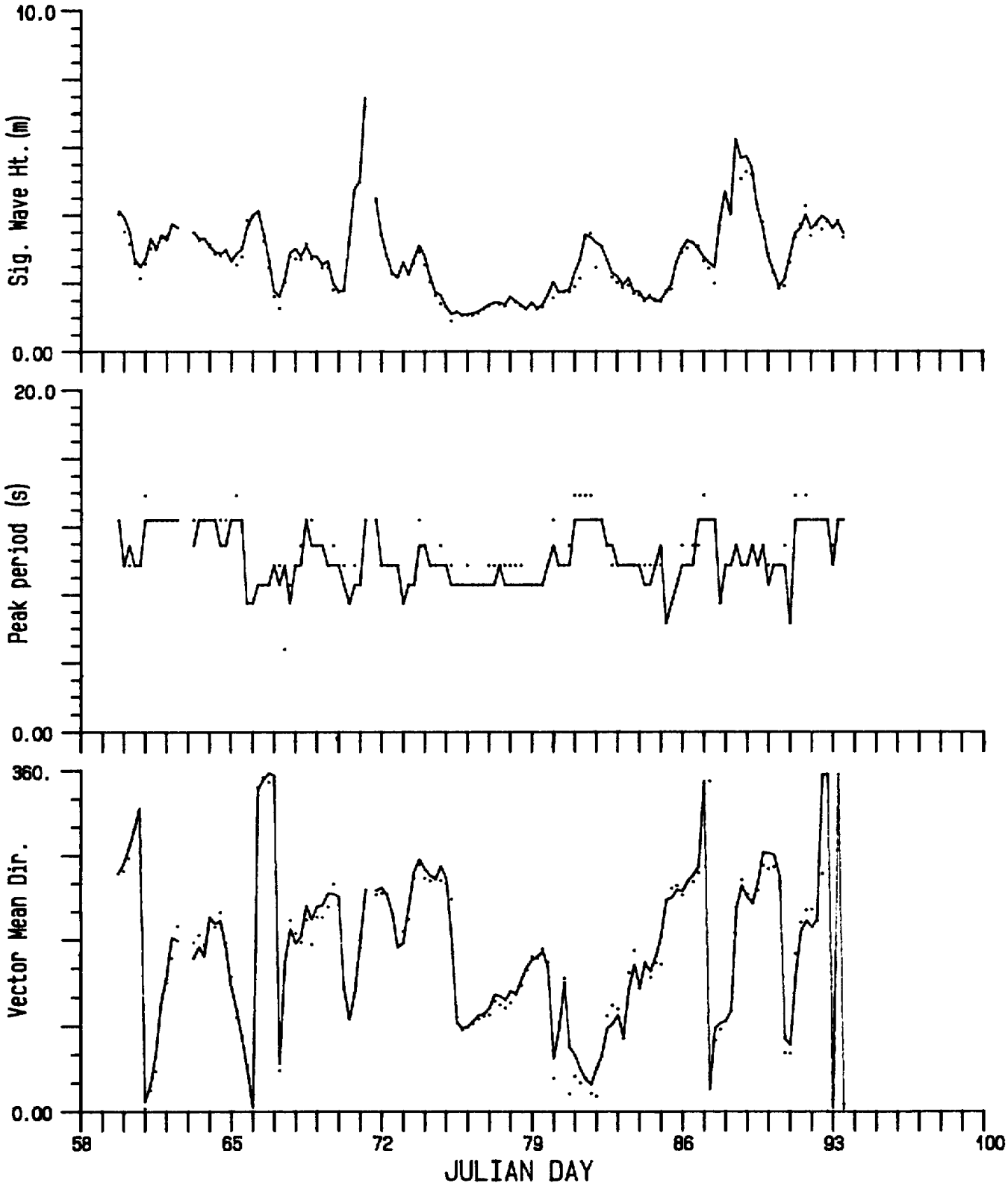

Fig. 19 Time series of HSIG, TP and VMD of the data (solid) and 10-parameter fit (dotted) spectra.

TABLE 2. Summary statistics for spectral properties of the WAVEC data (W) and corresponding 10-parameter fit (F) spectra.

	HSIG (m)	TP (sec)	VMD (rad)	PDIR (rad)	TDIR (sec)	P
No. of Observ.	133	133	133	133	133	126 97
Mean W	2.77	10.19	2.87	3.37	10.27	6.58
F	2.67	10.48	2.98	3.02	10.69	11.27
ADEV W	0.87	1.41	1.22	1.40	2.09	7.99
F	0.88	1.52	1.23	1.42	1.96	7.25
SDEV W	1.13	1.65	1.47	1.70	2.19	13.44
F	1.12	1.82	1.49	1.62	2.31	11.83
SKEW W	0.95	0.05	-0.65	-0.34	-0.24	3.57
F	0.89	-0.05	-0.38	-0.82	-0.37	2.88
KURT W	1.67	-1.04	-0.67	-0.78	-1.41	14.75
F	1.25	-0.29	-0.57	-1.07	-0.49	9.60
No.	133	133	133	133	133	94
ME	0.10	-0.29	0.06	0.07	-0.42	-3.28
RMSE	0.18	0.84	0.26	0.39	1.13	13.68
% SCAT	6.68	8.13	8.78	12.09	10.79	139.95
CC	0.99	0.90	0.71	0.49	0.89	0.54
SI.LEV	0	0	0	0	0	0

4.4.1 Qualitative Assessment

Appendix 1 contains contoured directional spectra associated with the WAVEC spectra (upper left), the fit to this spectra (lower left), the hindcast model spectra (upper right) and its corresponding fit (lower right). The contour intervals are set to: 0.01, 0.025, 0.05, 0.1, 0.25, 0.5, 1.0, 2.0, 4.0, 6.0, 8.0, 10.0, 15.0, 20.0 and 30.0 m**2/(rps-rad). The records selected represent the two major storms of March 1984. The model generally overpredicted the total energy during the storms of this particular data set. The overall features of the directional spectra are reproduced quite well (ie. positioning of the directional peaks; eg. 1200/87 with two swell and a sea peak) by the hindcast model, however, the peaks tend to be much sharper than seen in the data. Given that the contour intervals are not linear, this difference is more severe than the plots would indicate. Much of the discrepancy between the data sets are due to the presence (or absence) of additional swell peaks. The hindcast spectra will miss a swell peak due to a more rapid decay of the signal than observed (eg. 0000/70-0600/70; 0600/71-1800/71 where the swell signal persists in the data through day 72; 1200/88- through day 89) or add peaks not present in the data (eg. 0600/88). The storm seas appear to develop (ie. progress towards lower frequencies) more rapidly, and to lower frequencies, in the hindcast spectra (eg. 0600/70 to 1800/70; 0600/87 to 1800/87; 1200/90-1800/90). As the winds were initially from the east for all three development periods (associated with the upper edge of a low moving northeast) one would expect that they affect the measurement sites at similar times given the north-south orientation of the sites. As during the build-up of the second storm, the hindcast

winds were actually lower than observed while the sea progression was faster, it appears that this overly rapid development may be an intrinsic feature of the model. The development of the total energy in the spectrum due to storm seas, however, is linked more closely to the magnitude of the input winds. This can be seen in Fig. 20 containing overlayed hindcast model (solid) and data spectral statistics (dotted). The dashed lines axe the 95% confidence limits on the data significant wave height and indicate that differences between the two record sets axe not related to statistical uncertainties in the field measurements. During the build-up of the second storm, the hindcast HSIG lags the data while a similar lag was seen in the model and observed winds (Fig.11). Fig. 21 contains similar plots for the corresponding 10-parameter fit spectra and are almost identical to those in Fig. 20 which is to be expected given the correlation statistics in Tables 1 and 2 .

TABLE 3. Summary statistics for the ten fit parameters obtained from the non-linear fit to the original (O) and interpolated (I) WAVEC data spectra. 133 Observations.

	ω_{m1} (rps)	δ_1 (m)	λ_1	P1	θ_{m1} (rad)	ω_{m2} (rps)	δ_2 (m)	λ_2	P2	θ_{m2} (rad)
MEAN O	0.56	1.84	2.64	31.02	3.15	0.82	1.80	2.06	9.89	3.30
I	0.54	1.93	1.05	9.58	1.62	0.77	2.00	1.69	6.22	3.40
ADEV O	0.09	0.71	1.66	23.05	1.44	0.24	0.83	1.49	8.03	1.29
I	0.07	0.65	0.47	7.16	1.23	0.20	0.79	1.21	4.10	1.13
SDEV O	0.10	0.95	2.92	28.65	1.67	0.29	1.33	2.45	11.84	1.54
I	0.09	0.88	0.60	10.26	1.54	0.28	0.95	1.97	8.78	1.41
SKEW O	0.03	1.21	3.62	1.10	-.93	1.20	4.40	3.13	2.38	-0.16
I	0.41	1.44	0.88	2.31	1.12	1.58	0.66	3.16	7.48	-0.32
KURT O	-0.66	1.81	15.72	0.03	-.98	0.85	32.20	11.66	6.94	-0.90
I	-0.21	2.40	1.15	6.70	-.83	1.50	-0.14	12.60	70.92	-0.48
ME	0.02	-0.08	1.58	21.44	0.07	0.05	-0.20	0.36	3.67	0.05
RMSE	0.08	0.50	3.27	31.72	1.12	0.25	1.16	3.03	14.47	0.99
% SCAT	13.8	26.3	177.5	156.2	52.7	30.0	61.0	161.7	179.6	29.5
CC	0.71	0.86	0.18	0.64	0.62	0.66	0.54	0.08	0.10	0.54
SI.LEV	0	0	0.04	0	0	0	0	0.38	0.28	0

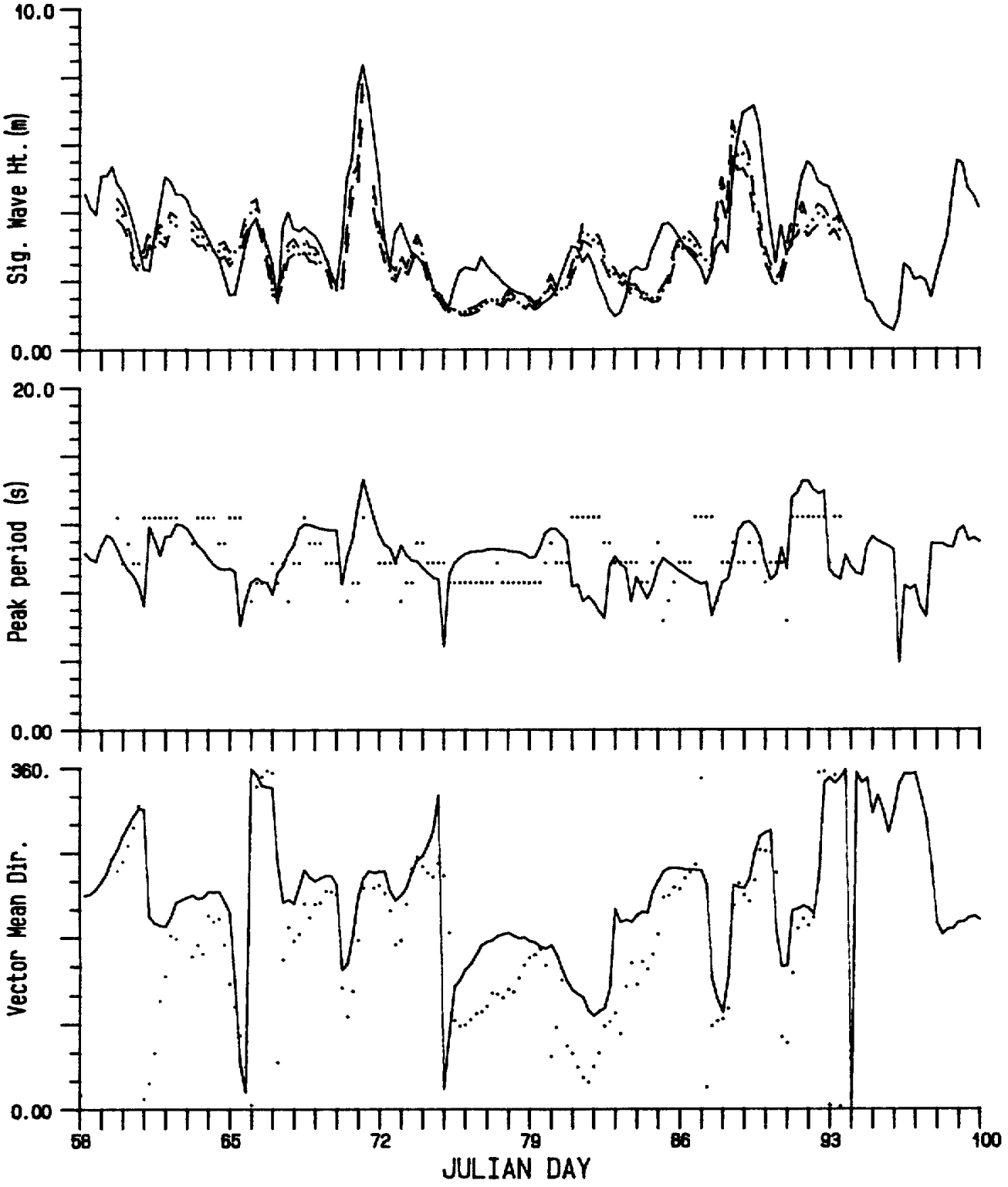

Fig. 20 Time series of HSIG, TP, VMD, PDIR, TDIR and P of the hindcast (solid) and data (dotted) spectra. The dashed lines are the 95% confidence limits on the data HSIG.

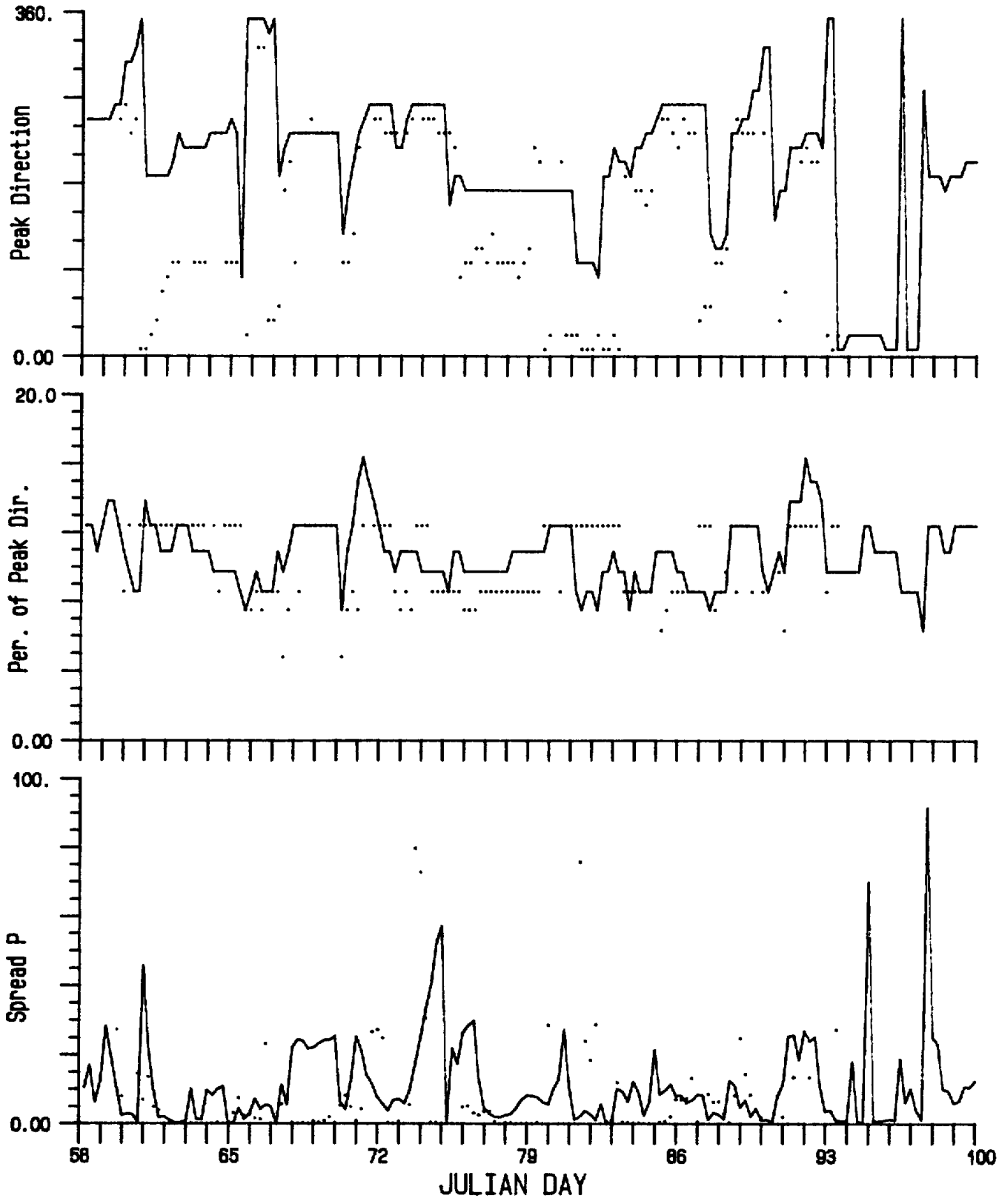

Fig. 20 (continued)

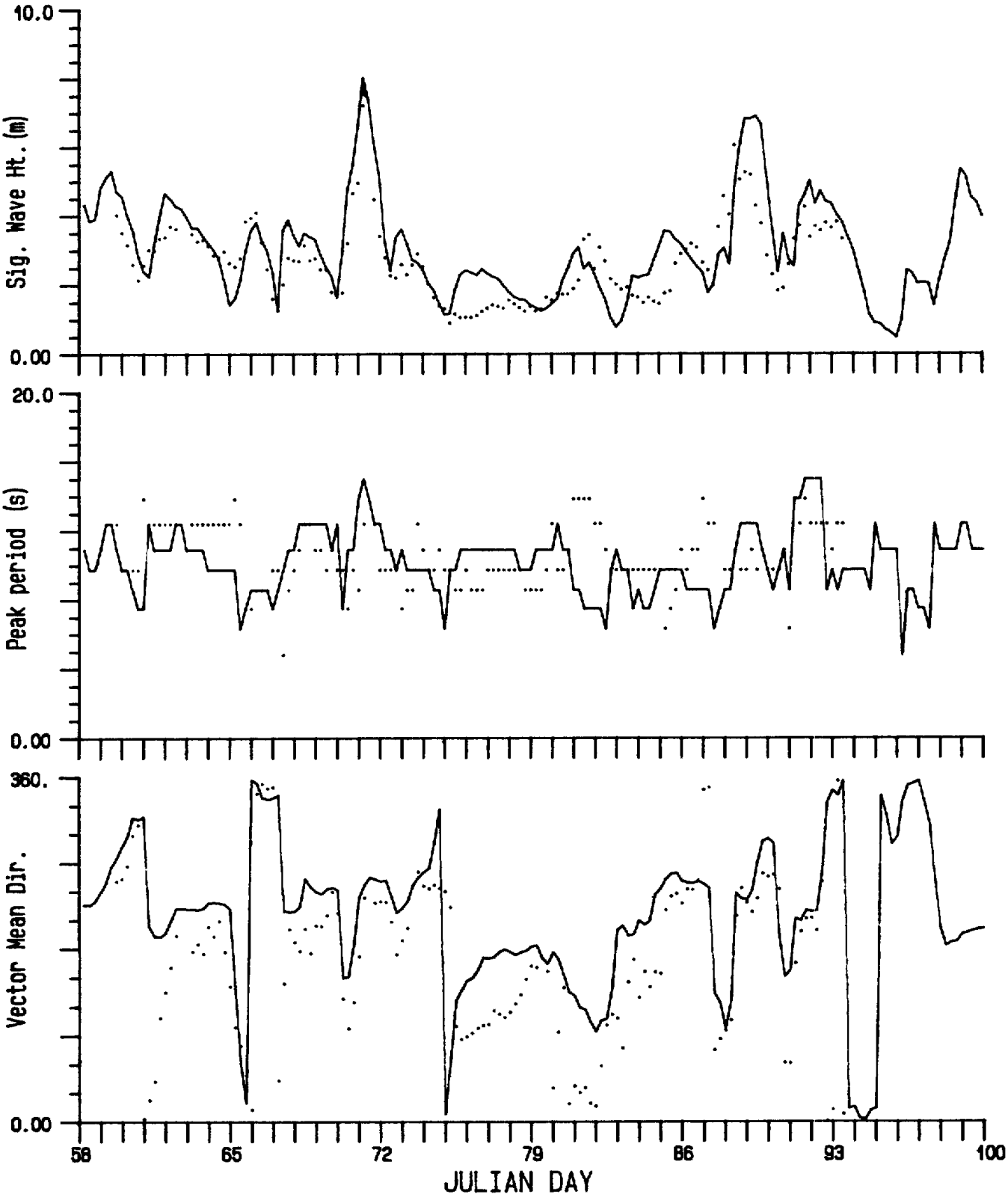

Fig. 21 As in Fig. 20 but for the corresponding 10-parameter fit spectra.

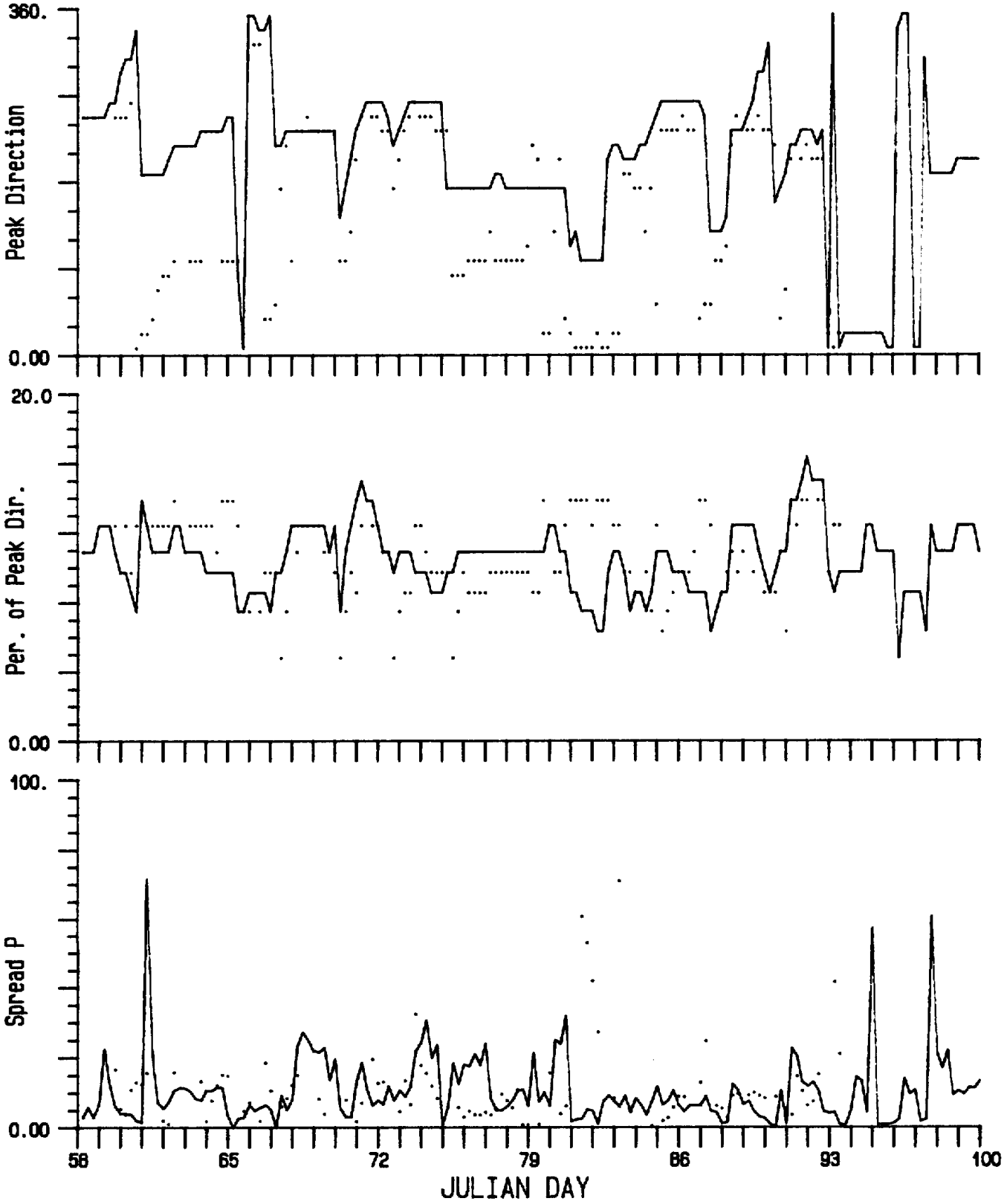

Fig. 21 (continued)

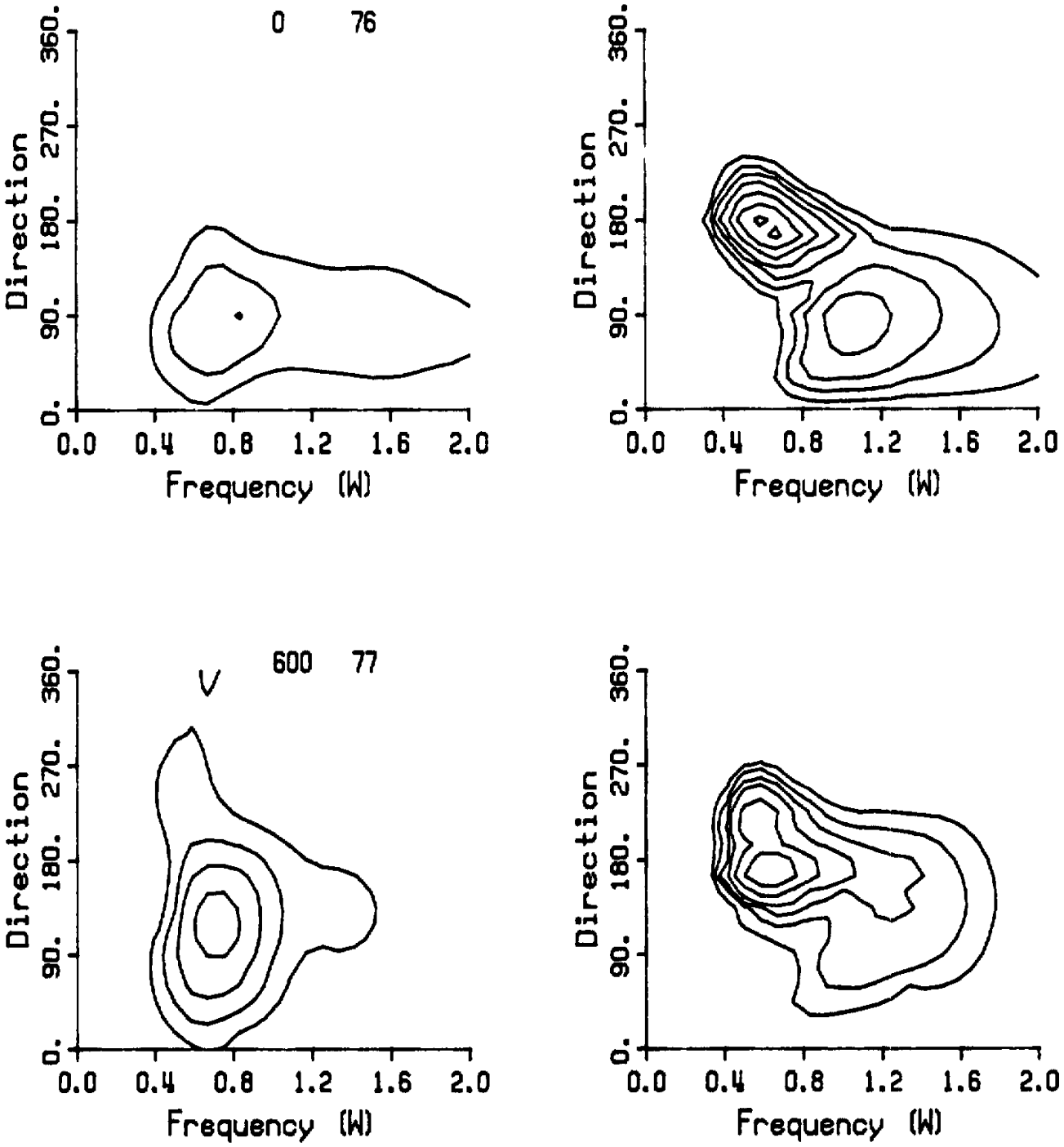

Fig. 22 Examples of contoured directional spectra for the data (left) and hindcast (right) spectra. Times as shown on the plots. Contour intervals set at: .01, .025, .05, .1, .25, .5, 1, 2, 4, 6, 8, 10, 15, 20 and 30 m**2/rps-rad.

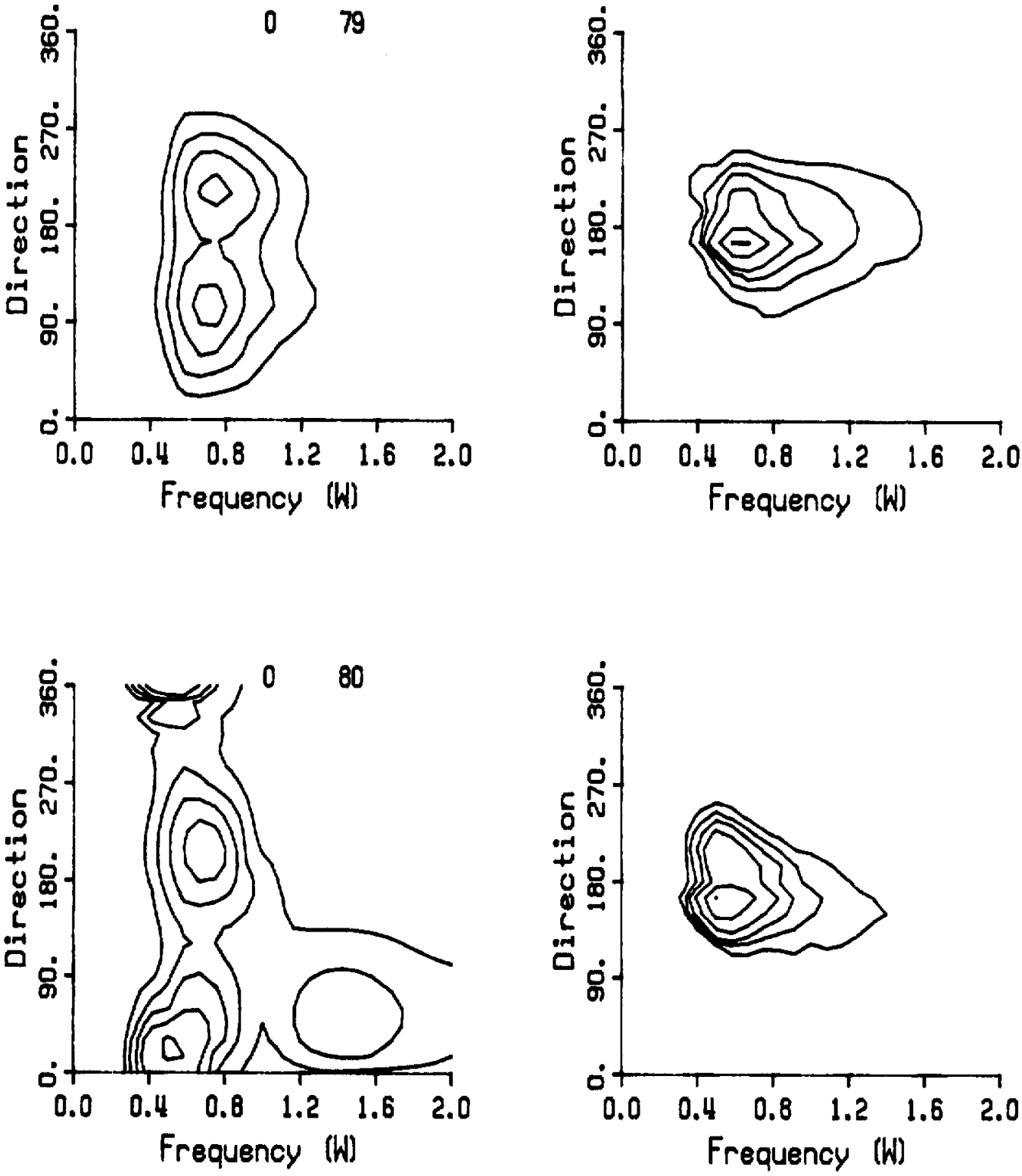

Fig. 23 As In Fig. 22

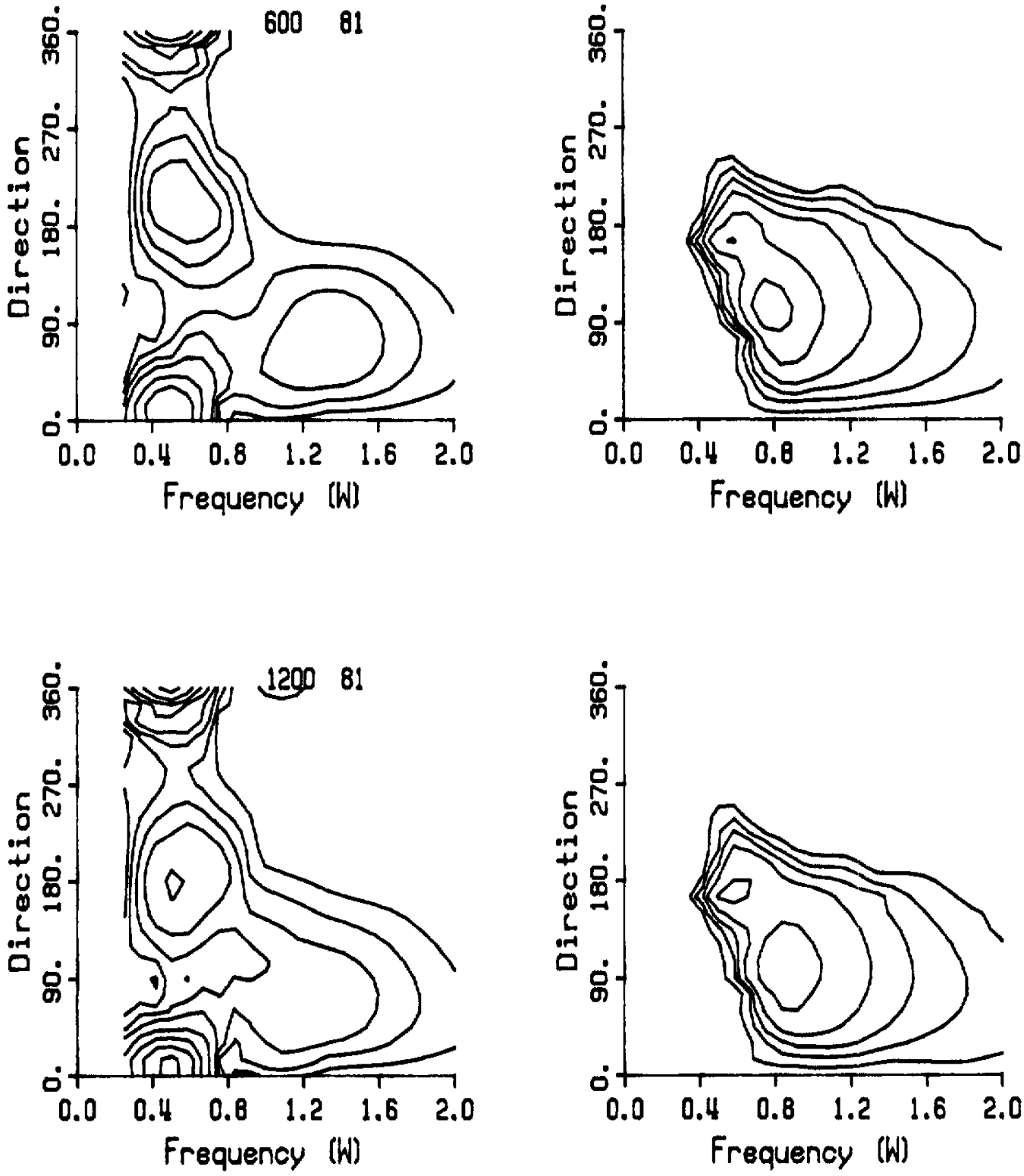

Fig. 24 As in Fig. 22

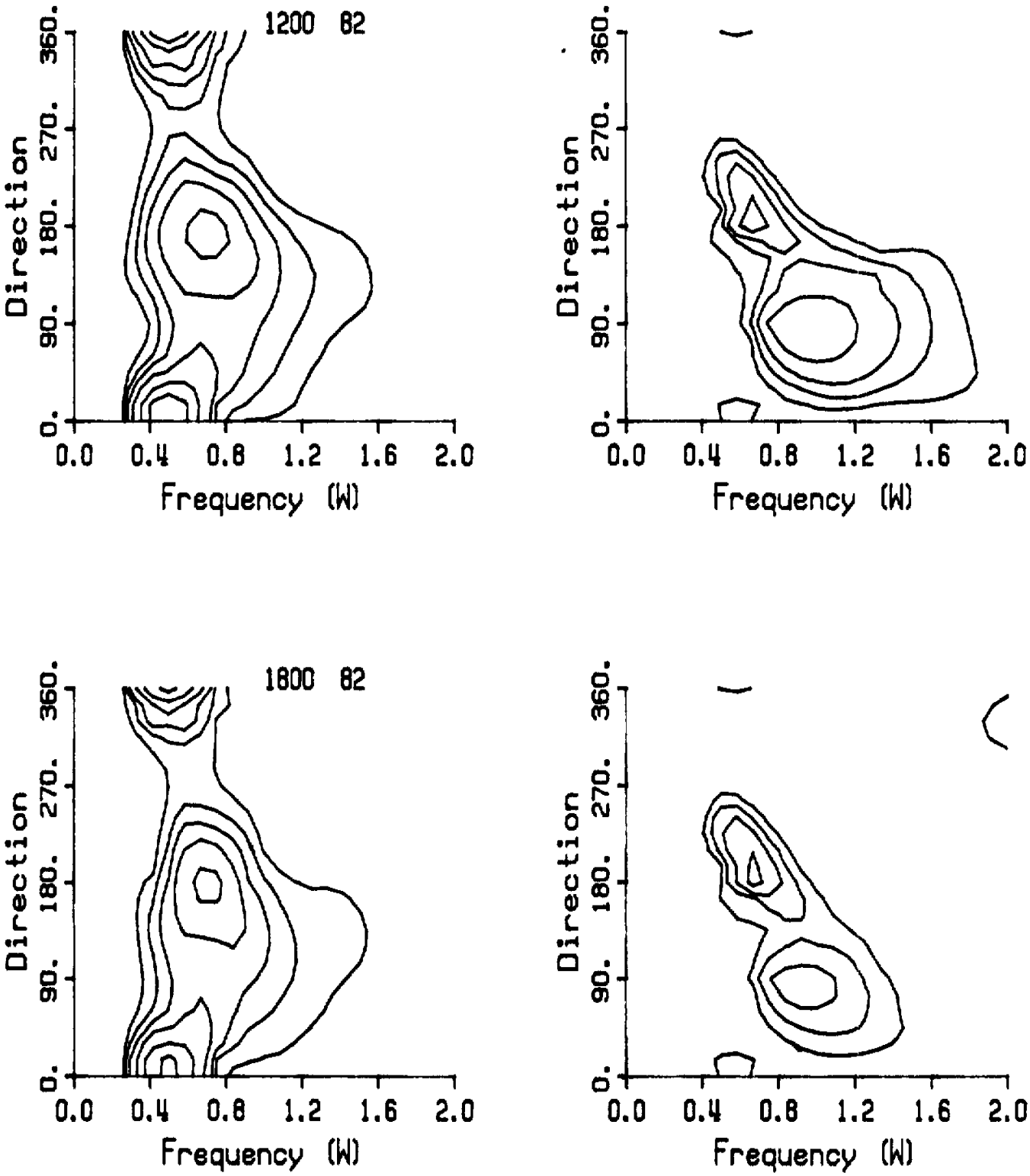

Fig. 25 As in Fig. 22

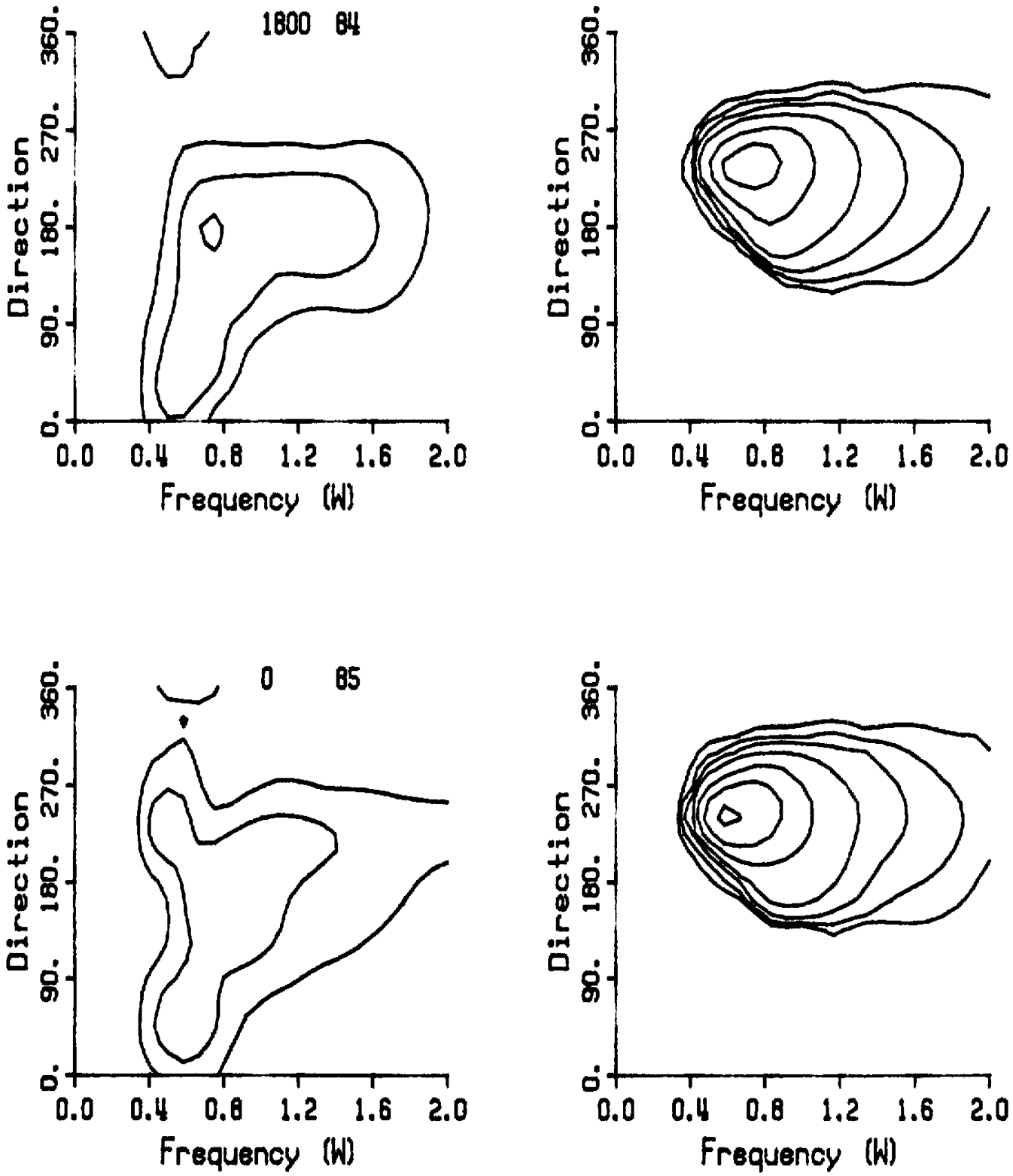

Fig. 26 As in Fig. 22

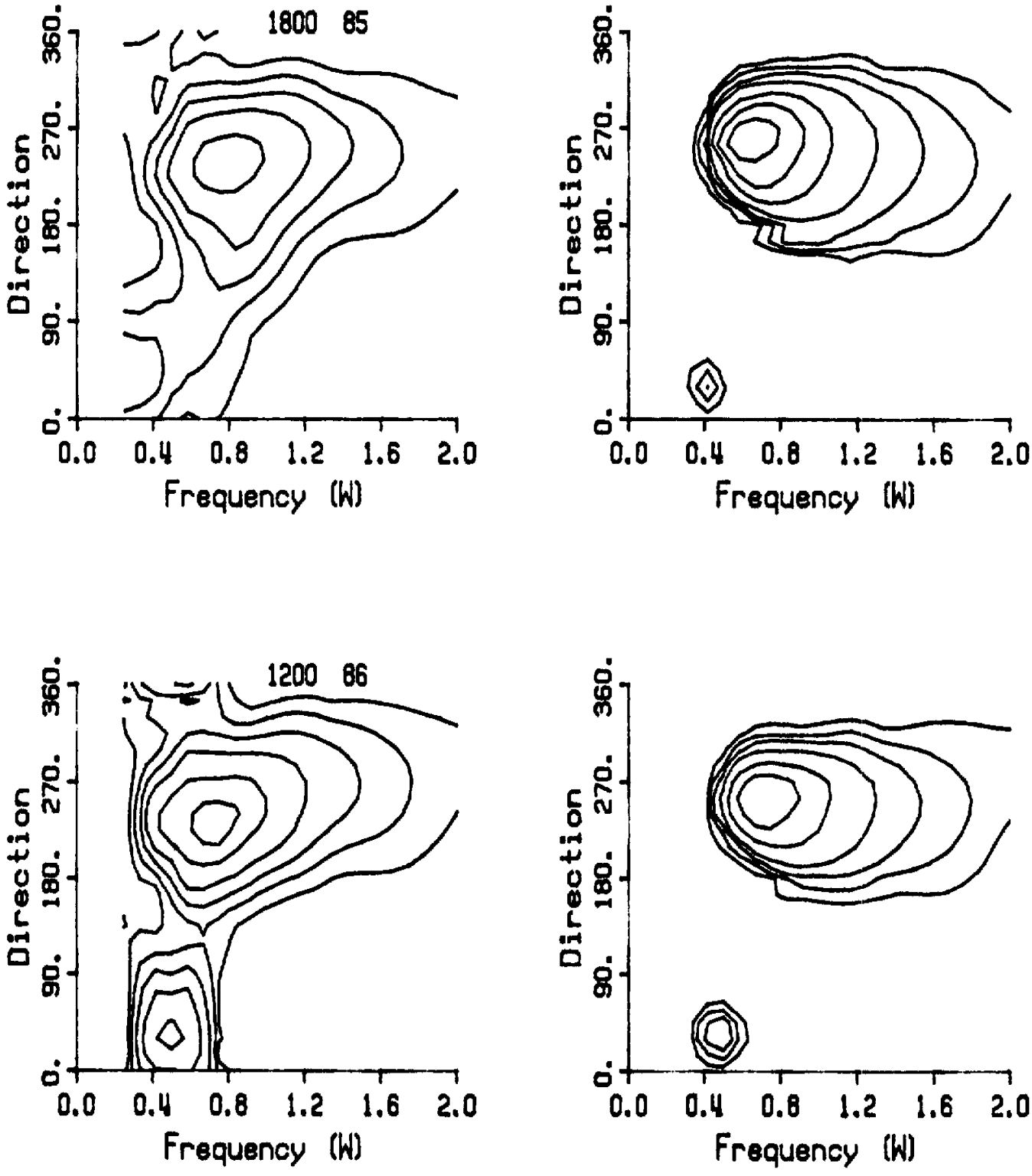

Fig. 27 As in Fig. 22

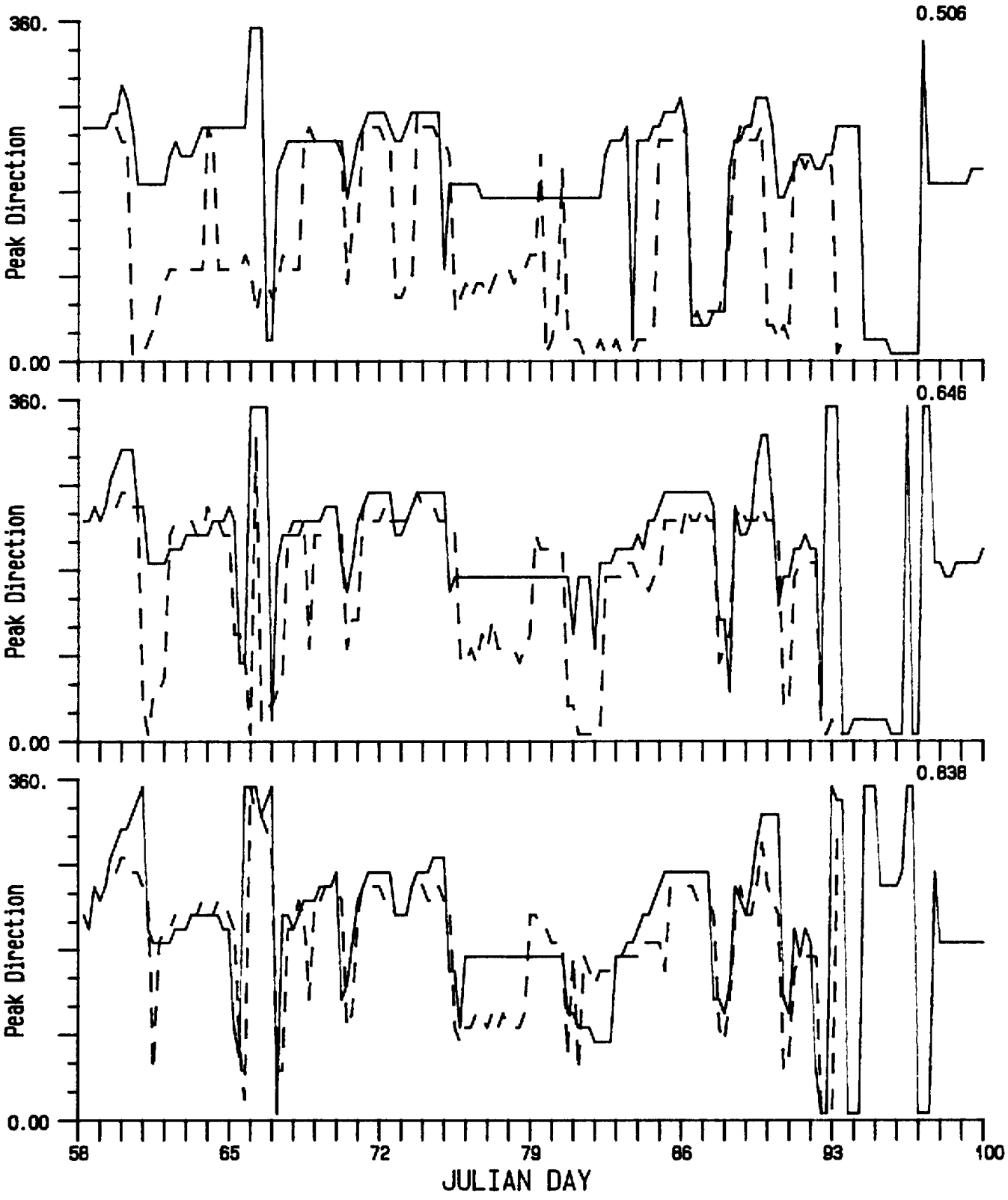

Fig. 28 Time series of PDIR at selected frequencies of the hindcast (solid) and data (dashed) spectra.

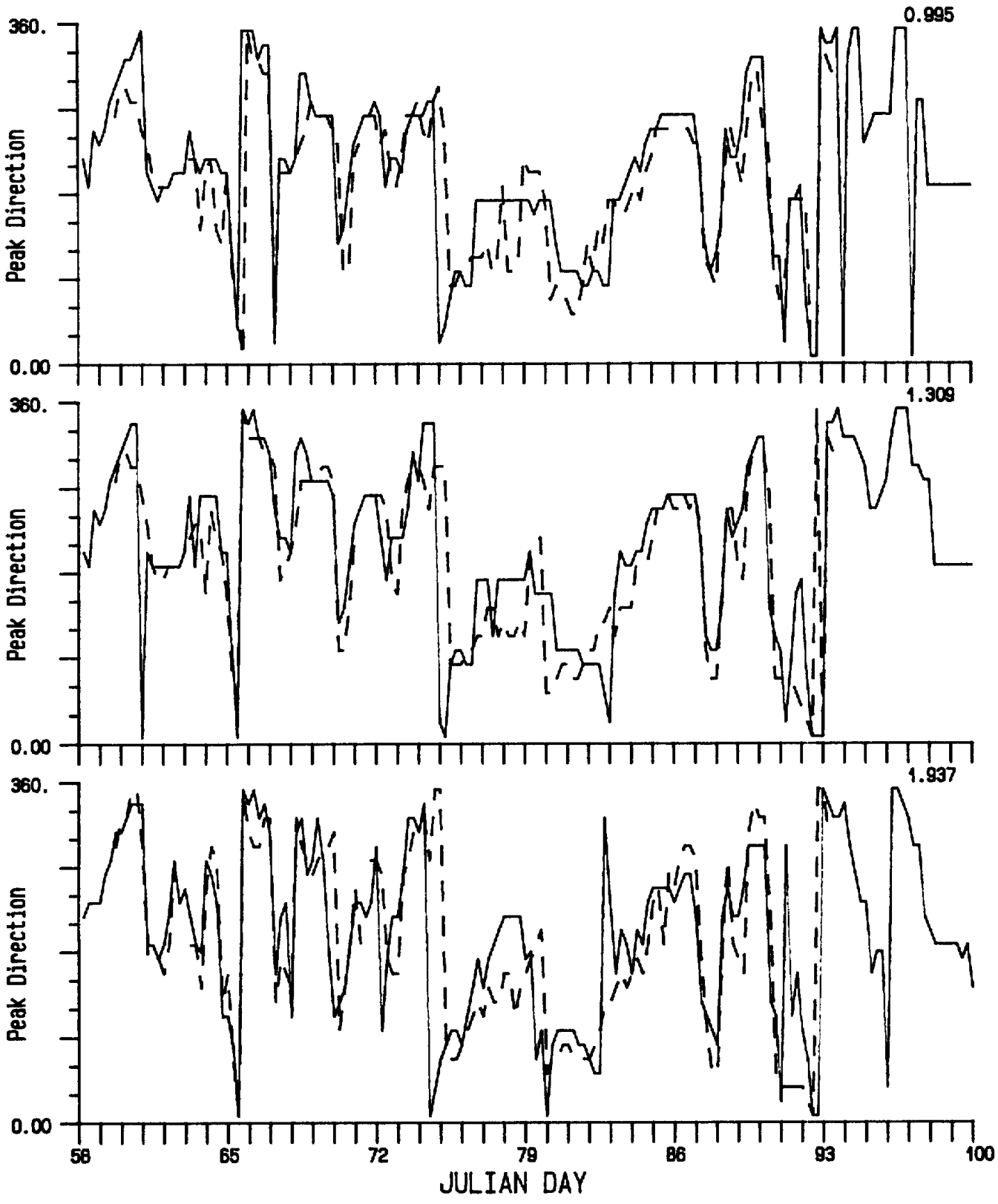

Fig. 28 (continued)

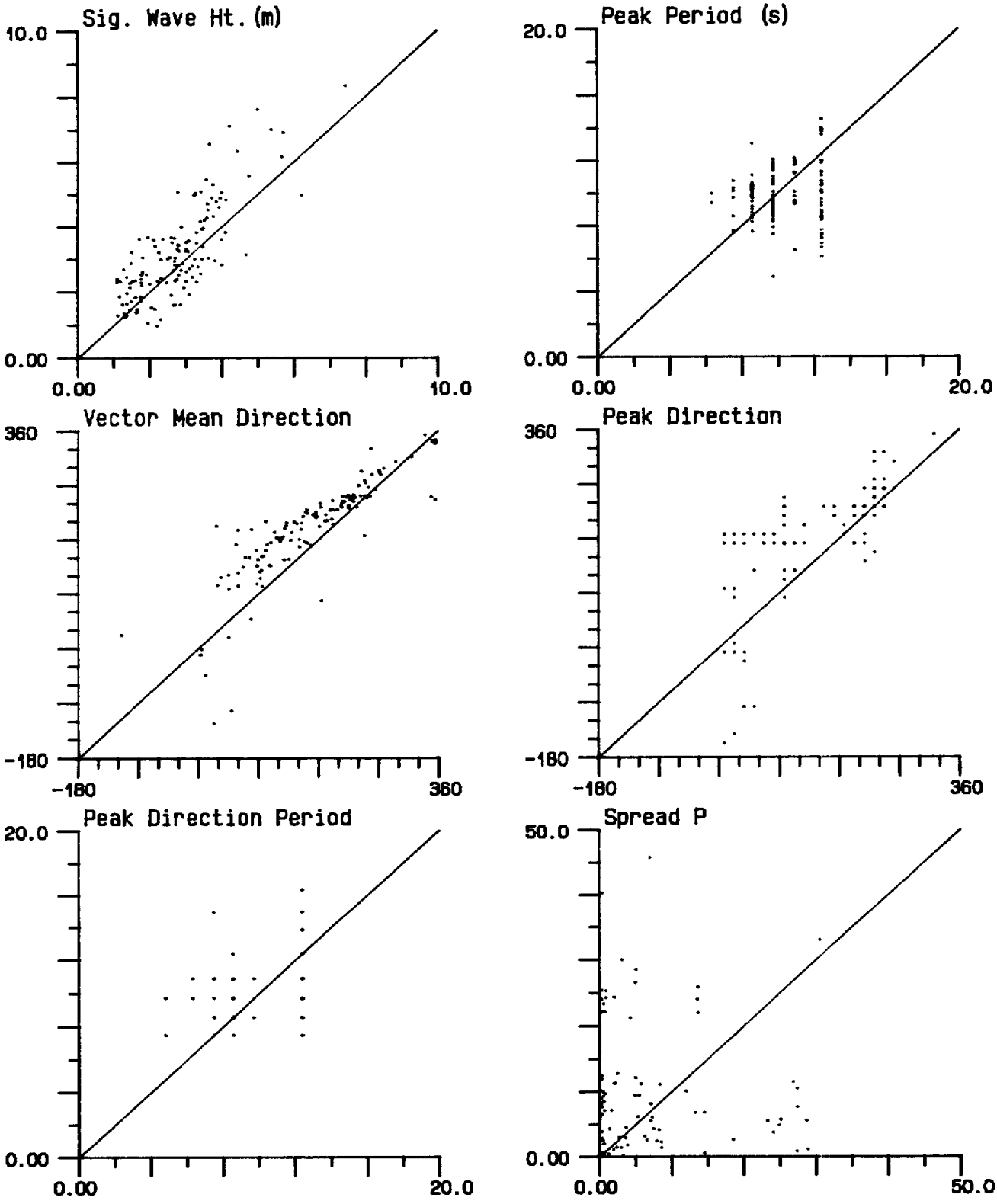

Fig. 29 Scatterplot of HSIG, TP, VMD, PDIR, TDIR and P of the hindcast (vertical axes) and data (horiz. axes) spectra.

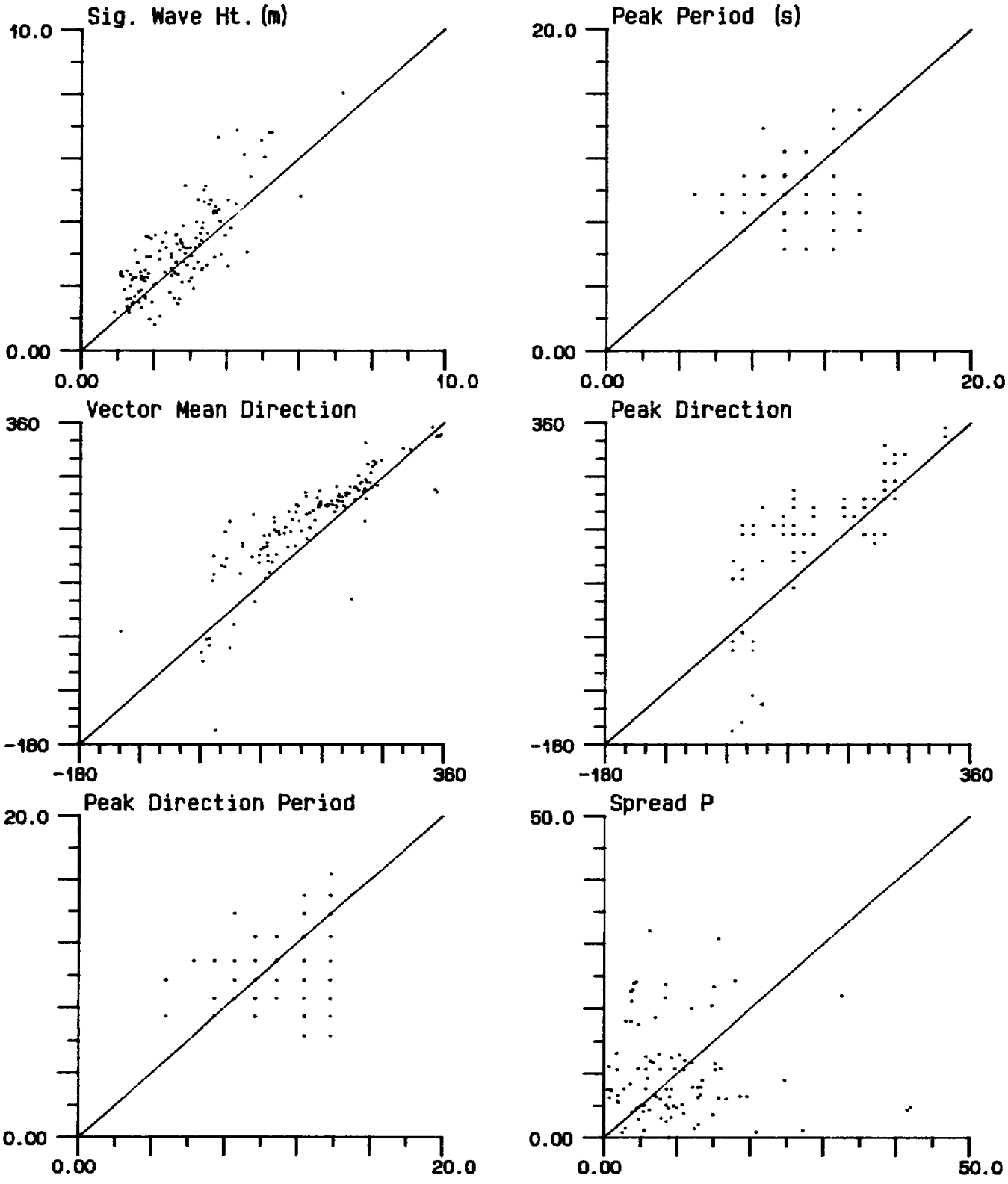

Fig. 30 As in Fig. 29 but for the corresponding 10-parameter fit spectra.

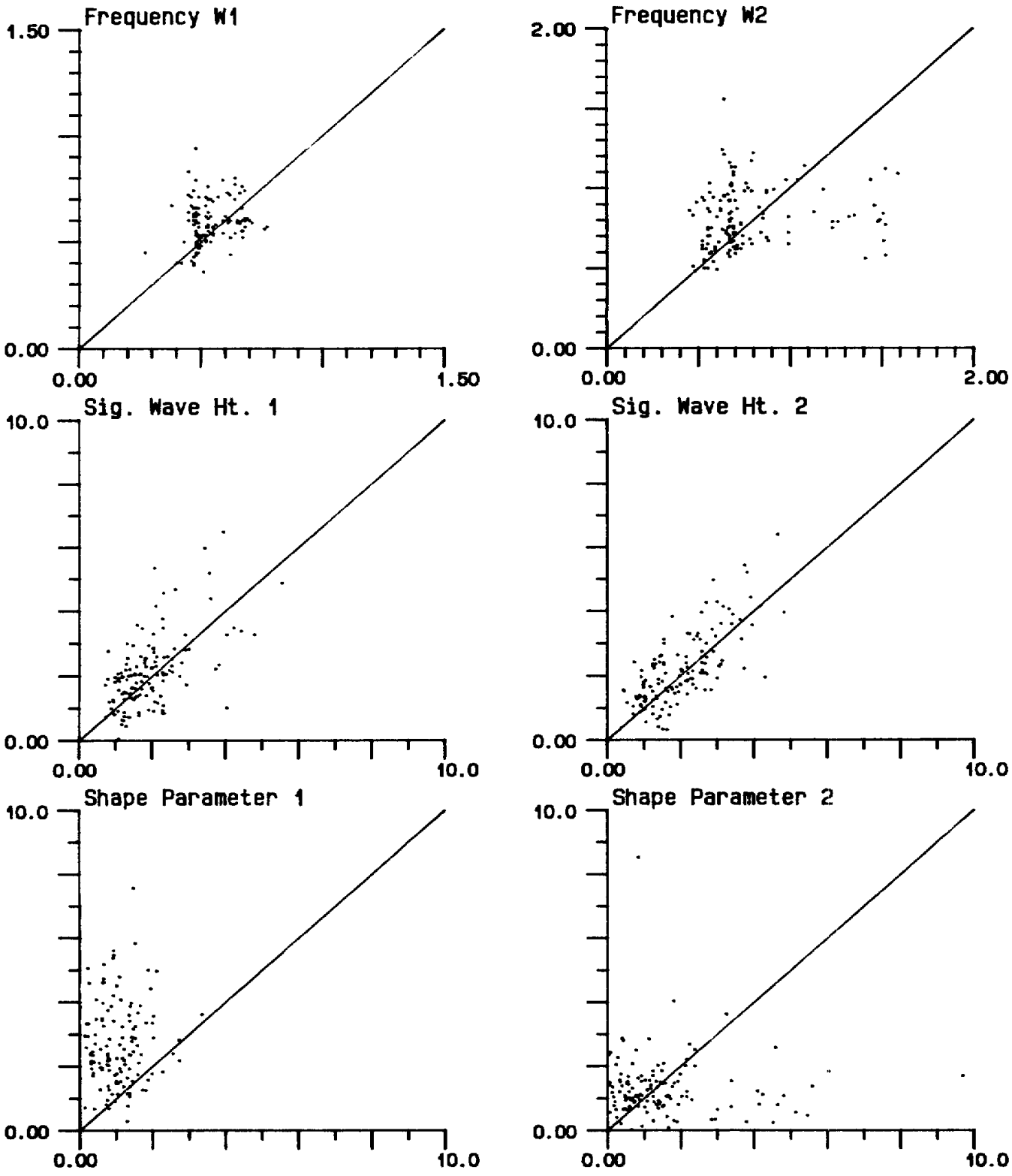

Fig. 31 Scatterplot of the directional fit parameters for the hindcast (vertical axes) and data (horiz. axes) fits.

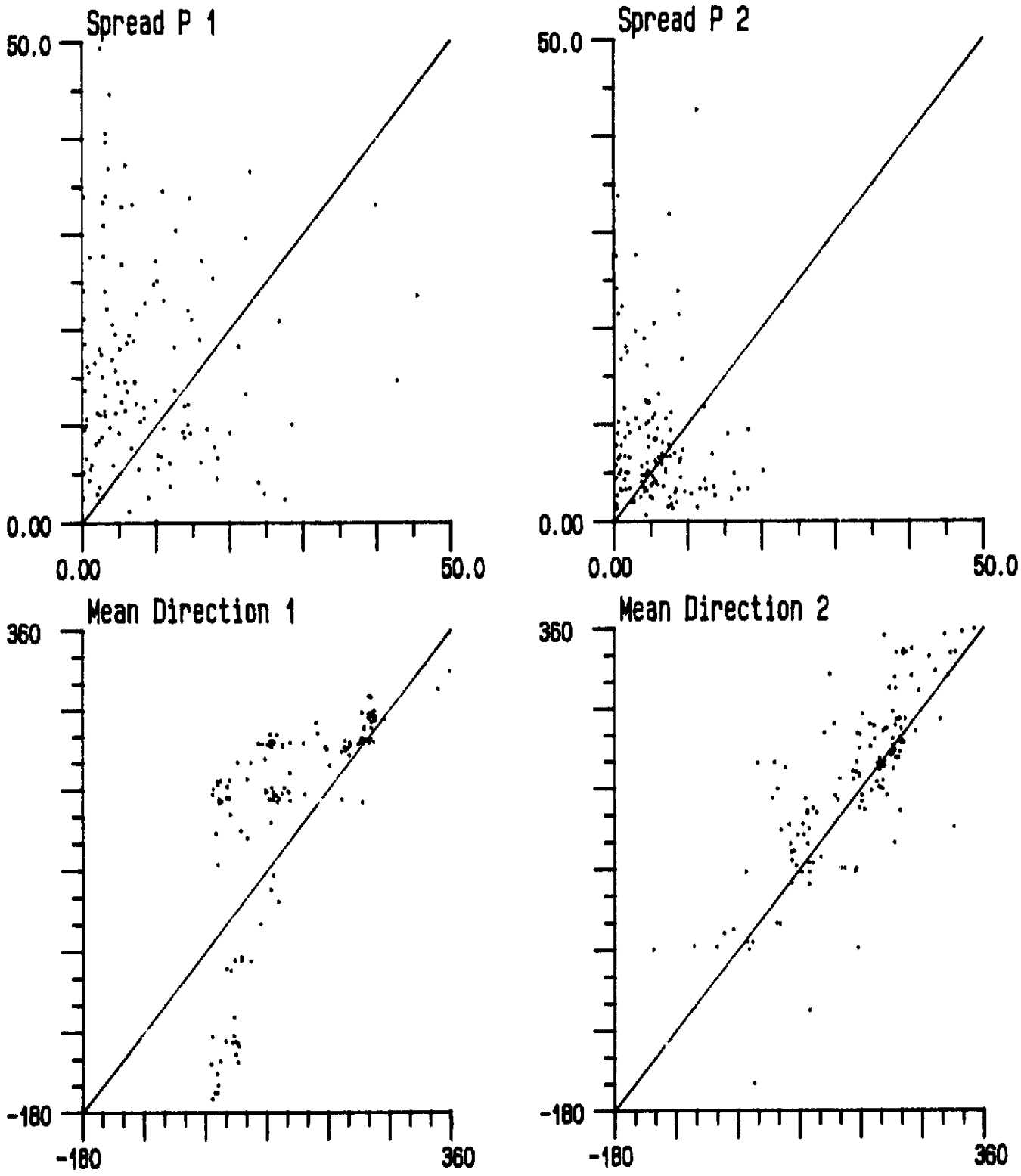

Fig. 31 (continued)

TABLE 4. Summary statistics for spectral properties of the data (W), hindcast (M) and ten-parameter fit spectra (WF and MF)

	HSIG (m)	TP (sec)	VMD (rad)	PDIR (rad)	TDIR (sec)	P
No. of	133	133	133	133	133	126
Obs. F	133	133	133	133	133	97
Mean W	2.77	10.19	2.87	3.37	10.27	6.58
WF	2.67	10.48	2.98	3.02	10.69	11.27
M	3.19	10.04	3.76	3.83	10.65	10.81
MF	3.07	10.15	3.79	3.83	10.45	10.25
ADEV W	0.87	1.41	1.22	1.40	2.09	7.99
WF	0.88	1.52	1.23	1.42	1.96	7.25
M	1.10	1.35	0.90	0.82	1.47	8.07
MF	1.05	1.50	0.91	0.81	1.54	6.23
SDEV W	1.13	1.65	1.47	1.70	2.19	13.44
WF	1.12	1.82	1.49	1.62	2.31	11.83
M	1.45	1.76	1.16	1.07	1.85	10.81
MF	1.38	1.90	1.17	1.06	1.97	9.01
SKEW W	0.95	0.05	-0.65	-0.34	-0.24	3.57
WF	0.89	-0.05	-0.38	-0.82	-0.37	2.88
M	1.10	0.25	0.34	0.32	0.65	1.69
MF	1.07	0.40	0.26	0.33	0.37	2.83
KURT W	1.67	-1.04	-0.67	-0.78	-1.41	14.75
WF	1.25	-0.29	-0.57	-1.07	-0.49	9.60
M	1.19	0.44	-0.07	0.14	0.28	3.29
MF	1.19	0.14	-0.19	0.23	0.13	14.49
ME	0.43	-0.15	0.52	0.68	0.38	4.37
F	0.40	-0.33	0.54	0.65	-0.23	-0.96
RMSE	0.98	2.21	0.96	1.34	2.34	17.83
F	0.93	2.46	0.99	1.35	2.67	15.62
% SCAT	33.00	21.85	27.78	35.81	22.38	203.36
F	32.30	23.89	28.20	36.54	25.29	144.77
CC	0.79	0.16	0.26	0.25	0.35	0.01
F	0.80	0.13	0.39	0.42	0.23	-0.08
SI.LEV	0	0.07	0.003	0.004	4.E-5	0.89
F	0	0.13	0	0	0.008	0.43
FOR HSIG > 3.0 m - 42 OBS.; (39 FOR P AND 34 FOR FIT P)						
ME	0.78	0.23	0.38	0.67	0.76	3.61
F	0.64	0.21	0.42	0.71	0.19	-1.41
RMSE	1.23	1.78	0.73	1.11	2.27	13.55
F	1.10	2.02	0.73	1.11	1.86	9.73
% SCAT	28.13	16.12	18.26	26.76	19.76	164.76
F	26.00	18.03	17.68	27.10	16.12	108.34
CC	0.70	0.50	0.71	0.76	0.45	-0.09
F	0.71	0.45	0.73	0.89	0.61	-0.12
SI.LEV	0	7.E-4	0	0	0.003	0.60
F	0	0.003	0	0	0	0.49

The period of largest discrepancy between the hindcast and data records, occurred from day 75 to day 86, Selected examples of the data (left) and hindcast (right) spectra are included in Figs. 22 to 27 . From day 75 to 79, there were low wind speeds and concurrent veering wind directions. Even though both the rig and model winds agree well, there was consistently more energy observed in the hindcast spectra which contained a very strong southerly swell signature not observed in the data from day 75 to 77 (eg. see Fig. 22). On days 78 to 80, bimodal swell in the data were not predicted by the model (Fig. 23). The minor peaks in HSIG on days 81–82 and 85 were offset while the model provided a broad featured rise on day 85. The characteristics of the data and hindcast directional spectra were quite different on days 81 and 82 (eg. Figs. 24 and 25) due to differences in both the time of sea development and the presence of swell. The initial conditions prior to the energy rise on day 85 were also quite different (Fig. 26) with the data showing a ”flat” energy distribution. The 0.6 rps southwest peak in the model persisted through this period while the field spectra ”caught up” to the model soon after the wind directions stabilized (late day 85 –86; Fig. 27). This feature also supports the observation that the hindcast model either developed too quickly or did not contain a large enough dissipation due to waves interacting under veering winds.

The progression of the directional signature down frequency and the response to veering winds, can be observed in Figure 28 . As one examines these time series, it becomes apparent that the agreement between the directions deteriorates at low frequencies. It is only during the two storms, that the direction tracking agrees at 0,503 rps (.08 Hz) as wind forced seas are occurring down to this frequency. At a mid frequency of .82 – 1.0 rps, the hindcast model directions tend to lead the field observations when veering occurs implying, again, that the models response was too rapid.

The behavior of selected spectral properties can be visualized by means of a scatterplot, as shown in Figs. 29 and 30 (for the 10–parameter fits). The 1:1 correspondence line is shown with the hindcast estimate associated with the vertical axes and the data estimate with the horizontal axes. There is considerable scatter in all the estimates though a significant correlation would be expected in HSIG, VMD, PDIR and TDIR. The directions coming from the SE through SW indicate that the hindcast values are shifted clockwise from the data while there is better agreement in directions from W through NE. This may reflect a time offset, the more rapid development of the hindcast model, or factors affecting only the field data such as refraction effects due to long period waves moving onto the bank from the southern half of the compass or, possibly, current–wave

interaction (ie. strong inertial currents which lag the winds). The larger P values in Fig. 30 , associated with the data fits, reflects either a choice being made by the 10–parameter model to fit one peak in a bimodal distribution or its lack of any noise component thereby allowing for the spread scanning procedure to resolve a better P estimate.

Similar scatterplots of the fit parameters can be seen in Fig. 31 . The scatter associated with $\delta 1$, $\delta 2$, and $\Theta m2$ indicate that these parameters should be significantly correlated. There was less agreement in $\Theta m1$ and no obvious agreement in the other parameters. The scatter would limit prediction of one set of parameters from the other which is also dependent, in cases of multiple peaks, on whether the same peaks are present in the two input spectra and were fit.

4.4.2 Quantitative Assessment

The behavior of the spectral properties can be examined quantitatively using summary and comparison statistics. These are listed in Table 4 (related to scatterplots of Figure 29) with the spectral properties calculated on both the model and data spectra and their corresponding ten–parameter fit spectra, fully expanded onto the model frequency–direction array. The statistics for the input spectra and their parameterized forms are almost identical. A positive ME (mean error) in a direction statistic indicates that the hindcast direction is shifted clockwise from the data. Correlations between HSIG, VMD, PDIR and TDIR are significant. Given any auto–correlation within the time series, neither the peak periods nor the scanned P values associated with the peak direction are correlated. Also shown in Table 4 are the correlations associated with records when HSIG > 3.0m. In these cases, all but the P values are significantly correlated with much better agreement in the direction statistics as expected when forced seas dominate.

A similar analysis can be performed on the fit parameters themselves, and not the spectral properties as in Table 4 , and the summary statistics axe given in Table 5 (relate to scatterplots of Fig. 31). The results generally agree with the qualitative observations of Section 4.4.1 . The modal frequencies, $\omega m1$ and $\omega m2$, show little bias between the data sets (as indicated by the ME), $\delta 1$ and $\delta 2$ of the hindcast fit are larger than for the data (ie. overestimating the spectral energy), and $\lambda 1$ and $\lambda 2$ and P1 and P2 uncorrelated (though larger than in the data) and $\Theta m1$ and $\Theta m2$ significantly correlated, with $\Theta m2$ showing better agreement due to less swell contribution to this statistic. The WAVEC directions are on average rotated counter–clockwise from the hindcast directions. The direction statistics are difficult to interpret in a bulk manner as

they are sensitive to whether or not a given peak was fit. Included in the table, are the statistics for cases when Θm1 and Θm2 of the two fits agree within 45 degrees and when the comparison is performed on the data fits calculated in Part 1 of this study. By limiting the directions, the frequency parameters show improved correlations, particularly for the ”sea” peak. The poorer agreement in the ”sea” parameters for the fit to the original, non–interpolated spectra, was expected given the discussion in Section 4.3 . The higher P values again may be indicating that the interpolation procedure, or the direction and frequency grid resolution, may be smoothing the spectra.

The percent of the variance that would be explained by means of a linear regression between the two sets of fit parameters (ie. hindcast and data), in order to predict one set from the other, is approximately equal to 100.(correlation coefficient**2). Given the CC values in Table 5 , only a regression between the sea significant wave heights, δ2, could account for slightly more than 50% of the variance. The predictive equation

Y = 0.643 + 0.6196*X

where X is the hindcast δ2 value and Y the expected data value, would account for 51.6% of the variance in Y (with the standard error on the intercept and slope of 0.128 and .0524, respectively).

The residual statistic, RESD, can be used to compare the hindcast and data spectra on a frequency–direction, point–by–point basis. The time series of these RESD values are shown in Fig. 32 with the solid line representing division by the hindcast energy and the dotted division by the WAVEC energy. The large errors in the latter are due to the generally lower energy values at the peaks due to the broader directional distributions. The poor point–by–point agreement is easily discerned by examining the histogram of RESD values (Fig. 33).

A coherence analysis, similar to that performed on the wind vectors, was performed on the average spectral energy vectors given by HSIG.COS(VMD) and HSIG.SIN(VMD), between the hindcast and data spectra. Like the winds, the analysis would supply an upper frequency limit of agreement between the two data sets. The results are shown in Fig. 34 . There were 16 degrees of freedom and a frequency resolution of 0.25 cpd associated with the analysis. A positive phase would represent the hindcast spectra leading the data. The approximate cut–off time scale, for 50% coherence, was similar to the input winds at 0.75 cpd (ie. 1.25 to 1.5 days) and showed a corresponding peak in the clockwise component.

TABLE 5. Summary statistics for the ten fit parameters obtained from the non-linear fit to the hindcast model (M) and WAVEC data (W) spectra.
133 Observations.

		ω_{m1} (rps)	δ_1 (m)	λ_1	P1	θ_{m1} (rad)	ω_{m2} (rps)	δ_2 (m)	λ_2	P2	θ_{m2} (rad)
MEAN	M	0.59	2.12	2.80	20.07	3.87	0.81	2.19	1.43	8.26	3.64
	W	0.54	1.93	1.05	9.58	1.62	0.77	2.00	1.69	6.22	3.40
ADEV	M	0.08	0.81	1.14	12.63	0.72	0.15	0.85	0.73	4.97	1.16
	W	0.07	0.65	0.47	7.16	1.23	0.20	0.79	1.21	4.10	1.13
SDEV	M	0.10	1.12	1.70	19.05	0.95	0.19	1.11	1.72	7.13	1.47
	W	0.09	0.88	0.60	10.26	1.54	0.28	0.95	1.97	8.78	1.41
SKEW	M	0.37	1.26	3.36	2.42	0.04	0.71	1.01	7.23	2.09	0.39
	W	0.41	1.44	0.88	2.31	1.12	1.58	0.66	3.16	7.48	-0.32
KURT	M	0.53	2.28	21.39	6.56	1.16	0.66	1.16	63.57	5.06	-0.61
	W	-0.21	2.40	1.15	6.70	-0.83	1.50	-0.14	12.60	70.92	-0.48
ME		0.05	0.19	1.75	10.49	0.55	0.04	0.19	-0.26	2.04	0.31
RMSE		0.13	0.97	2.50	24.26	1.70	0.31	0.81	2.67	11.75	1.10
% SCAT		22.2	47.8	129.7	163.6	48.1	39.5	38.5	170.5	162.3	31.2
CC		0.22	0.57	0.01	-0.04	0.20	0.15	0.72	-0.04	-0.06	0.57
SI.LEV		0.01	0	0.89	0.69	0.02	0.09	0	0.66	0.52	0
FOR DIRECTION DIFFERENCES < 45 DEGREES											
29 OBSERVATIONS											
ME		0.03	0.03	1.85	7.32	0.11	0.003	0.38	-0.13	2.99	0.07
RMSE		0.11	1.24	2.44	16.21	0.46	0.17	0.89	1.65	9.19	0.73
% SCAT		19.1	48.9	125.8	110.5	11.4	22.3	34.3	107.5	144.1	16.9
CC		0.48	0.53	-0.05	0.16	0.12	0.77	0.81	-0.09	0.15	0.89
SI.LEV		0.01	0.003	0.80	0.41	0.55	0	0	0.63	0.45	0
FOR NON-INTERPOLATED DATA SPECTRA											
133 OBSERVATIONS											
ME		0.02	0.27	0.17	-10.96	0.57	-0.01	0.39	-0.62	-1.63	0.25
RMSE		0.13	1.02	3.42	36.43	1.54	0.33	1.39	3.18	14.06	1.13
% SCAT		22.6	51.5	125.7	142.6	41.0	40.1	69.7	182.4	154.8	32.2
CC		0.19	0.56	-0.03	-0.03	0.41	0.13	0.41	-0.10	-0.03	0.48
SI. LEV		0.04	0	0.71	0.74	0	0.12	0	0.24	0.71	0

As different frequency ranges in a wave spectrum can be considered to reflect different generation processes, the hindcast model may be reproducing certain frequency bands more accurately than others. The frequency dependent behavior of the hindcast spectra was assessed by performing the coherence analysis on spectral energy vectors again given by HSIG*COS(VMD) and HSIG*SIN(VMD) where HSIG and VMD were calculated over selected frequency bands as opposed to the entire spectrum. Three regions were chosen: bands 1 to 8 (0.25 to 0.5 rps) to represent swell, bands 9 to 12 (.58 to .84 rps) associated with storm sea peaks primarily influenced by non-linear interaction transferring energy from higher frequencies and bands 13 to 15 (1.0 to

2.0 rps) being the region of directly wind forced seas. The results are shown in Fig. 35a for the clockwise rotating component and 35b for the counter–clockwise component. The ”swell” bands were incoherent. The high frequency bands 13–15 showed the best coherence with the clockwise component being significant to time scales as short as 1.0 day. The increased coherence at shorter time scales may be reflecting periods of no energy in the selected bands. The peak in the mid–frequencies, was the main contributing factor to the similar peak present in Fig. 34 and corresponded to the clockwise peak in the wind analysis of Fig. 12 . The phases are generally positive (ie. hindcast leading the data) though somewhat confused in the clockwise component.

5. DISCUSSION

A 10–parameter model was fitted, by means of a non–linear, least–squares iterative technique, to directional wave spectra produced by the ODGP wave hindcast model. Approximately 93% of the fits contained residual errors of less than 20% with close to 70% of the records having errors less than 10%. This agreement was better than for the equivalent fits to field measured spectra (89.5% and 39%, respectively). The improvement may be a result of the sharper directional peaks in the hindcast spectra which could provide a better target signal and the absence of isotropic noise which reduces the error contributions from background energy away from the peak. The fitting procedure was generally able to select the two major directional peaks of the record. The fit was less successful when there existed multiple swell and sea peaks of approximately equal energy, travelling in different directions. The hindcast spectra, unlike either the processed data or the parametric model, may contain more than two directional peaks per frequency band, in which case the parametric model (with a maximum of two direction peaks per record) is inappropriate.

The hindcast spectra were compared to field measured directional wave spectra. The most obvious features, when comparing the two sets of contoured directional energy spectra, was the difference in the directional widths of the peaks and the absence of isotropic noise in the hindcast spectra. From the current state of knowledge, it is not clear whether the sharp model peak or the broader data peak are the most representative of actual conditions. However, from simulations (see Marsden and Juszko, 1987), the data processing method accurately reproduces test uni–modal peaks, including various levels of isotropic noise. When the test signal is bimodal, it consistently provides too broad a distribution. The true distribution probably lies somewhere in between the observed hindcast and data directional spectra. The hindcast spectra did model the overall energy and direction

properties, as indicated by correlations levels between the significant wave heights and vector mean directions. It provided a poor representation, however, of the swell regime (approximately the first eight frequency bands) even with the higher frequency resolution in this region.

A coherence analysis was performed between the model input winds and directly measured MANMAR winds, and between the overall spectral directional energy vectors of the hindcast and WAVEC spectra. The results indicated that the coherence–squared value falls below 0.5 at approximately 0.75 cpd (ie. approx, 30 hrs.). The man–machine mix of wind information, used to provide the hindcast model input winds, shows an improvement over pure geostrophic wind estimates (cutoff at approx. 0.5 cpd). The implications are that geophysical features, having time scales of less than 30 hours, would not be modelled in a statistically confident manner. Given the six–hourly sampling rate, features with time scales of less than 12 hours would be aliased. Therefore, one must be careful when interpreting specific model behavior. For example, the model may be reproducing a storm signature though not the detailed spectral behavior during build–up. This is also true when interpreting bulk statistics (eg. mean error, correlation coefficient, etc.) which do not have any time scale associated with them. When the coherence analysis was performed on selected frequency bands, the results showed that the directional energy for bands 1 to 8 (.25 to .5 rps – ”swell”) were incoherent and the coherence improved at the higher frequencies. As hindcast models axe tuned to the wind input, it is not surprising that the directly forced ”seas” showed better agreement. The analysis indicated that the hindcast model did not accurately reproduce wave spectral features for frequencies less than 0.5 rps and applications requiring proper representation of these frequencies should not use the hindcast spectra as input.

The results are based on a data set with limited temporal and spatial coverage and may not reflect the hindcast model behavior in different areas or over longer averaging periods. The study period contained two storms of different character, numerous wind veering episodes and a swell dominated, low energy period of over a week duration. This should provide a good preliminary test of both the 10–parameter fit and the hindcast model itself. One would not expect that the behavior of the 10–parameter fit be much different if examined over a long time series. A proper assessment of the hindcast model would require concurrent field measured directional wave spectra for a few years at more than one location as both the model and wind input accuracy must be addressed and the spatial coverage of the latter is variable. Given the practice of modelling only selected storms for extreme analysis, one would have to be careful in interpreting the modelled extremes as these can occur on short time

scales. Improved wind input estimates would most likely result in an improved coherence for the observed ”seas”. Improved winds may not necessarily improve the ”swell” modelling and the use of hindcast spectra in applications where swell is an important contributor may be limited.

6. REFERENCES

de Young B. and C.L. Tang, 1989. An analysis of fleet numerical oceanographic winds on the Grand Banks. Atmos. Ocean, 27, 414–427.

Gonella J., 1972. A rotary–component method fox analysing meteorological and oceanographic vector time series. Deep Sea Res., 19, 833–846.

Juszko B.–A., 1989, High resolution of the directional wave field on the Grand Banks. Contractor Report SSC File No. 52SS–FPB02–7–2719. Unpub, Manuscript.

Juszko B.–A., 1989. Parameterization of directional spectra – Part 1. Contractor Report CR/89/414 prepared for the Dept. of National Defense. 141 pages.

MacLaren Plansearch Ltd. Development and evaluation of a wave climate data base for the East Coast of Canada. Draft Report dated March 1988, prepared for the Marine Environmental Data Service, Dept. of Fisheries and Oceans.

Marsden R.F., 1987. A comparison between geostrophic and directly measured surface winds over the northeast Pacific Ocean. Atmos. Ocean, 25, 387–401.

Marsden R.F. and B.–A. Juszko, 1987. An eigenvector method for the calculation of directional spectra from heave, pitch and roll buoy data. J. Phys. Ocean. 17: 2157–2167.

Marsden R.F. and B.–A. Juszko, 1989. Wind estimates from wave slopes. J. Geophys. Res., 94, 6266–6272.

Ochi M.K. and E.N. Hubble, 1976. Six–parameter wave spectra. In: Proceedings of the 15th Coastal Engineering Conference, Honolulu, Hawaii. P 301–328.

Young T.L. and M.L. Van Woert, 1989. PLOT88 Software Library Reference Manual, Third Edition. Plotworks Inc. Ramona, Calif. 342 pp.

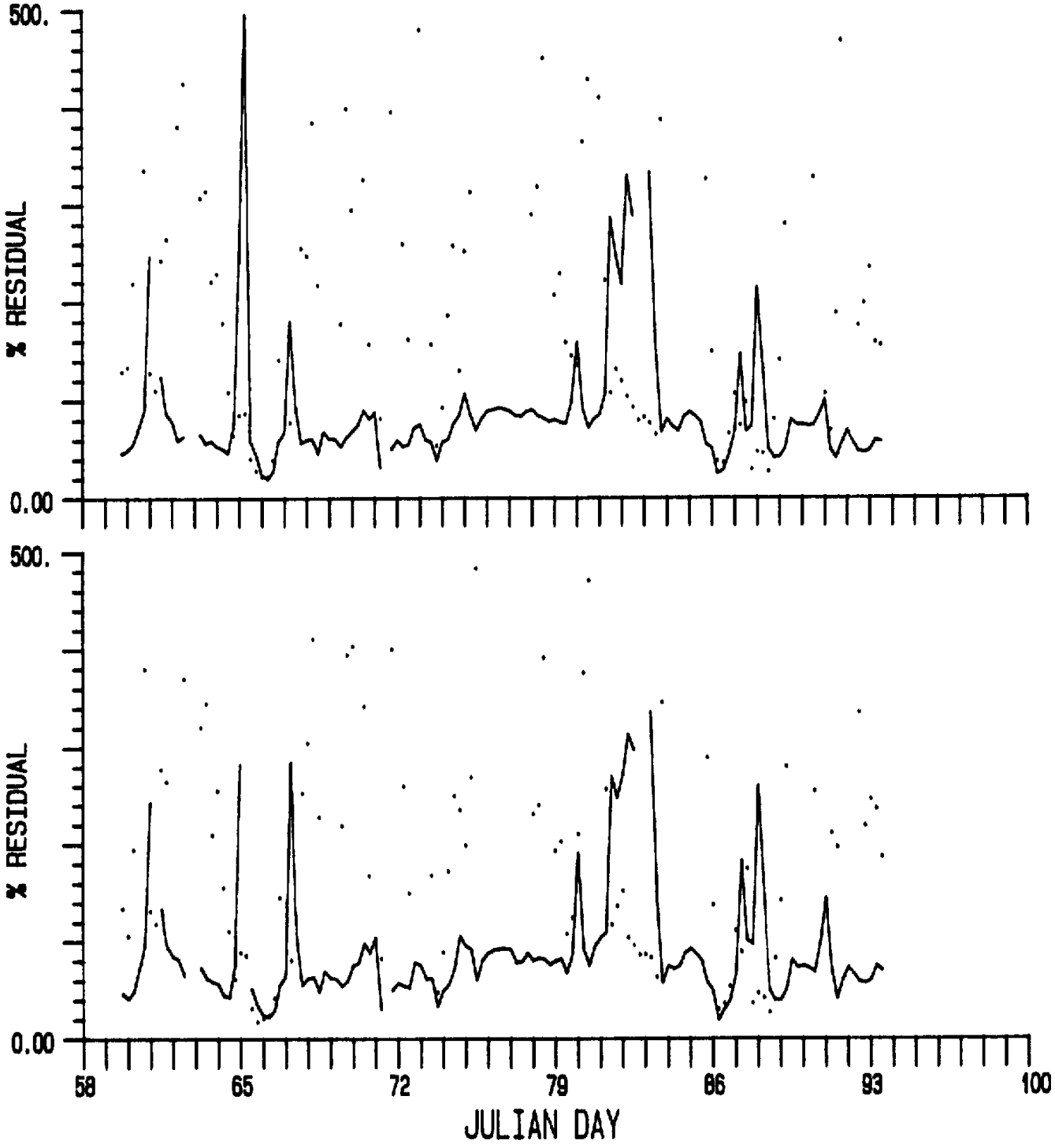

Fig. 32 Time series of RESD values calculated between the hindcast and data spectra (upper) and their corresponding fits (lower). Solid: weighted by hindcast energy; Dotted: weighted by data energy.

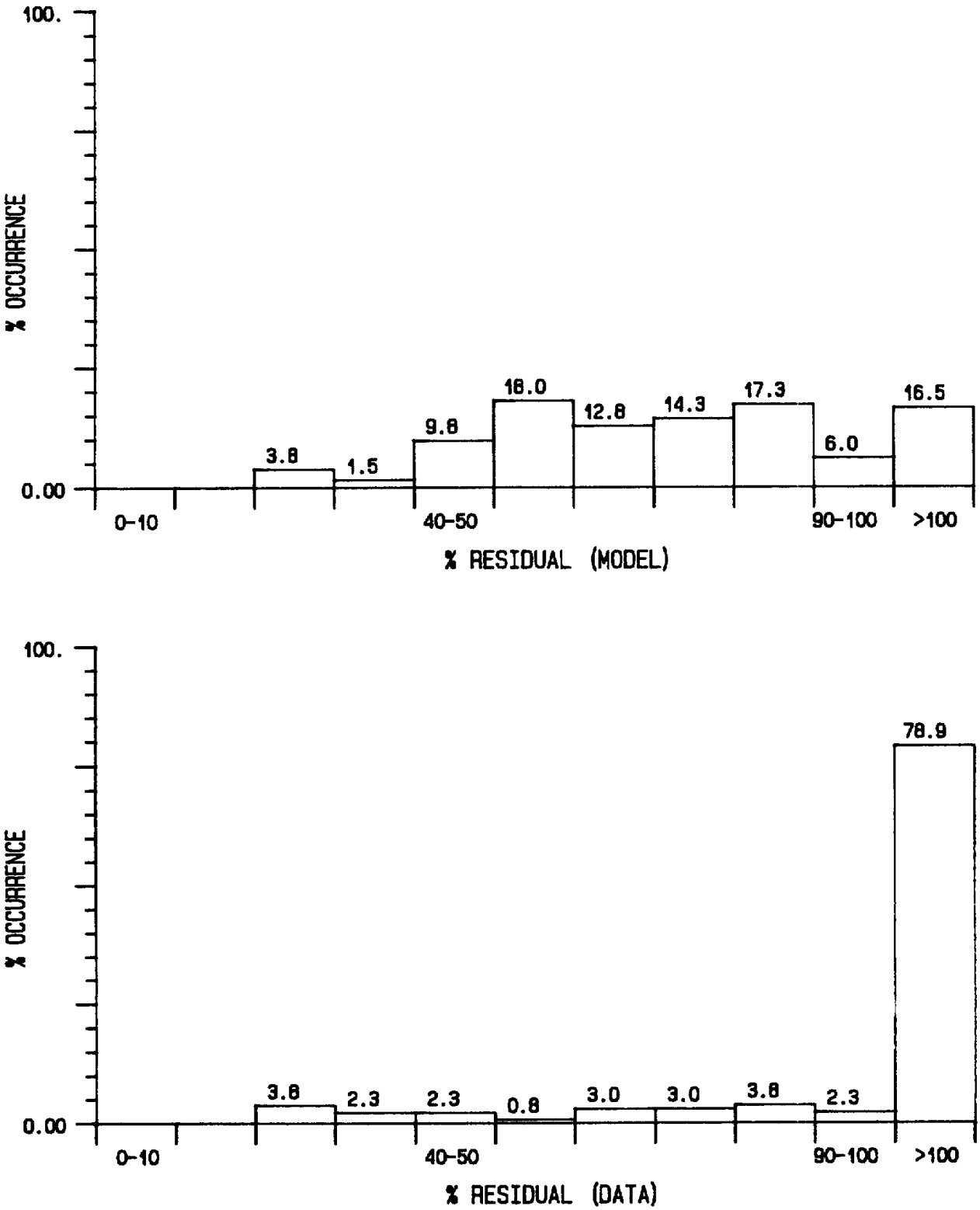

Fig. 33 Percent occurrence of RESD values calculated between the hindcast and data spectra. Upper: weighted by hindcast; Lower: by the data energy.

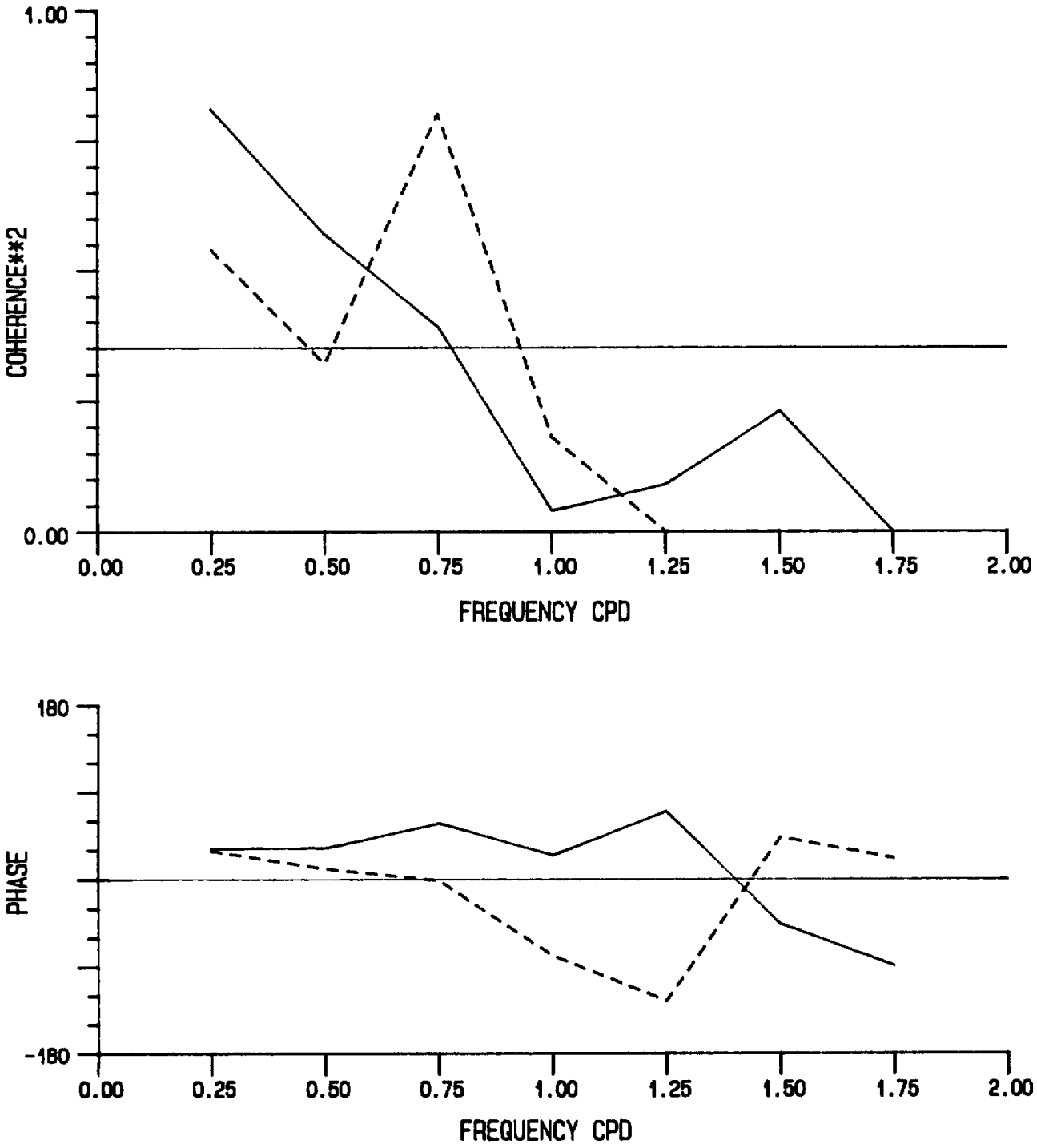

Fig. 34 Inner coherence squared and phase of spectral directional energy vectors of the hindcast and data spectra. Solid: Counter-clockwise; Dashed: Clockwise vectors. Horizontal lines are the 95% confidence limit on the coherence**2 and the zero phase line.

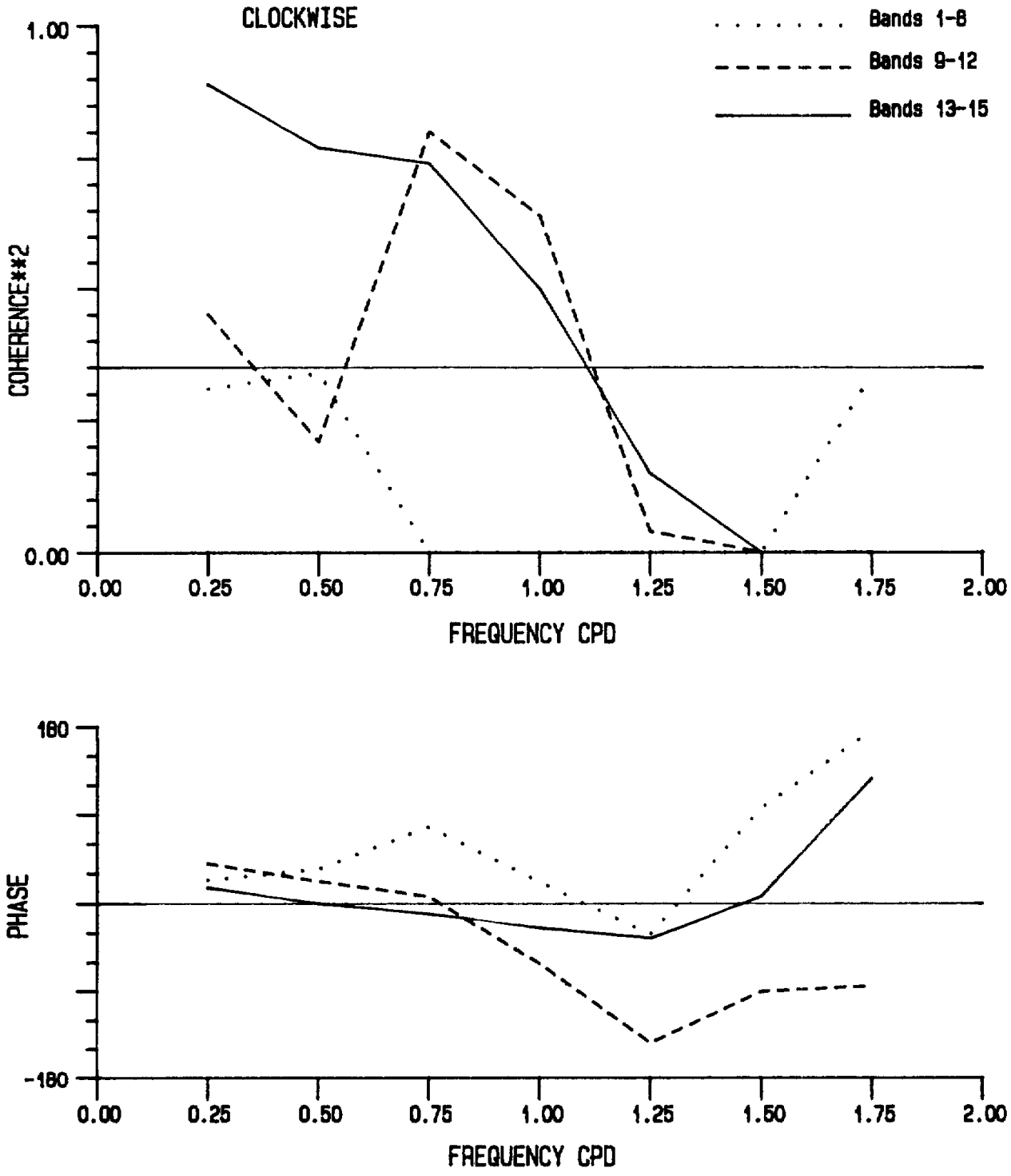

Fig. 35a Inner coherence squared and phase of spectral directional energy vectors associated with selected frequency bands. Horizontal lines are the 95% confidence limit on the coherence**2 and the zero phase line. Clockwise component.

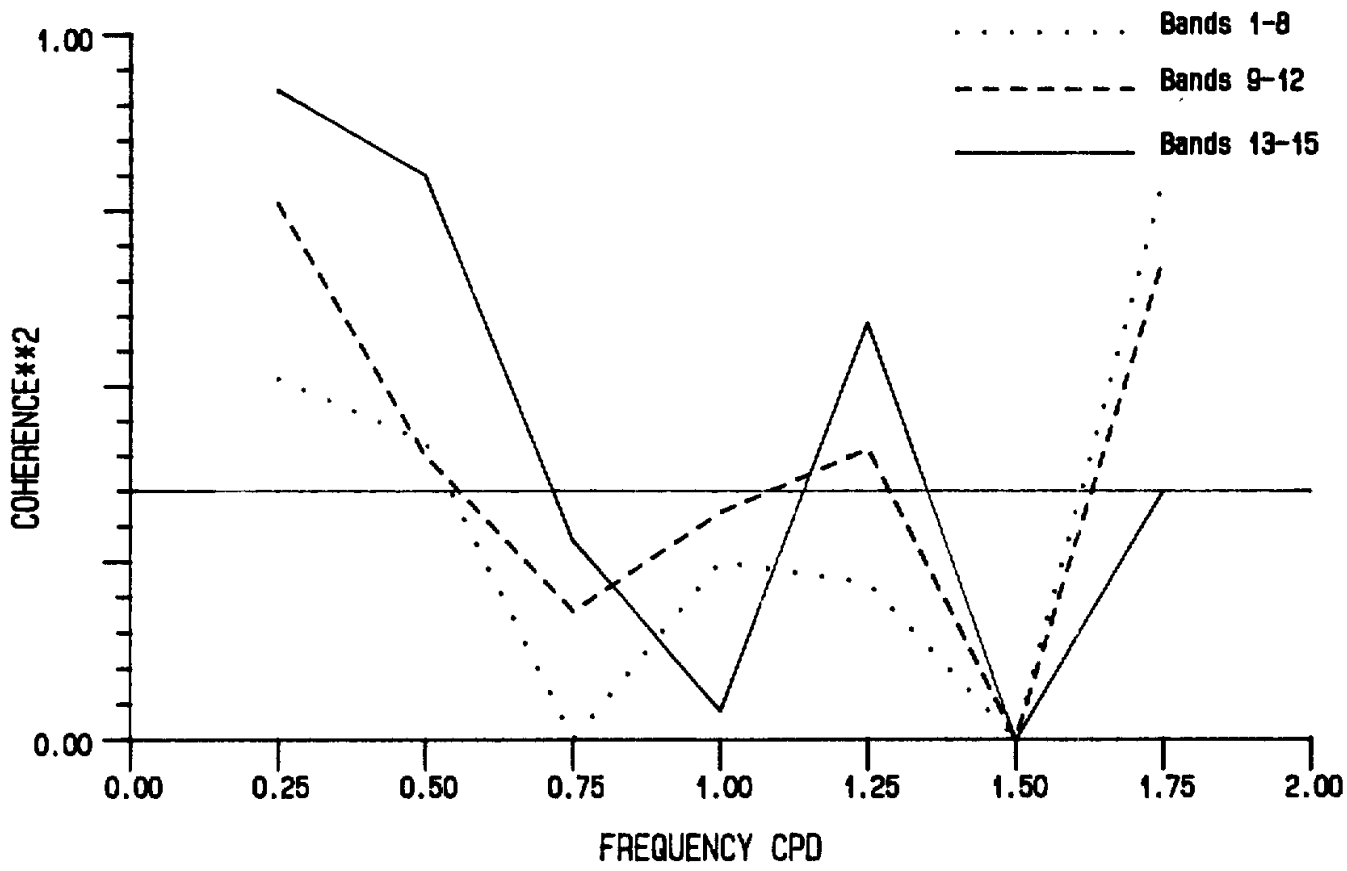

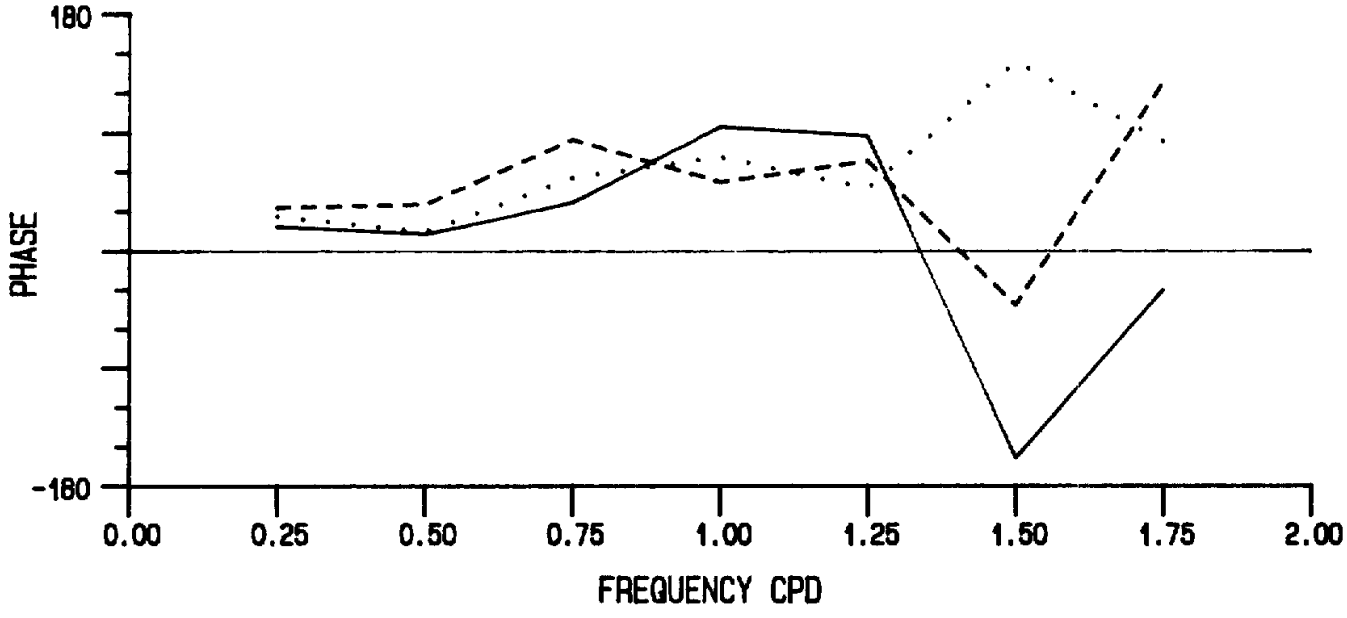

Fig. 35b Counter-clockwise component.

7. ACKNOWLEDGEMENTS

This work was supported by a Department of Supply and Services Contract No. W7707–9–0214/01–OSC. Special thanks to the Scientific Authority, Dr. Ross Graham of the Defense Research Establishment Atlantic, Dept, of National Defense, for his support and helpful comments through the course of this study.

APPENDIX 1.

SELECTED CONTOURED DIRECTIONAL SPECTRA

Contour lines at: 0.01, 0.025, 0.05, 0.1, 0.25, 0.5, 1.0, 2.0, 4.0, 6.0, 8.0, 10.0, 15.0, 20.0 and 30.0 m**2/(rps–radians)

Upper left: WAVEC data spectrum
Upper right: Hindcast model spectrum
Lower left: 10–Parameter fit spectrum to the WAVEC spectrum; RESD value included.
Lower right: 10–Parameter fit spectrum to the hindcast spectrum; RESD value included,

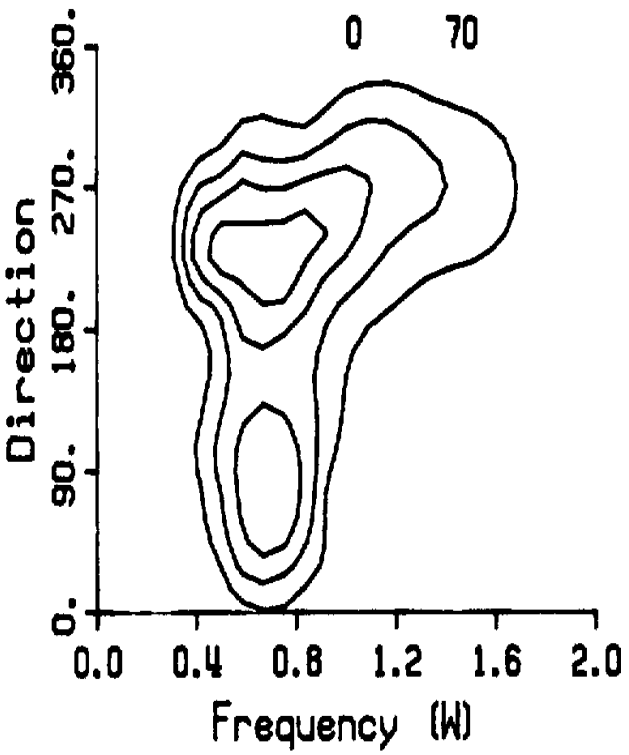
0 70
Direction
360.
270.
180.
90.
0.
0.0 0.4 0.8 1.2 1.6 2.0
Frequency (W)

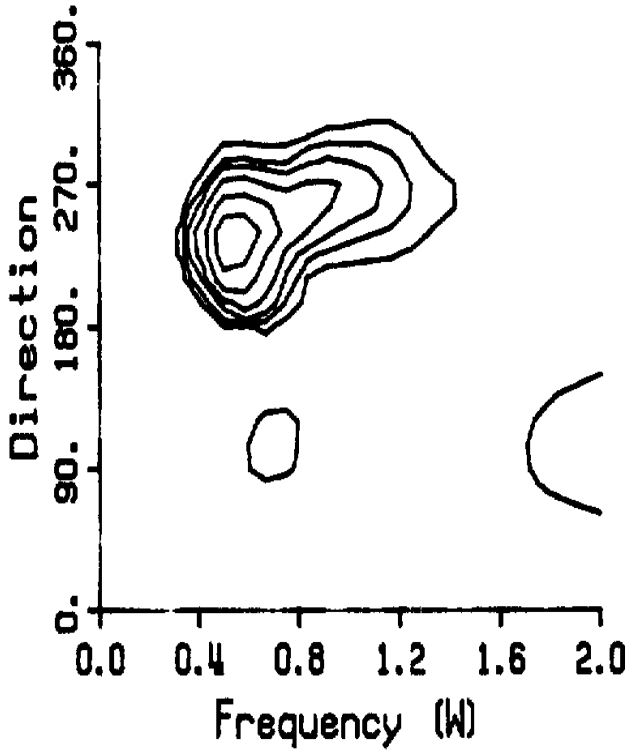
Direction
360.
270.
180.
90.
0.
0.0 0.4 0.8 1.2 1.6 2.0
Frequency (W)

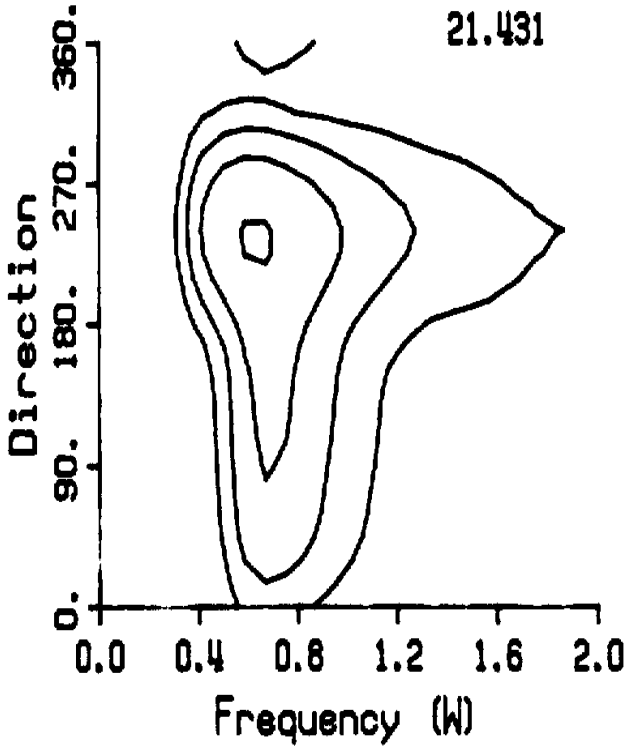
21.431
Direction
360.
270.
180.
90.
0.
0.0 0.4 0.8 1.2 1.6 2.0
Frequency (W)

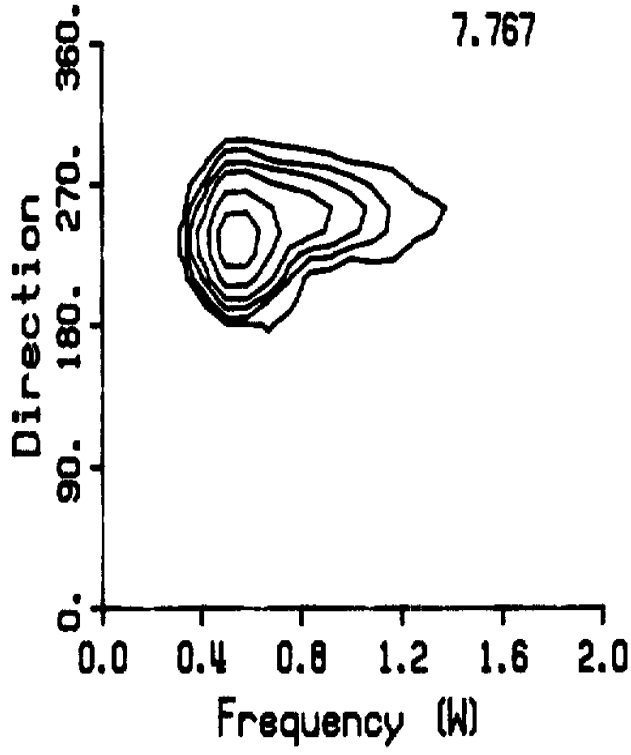
7.767
Direction
360.
270.
180.
90.
0.
0.0 0.4 0.8 1.2 1.6 2.0
Frequency (W)

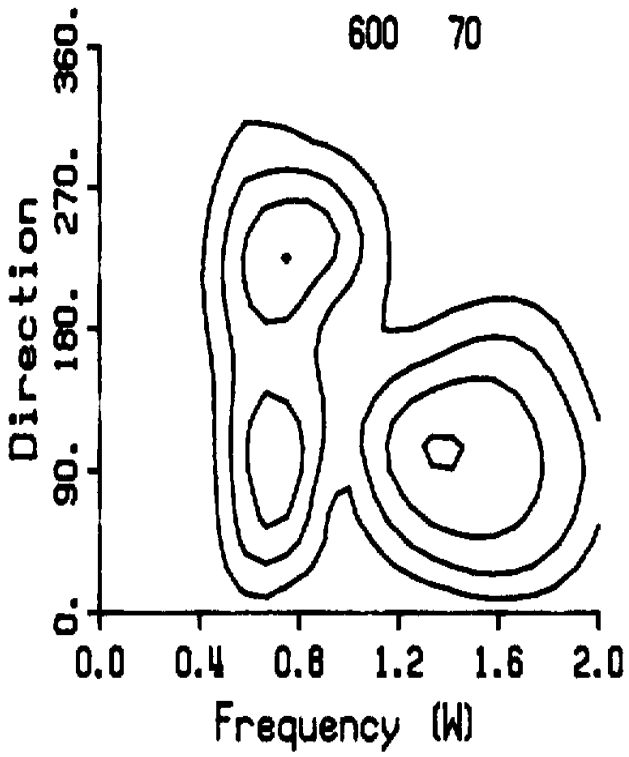
600 70
Direction
0.
90.
180.
270.
360.
0.0
0.4
0.8
1.2
1.6
2.0
Frequency (W)

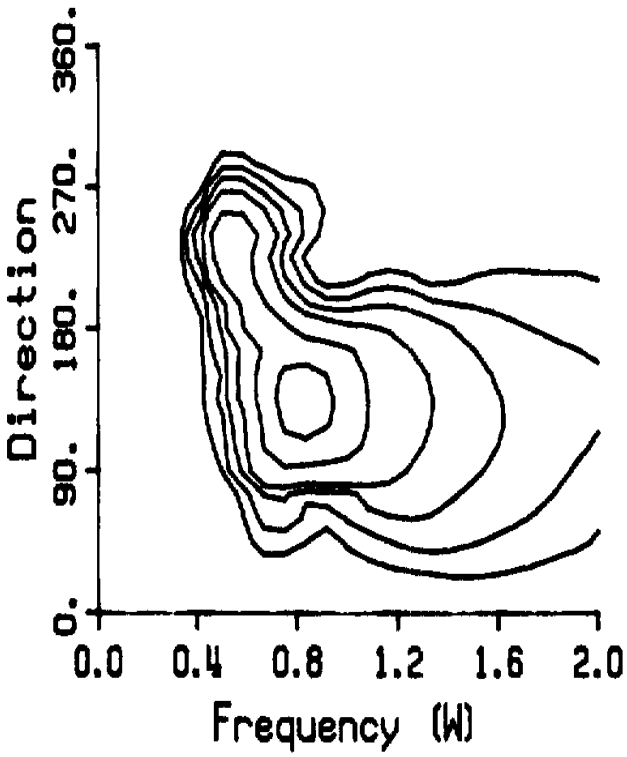
Direction
0.
90.
180.
270.
360.
0.0
0.4
0.8
1.2
1.6
2.0
Frequency (W)

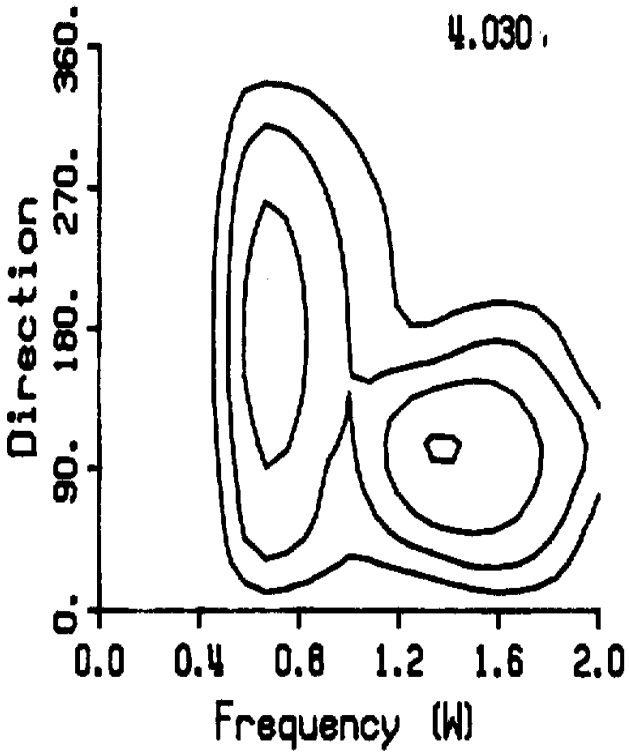
4.030
Direction
0.
90.
180.
270.
360.
0.0
0.4
0.8
1.2
1.6
2.0
Frequency (W)

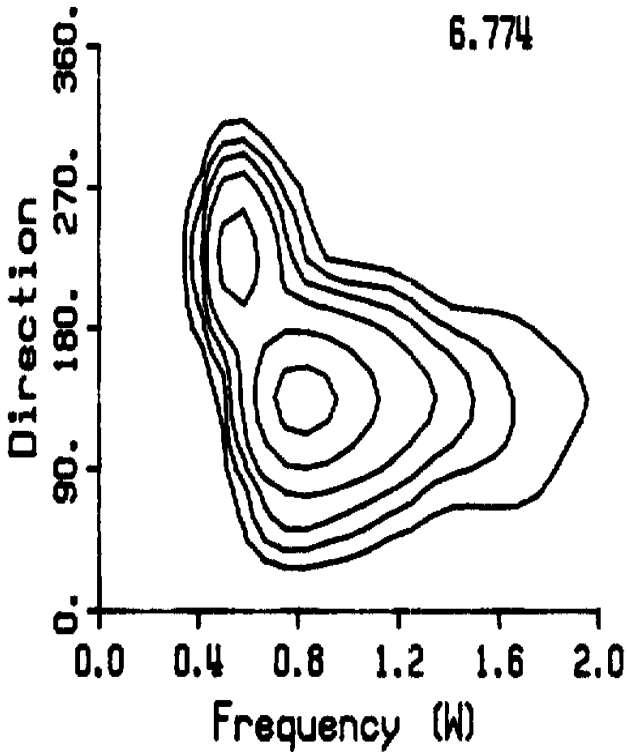
6.774
Direction
0.
90.
180.
270.
360.
0.0
0.4
0.8
1.2
1.6
2.0
Frequency (W)

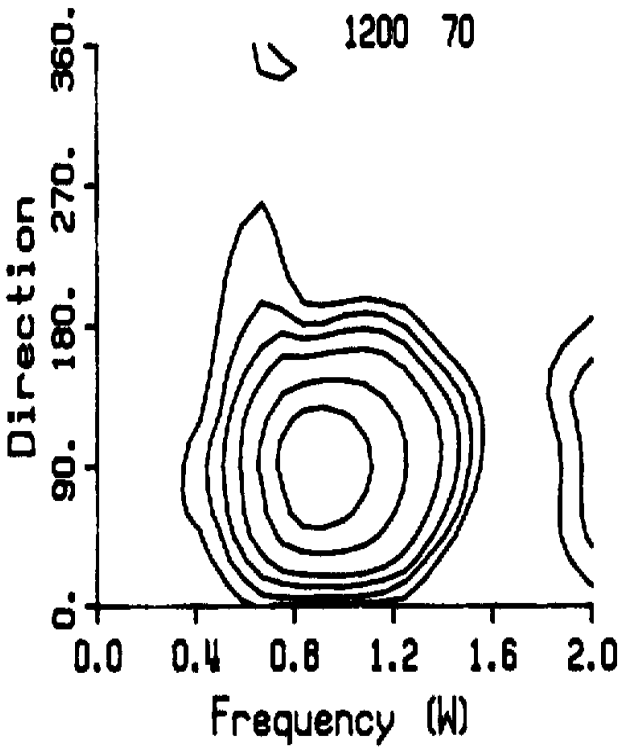
1200 70
Direction
360.
270.
180.
90.
0.
0.0 0.4 0.8 1.2 1.6 2.0
Frequency (W)

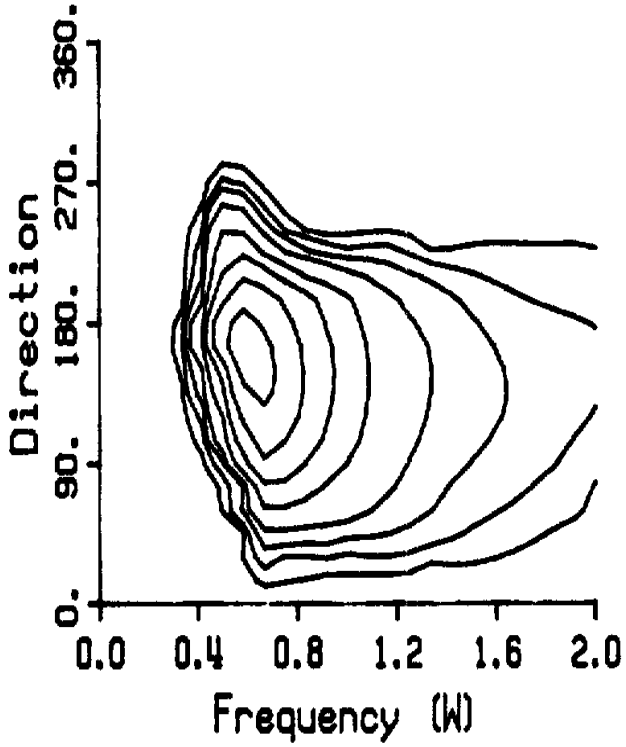
Direction
360.
270.
180.
90.
0.
0.0 0.4 0.8 1.2 1.6 2.0
Frequency (W)

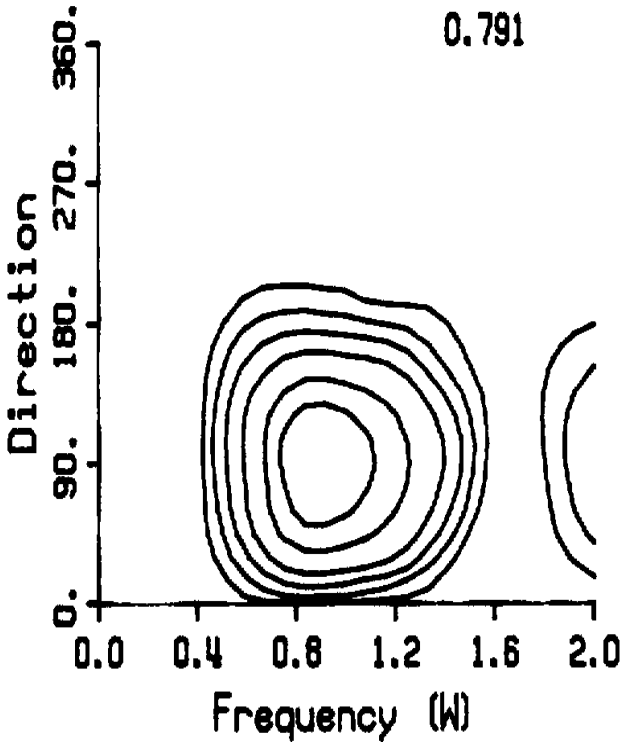
0.791
Direction
360.
270.
180.
90.
0.
0.0 0.4 0.8 1.2 1.6 2.0
Frequency (W)

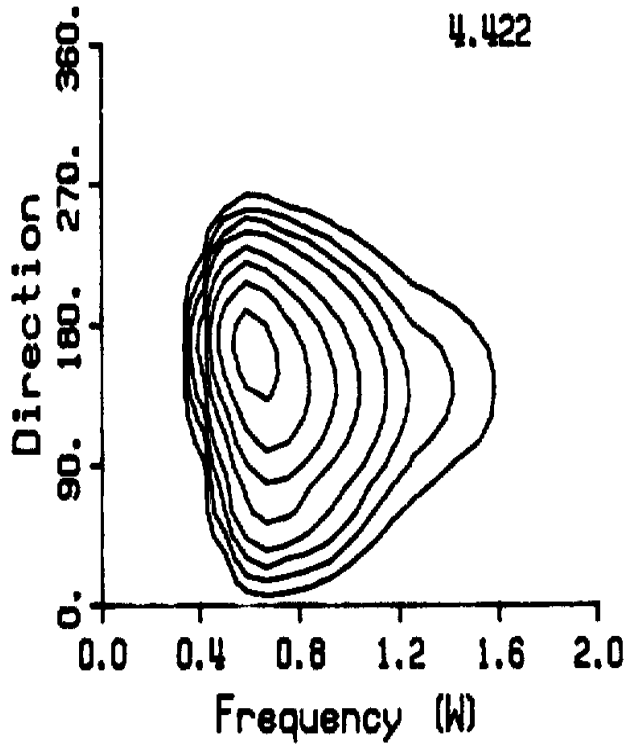
4.422
Direction
360.
270.
180.
90.
0.
0.0 0.4 0.8 1.2 1.6 2.0
Frequency (W)

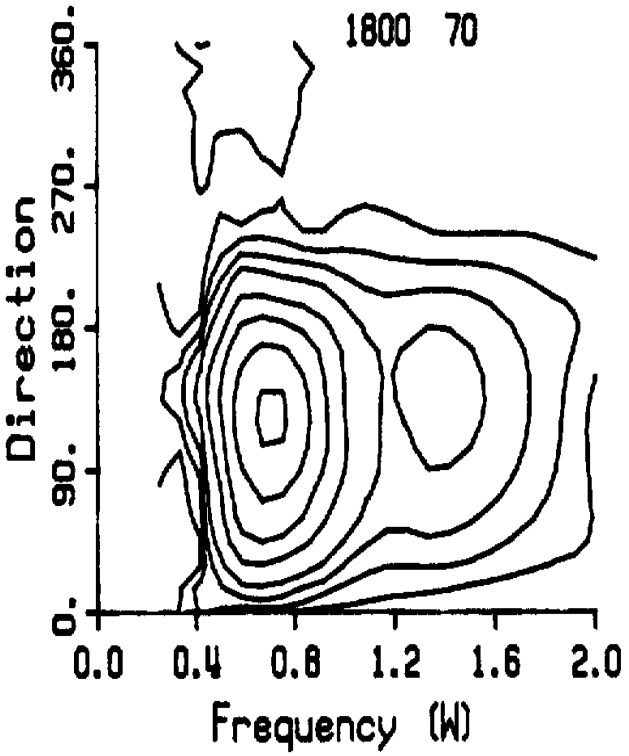
1800 70
Direction
360.
270.
180.
90.
0.
0.0 0.4 0.8 1.2 1.6 2.0
Frequency (W)

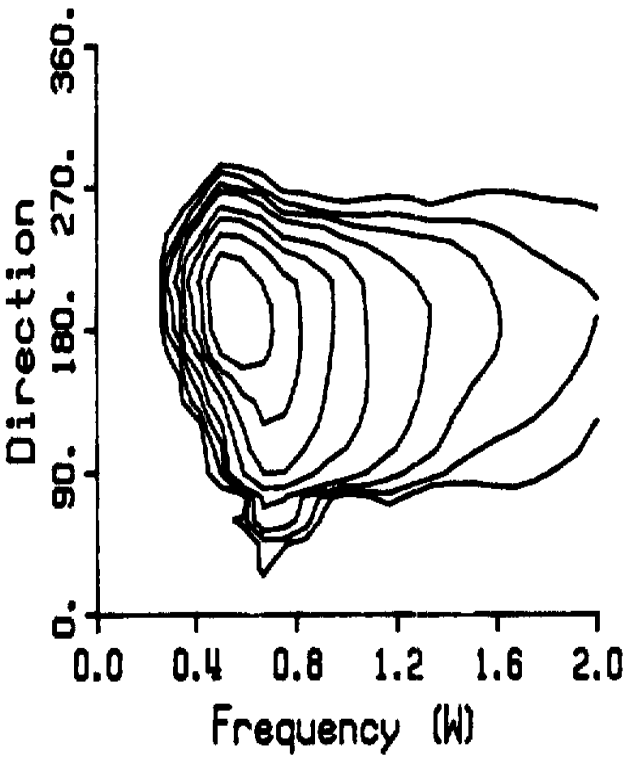
Direction
360.
270.
180.
90.
0.
0.0 0.4 0.8 1.2 1.6 2.0
Frequency (W)

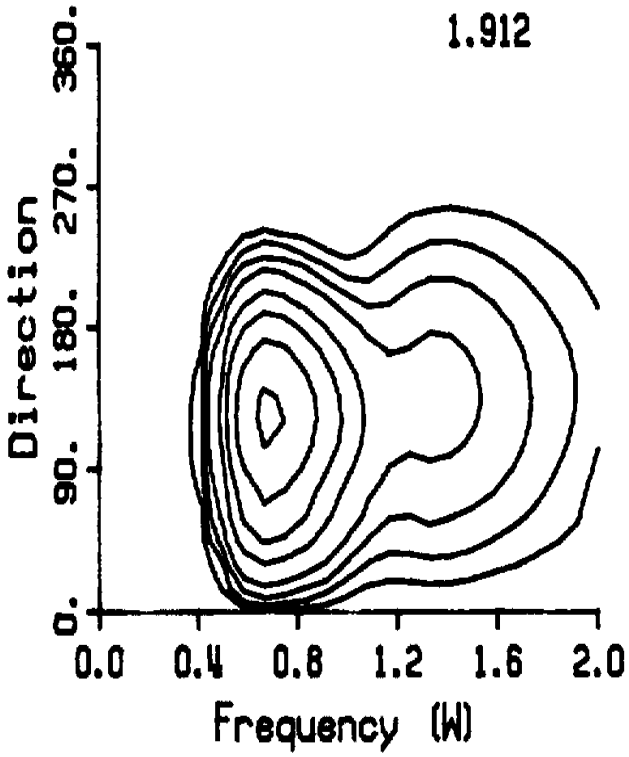
1.912
Direction
360.
270.
180.
90.
0.
0.0 0.4 0.8 1.2 1.6 2.0
Frequency (W)

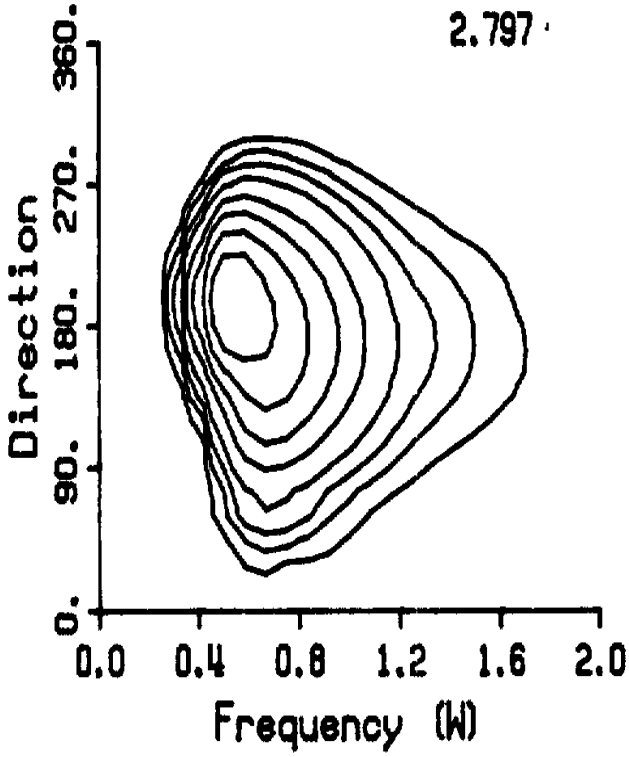
2.797
Direction
360.
270.
180.
90.
0.
0.0 0.4 0.8 1.2 1.6 2.0
Frequency (W)

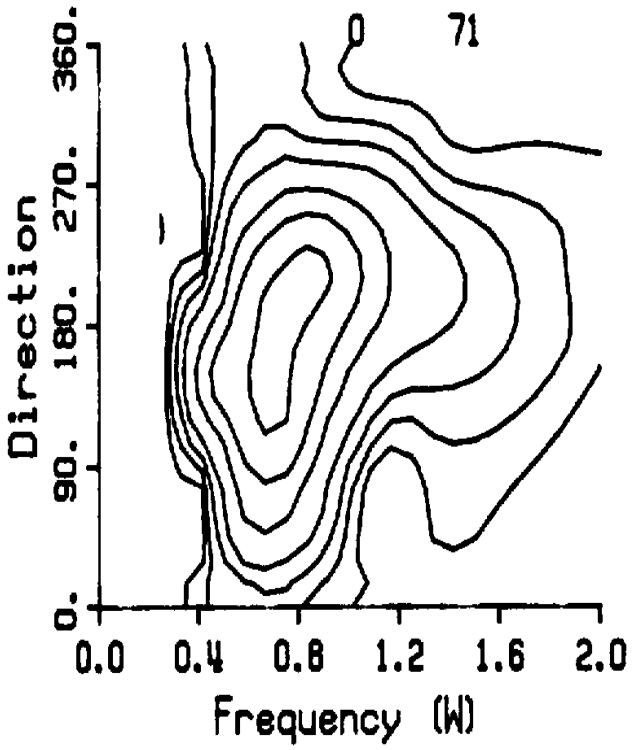
71
Direction
360.
270.
180.
90.
0.
0.0
0.4
0.8
1.2
1.6
2.0
Frequency (W)

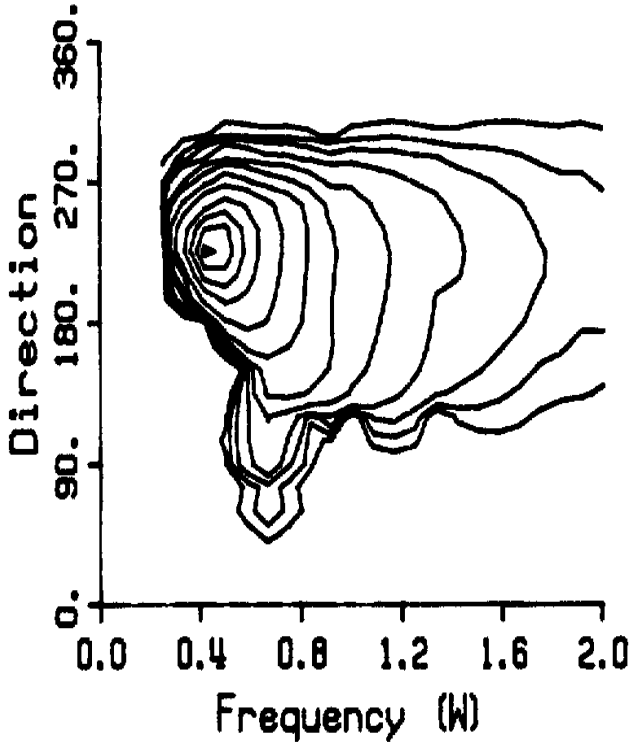
Direction
360.
270.
180.
90.
0.
0.0
0.4
0.8
1.2
1.6
2.0
Frequency (W)

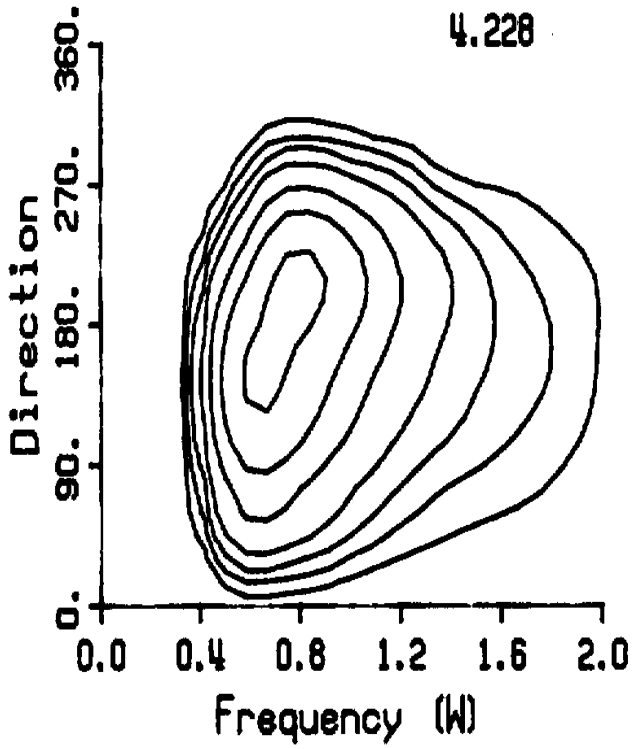
4.228
Direction
360.
270.
180.
90.
0.
0.0
0.4
0.8
1.2
1.6
2.0
Frequency (W)

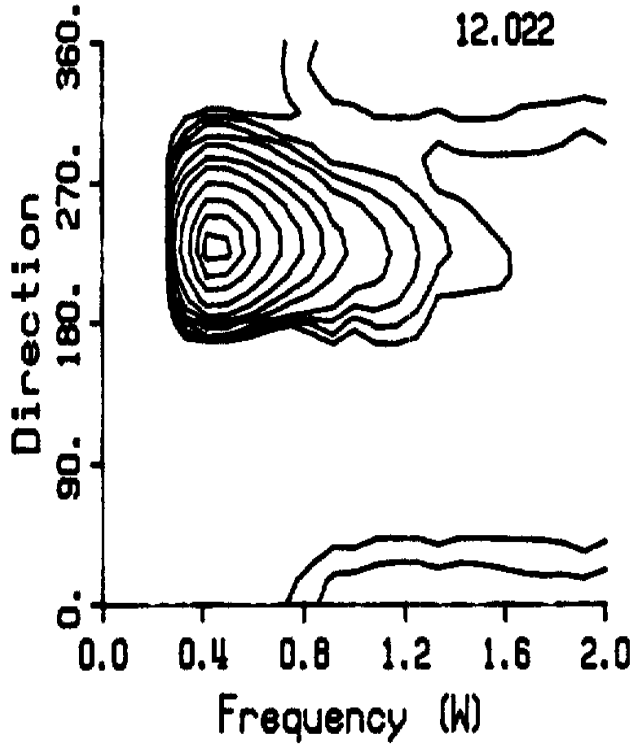
12.022
Direction
360.
270.
180.
90.
0.
0.0
0.4
0.8
1.2
1.6
2.0
Frequency (W)

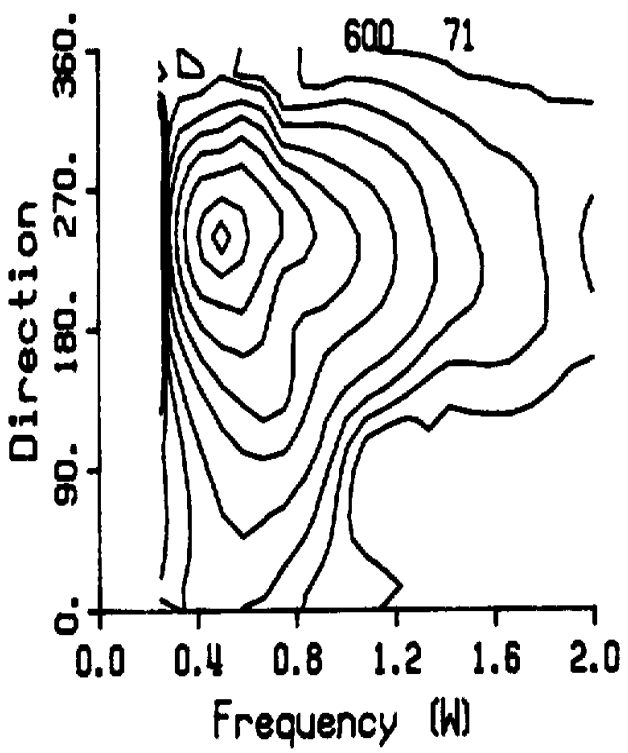
600 71
Direction
360.
270.
180.
90.
0.
0.0 0.4 0.8 1.2 1.6 2.0
Frequency (W)

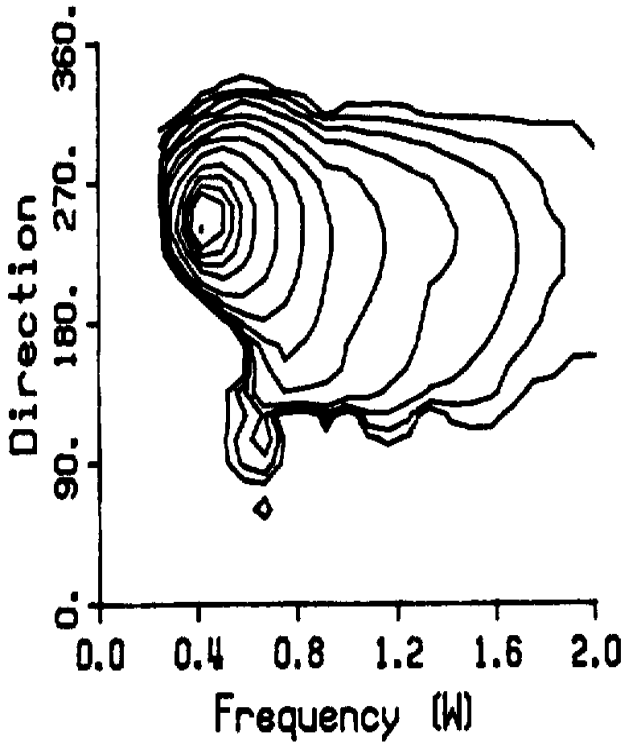
Direction
360.
270.
180.
90.
0.
0.0 0.4 0.8 1.2 1.6 2.0
Frequency (W)

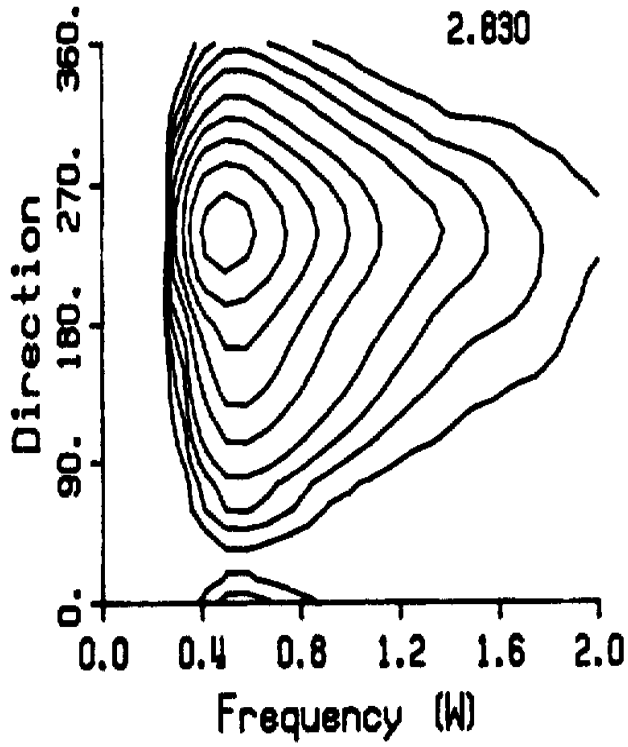
2.830
Direction
360.
270.
180.
90.
0.
0.0 0.4 0.8 1.2 1.6 2.0
Frequency (W)

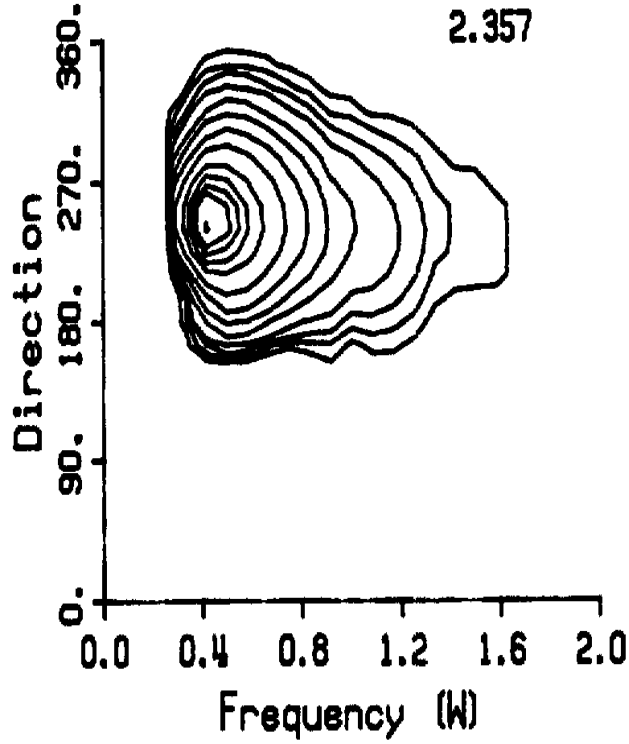
2.357
Direction
360.
270.
180.
90.
0.
0.0 0.4 0.8 1.2 1.6 2.0
Frequency (W)

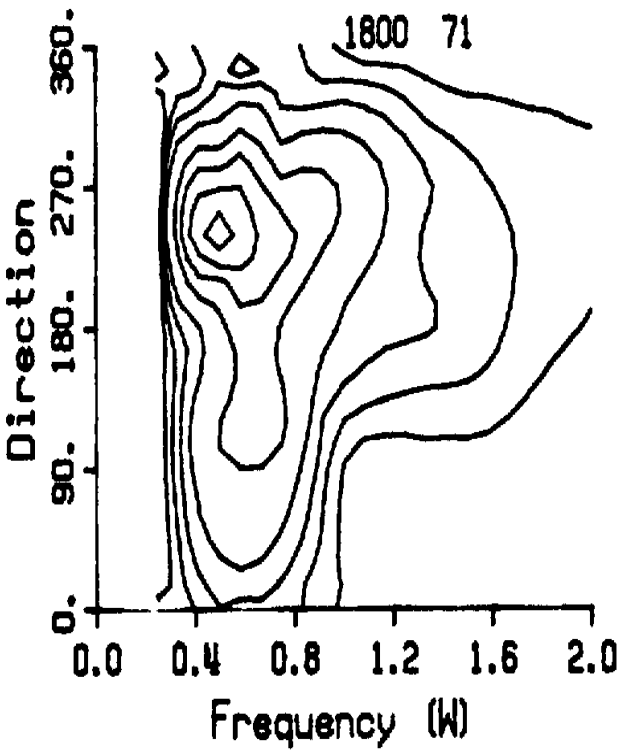
1800 71
Direction
360.
270.
180.
90.
0.
0.0 0.4 0.8 1.2 1.6 2.0
Frequency (W)

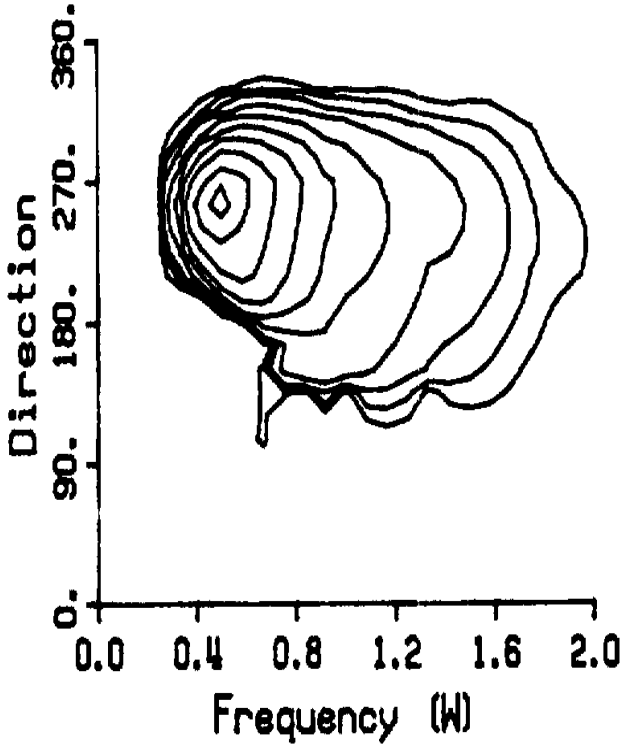
Direction
360.
270.
180.
90.
0.
0.0 0.4 0.8 1.2 1.6 2.0
Frequency (W)

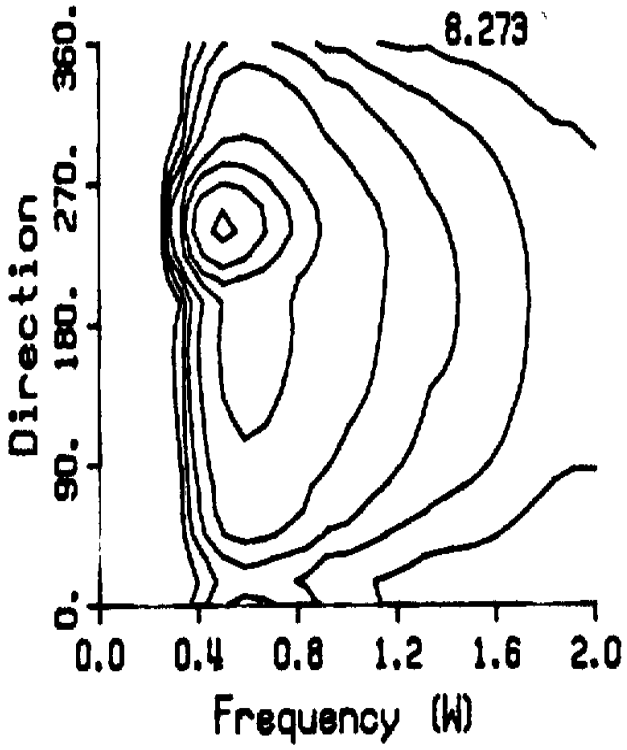
8.273
Direction
360.
270.
180.
90.
0.
0.0 0.4 0.8 1.2 1.6 2.0
Frequency (W)

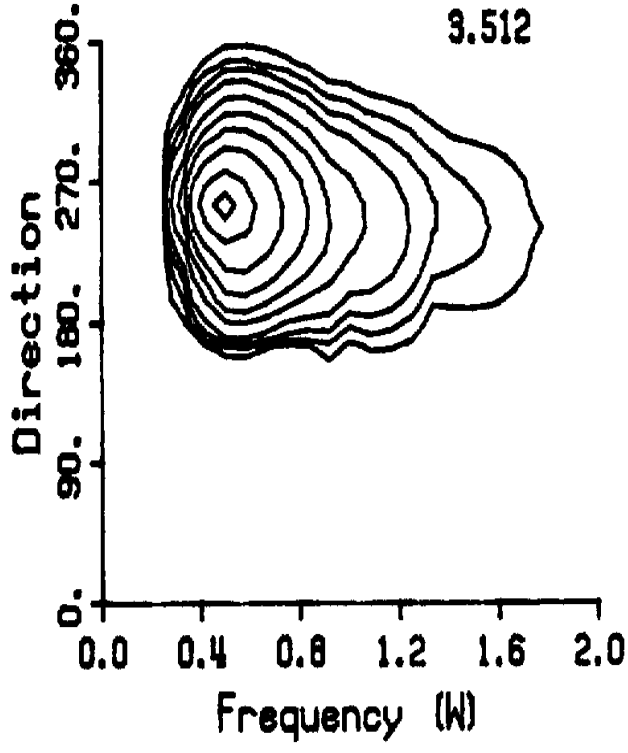
3.512
Direction
360.
270.
180.
90.
0.
0.0 0.4 0.8 1.2 1.6 2.0
Frequency (W)

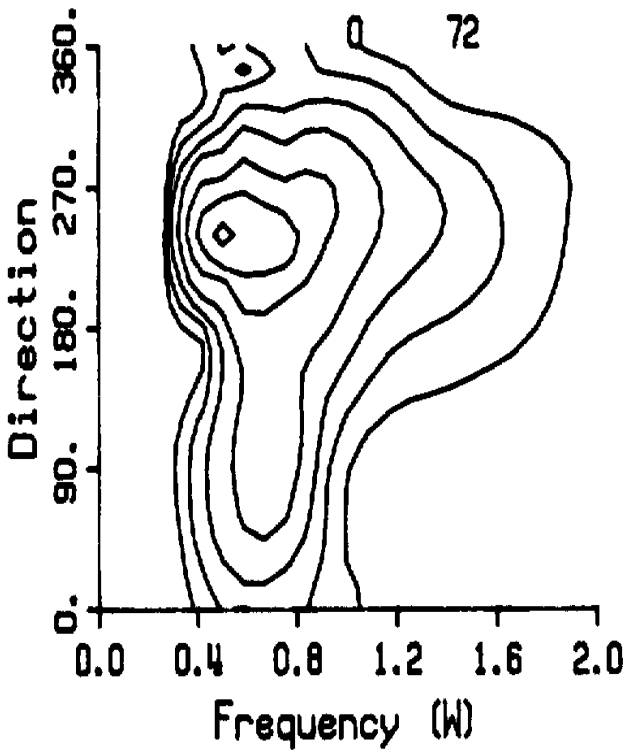
72
Direction
0.
90.
180.
270.
360.
0.0
0.4
0.8
1.2
1.6
2.0
Frequency (W)

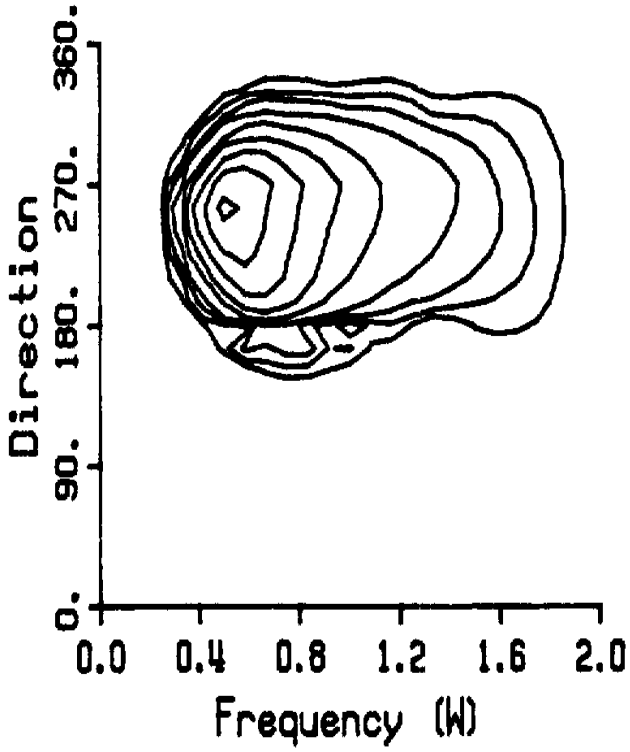
Direction
0.
90.
180.
270.
360.
0.0
0.4
0.8
1.2
1.6
2.0
Frequency (W)

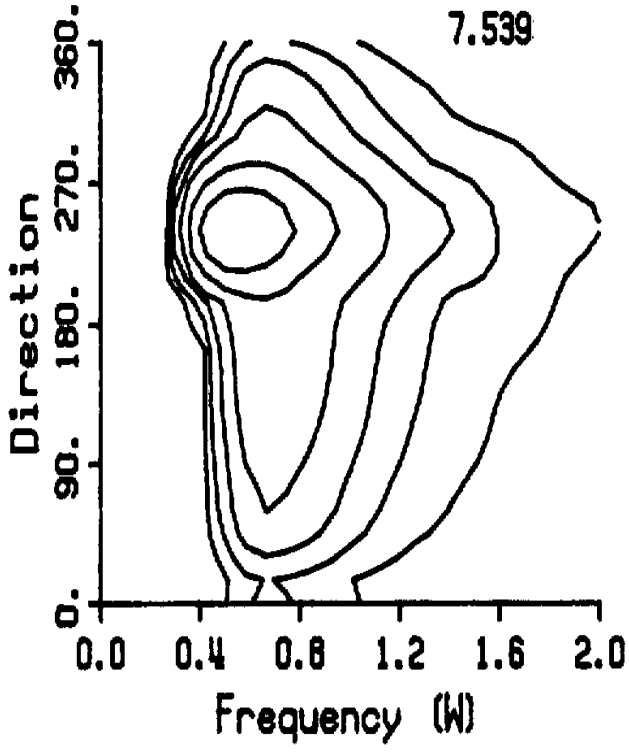
7.539
Direction
0.
90.
180.
270.
360.
0.0
0.4
0.8
1.2
1.6
2.0
Frequency (W)

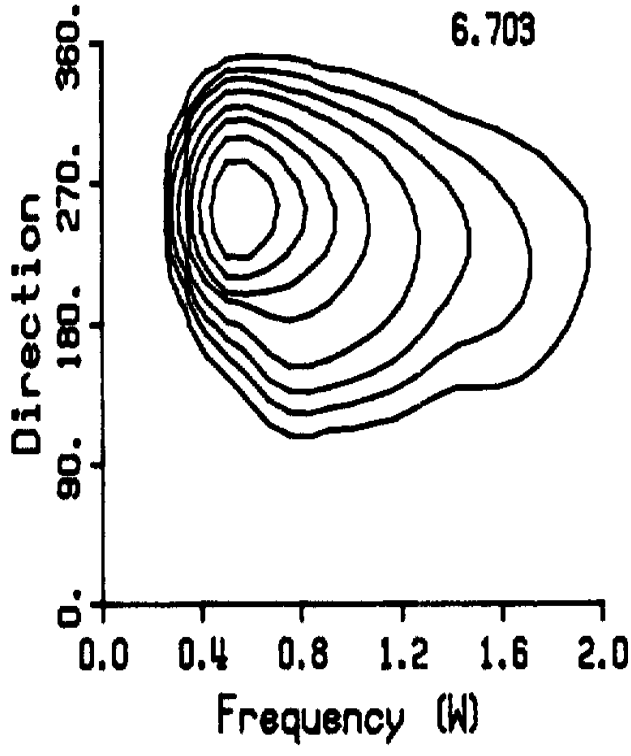
6.703
Direction
0.
90.
180.
270.
360.
0.0
0.4
0.8
1.2
1.6
2.0
Frequency (W)

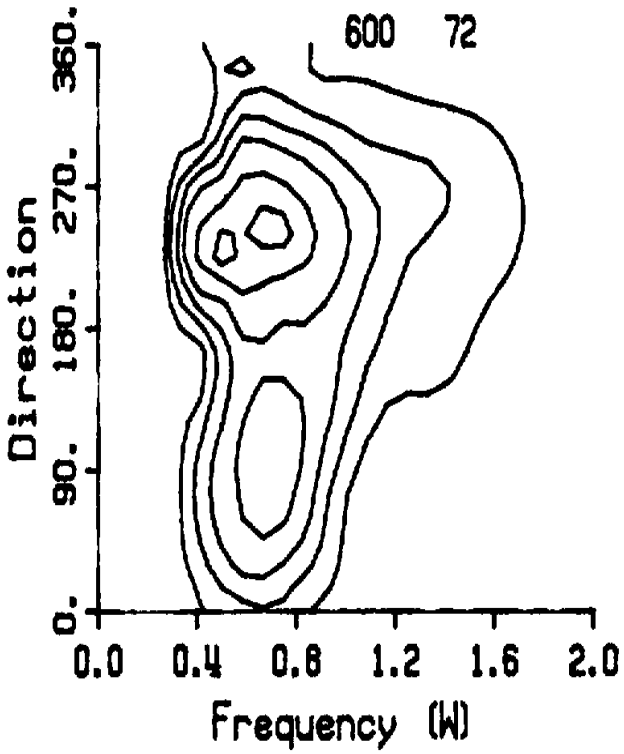
600 72
Direction
360.
270.
180.
90.
0.
0.0 0.4 0.8 1.2 1.6 2.0
Frequency (W)

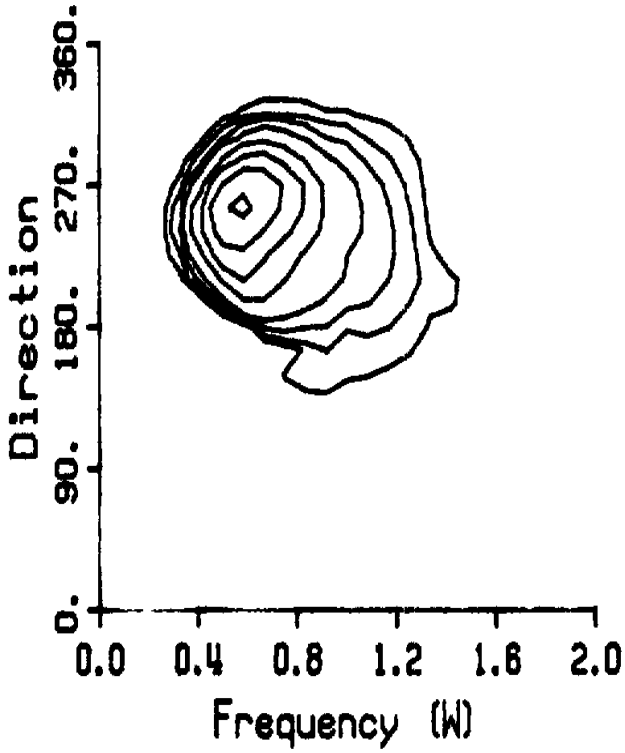
Direction
360.
270.
180.
90.
0.
0.0 0.4 0.8 1.2 1.6 2.0
Frequency (W)

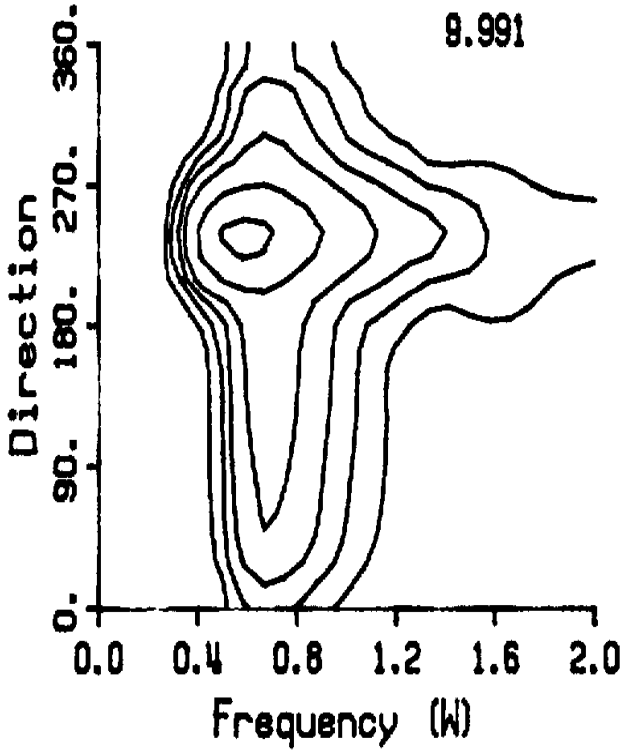
9.991
Direction
360.
270.
180.
90.
0.
0.0 0.4 0.8 1.2 1.6 2.0
Frequency (W)

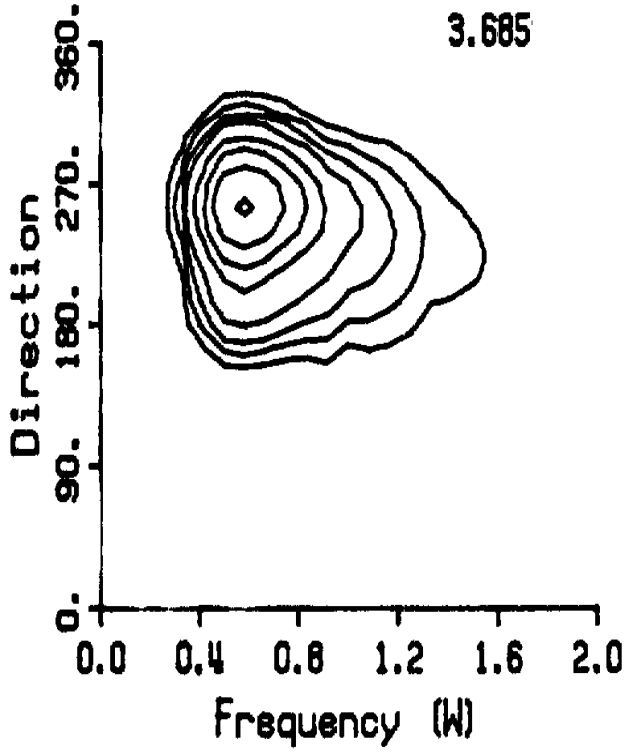
3.685
Direction
360.
270.
180.
90.
0.
0.0 0.4 0.8 1.2 1.6 2.0
Frequency (W)

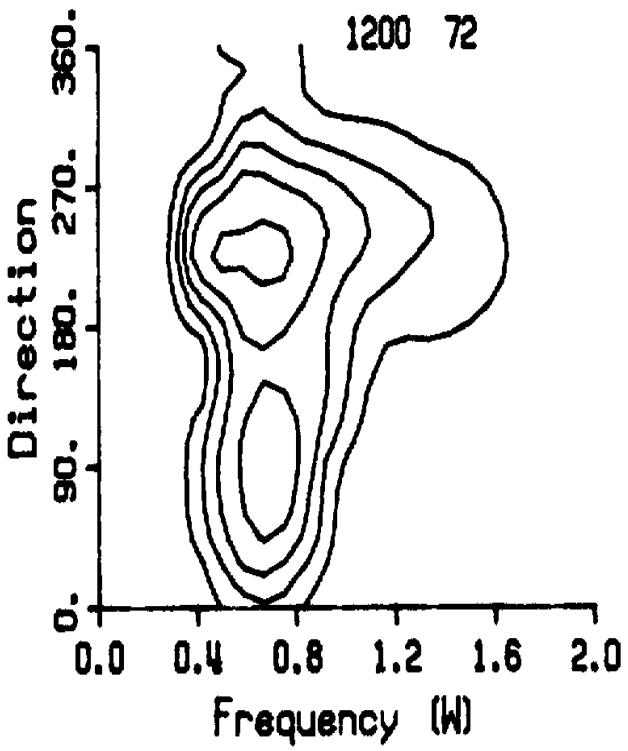
1200 72
Direction
360.
270.
180.
90.
0.
0.0 0.4 0.8 1.2 1.6 2.0
Frequency (W)

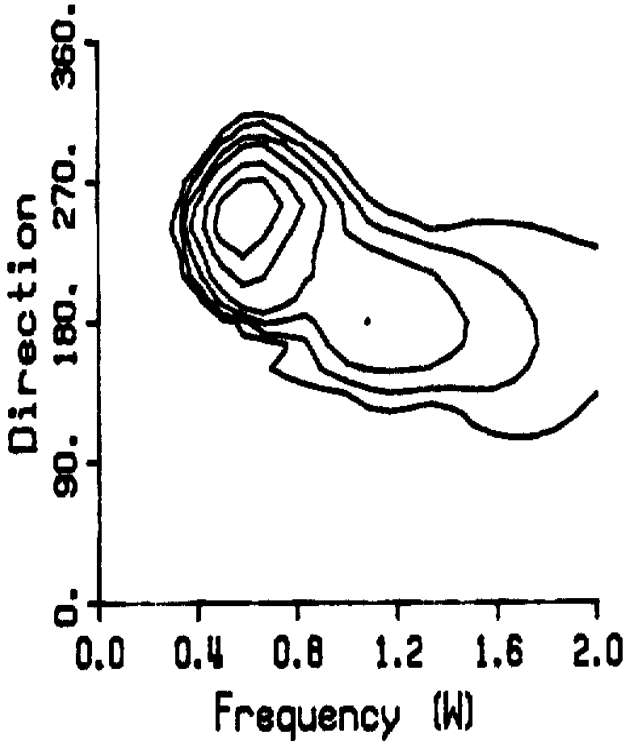
Direction
360.
270.
180.
90.
0.
0.0 0.4 0.8 1.2 1.6 2.0
Frequency (W)

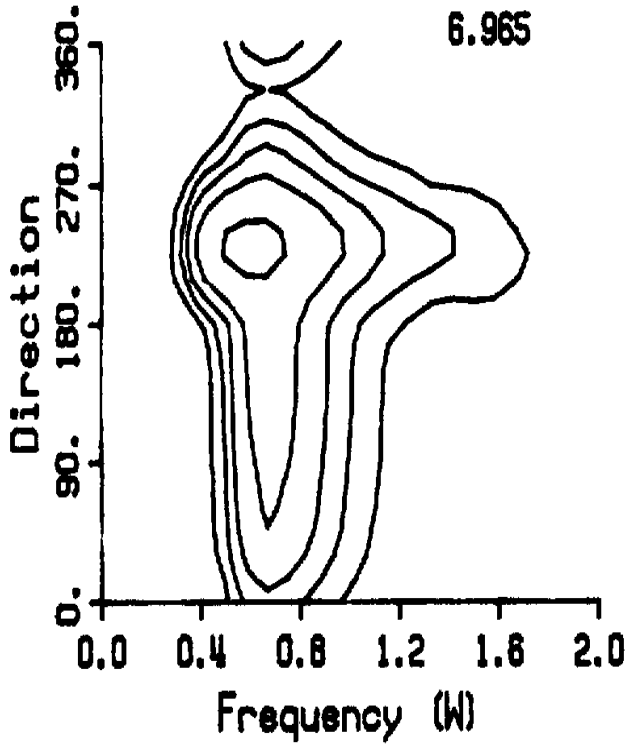
6.965
Direction
360.
270.
180.
90.
0.
0.0 0.4 0.8 1.2 1.6 2.0
Frequency (W)

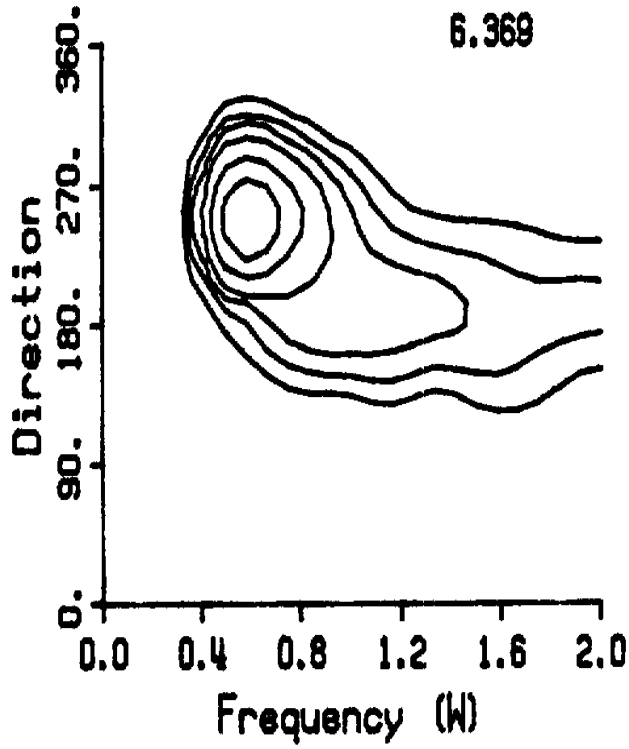
6.369
Direction
360.
270.
180.
90.
0.
0.0 0.4 0.8 1.2 1.6 2.0
Frequency (W)

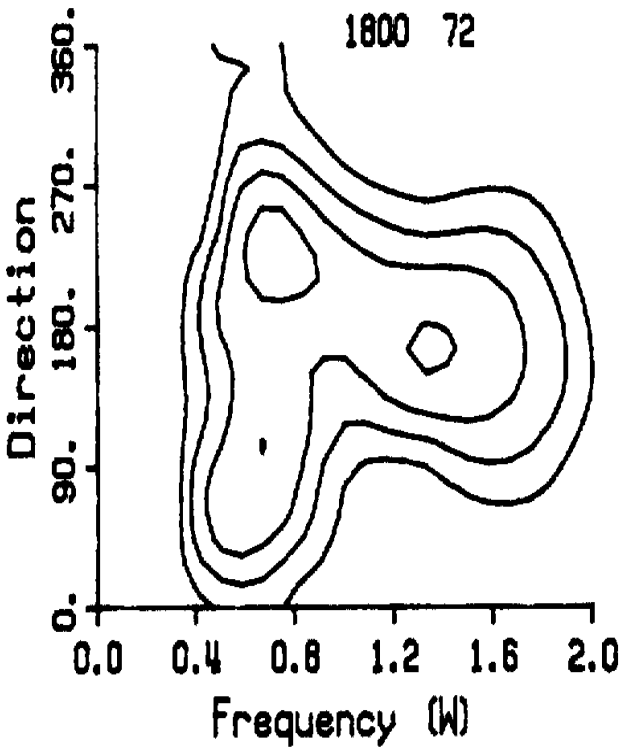
1800 72
Direction
360.
270.
180.
90.
0.
0.0 0.4 0.8 1.2 1.6 2.0
Frequency (W)

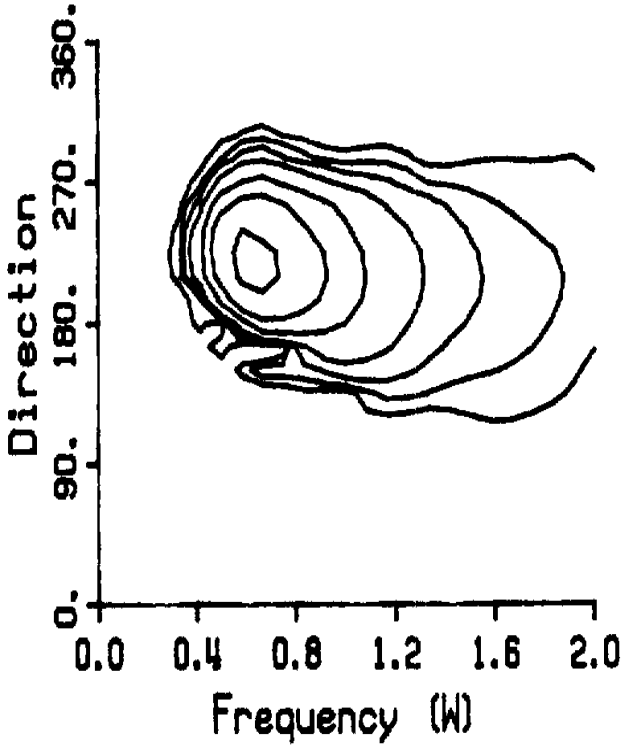
Direction
360.
270.
180.
90.
0.
0.0 0.4 0.8 1.2 1.6 2.0
Frequency (W)

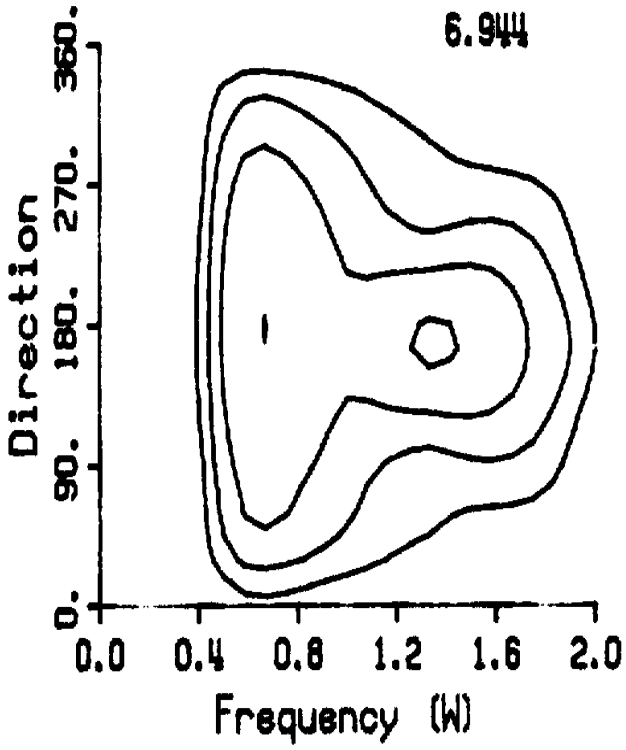
6.944
Direction
360.
270.
180.
90.
0.
0.0 0.4 0.8 1.2 1.6 2.0
Frequency (W)

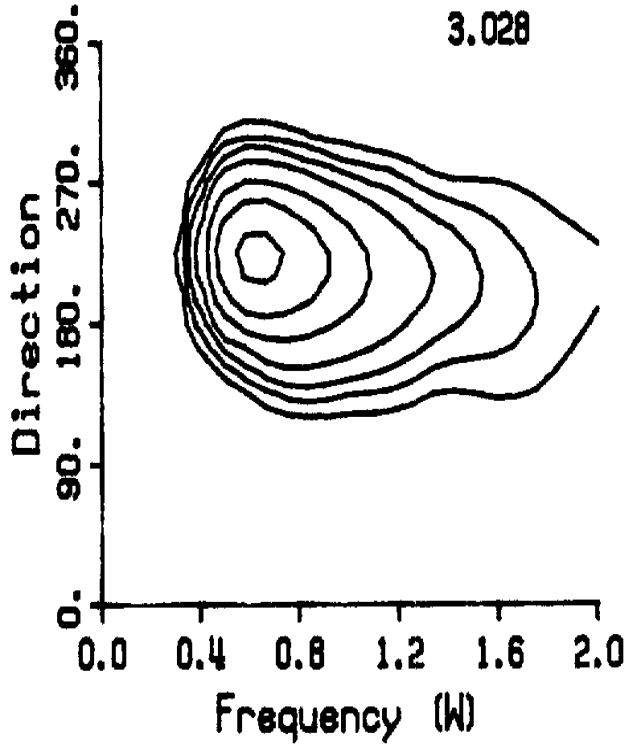
3.028
Direction
360.
270.
180.
90.
0.
0.0 0.4 0.8 1.2 1.6 2.0
Frequency (W)

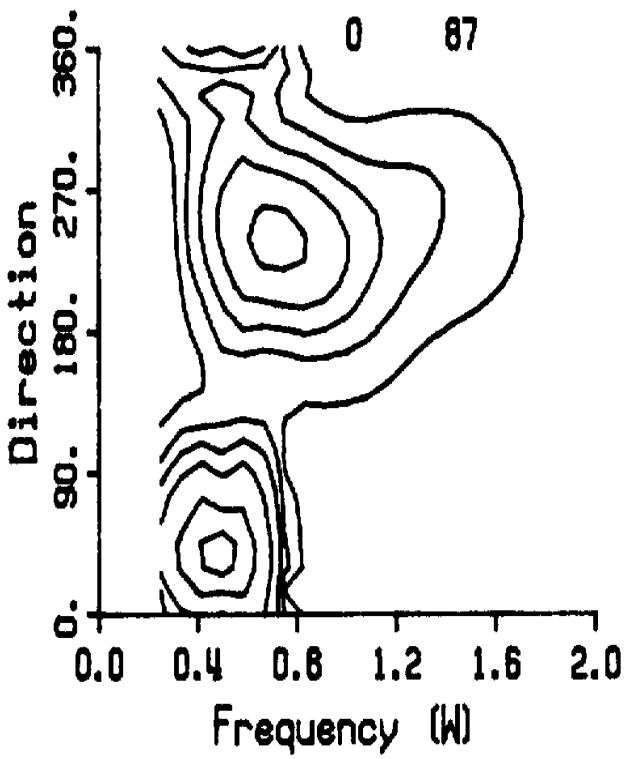
0 87
Direction
360.
270.
180.
90.
0.
0.0 0.4 0.8 1.2 1.6 2.0
Frequency (W)

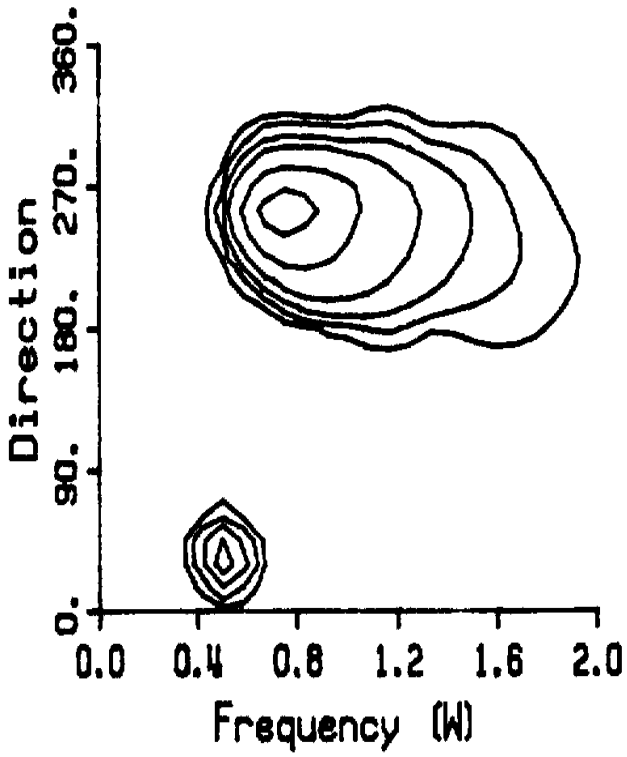
Direction
360.
270.
180.
90.
0.
0.0 0.4 0.8 1.2 1.6 2.0
Frequency (W)

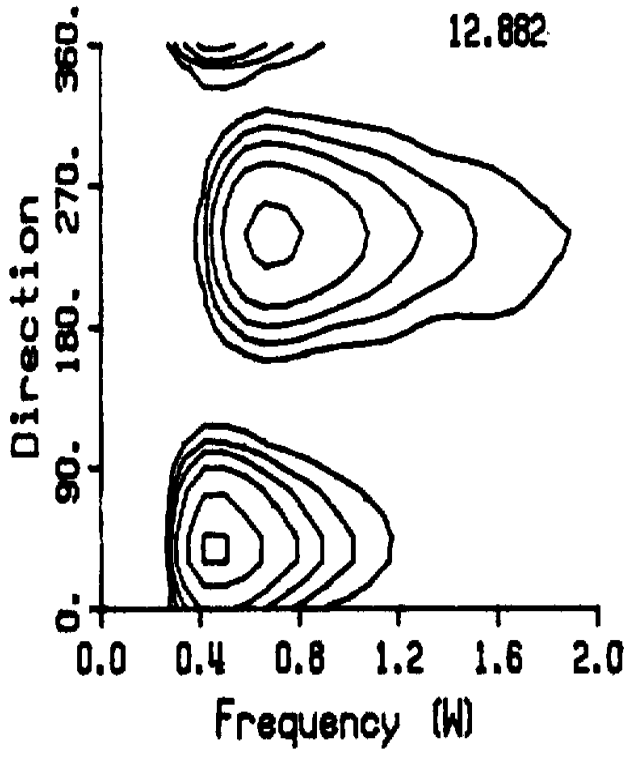
12.882
Direction
360.
270.
180.
90.
0.
0.0 0.4 0.8 1.2 1.6 2.0
Frequency (W)

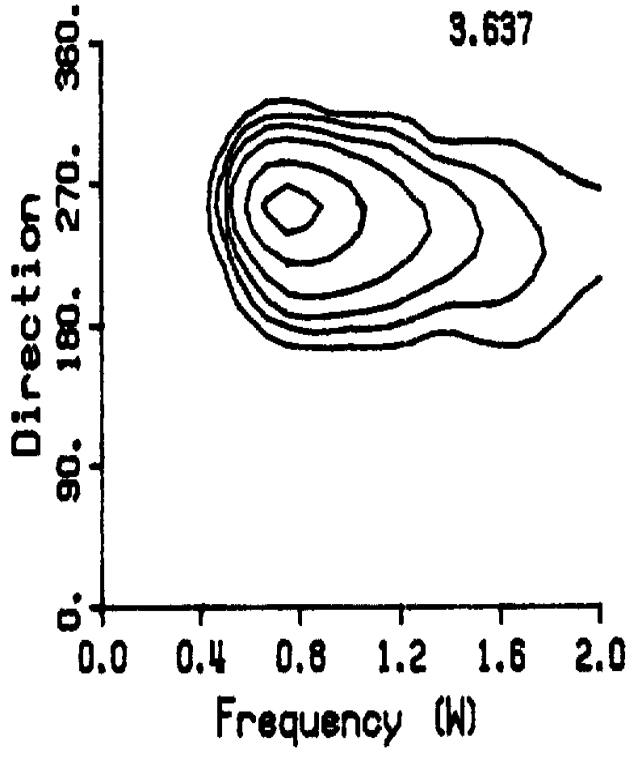
3.637
Direction
360.
270.
180.
90.
0.
0.0 0.4 0.8 1.2 1.6 2.0
Frequency (W)

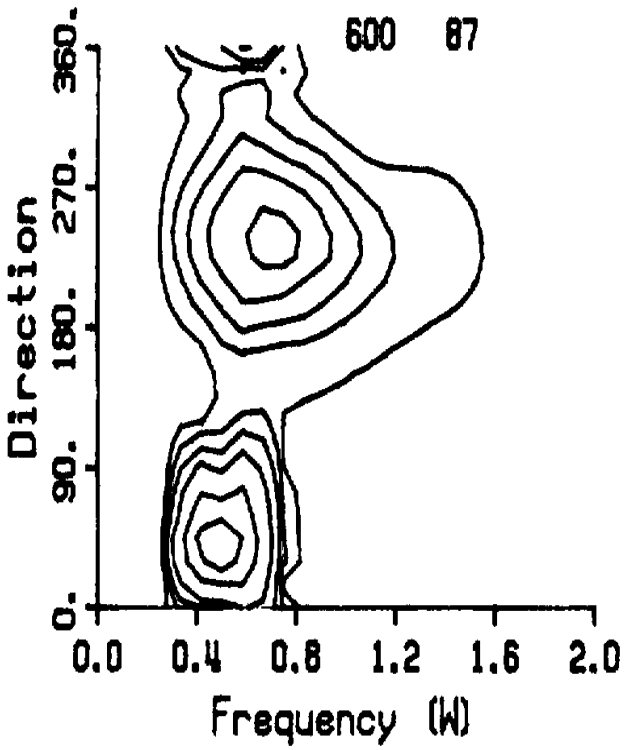
600 87
Direction
360.
270.
180.
90.
0.
0.0 0.4 0.8 1.2 1.6 2.0
Frequency (W)

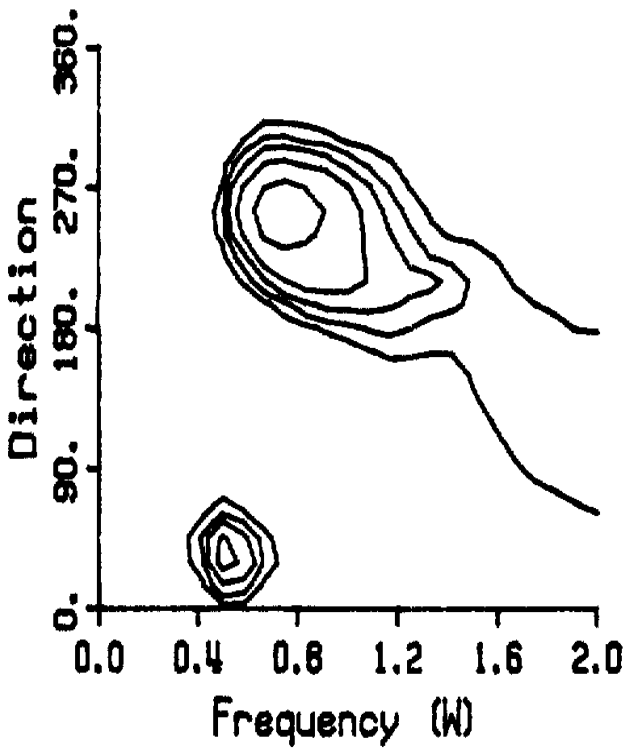
Direction
360.
270.
180.
90.
0.
0.0 0.4 0.8 1.2 1.6 2.0
Frequency (W)

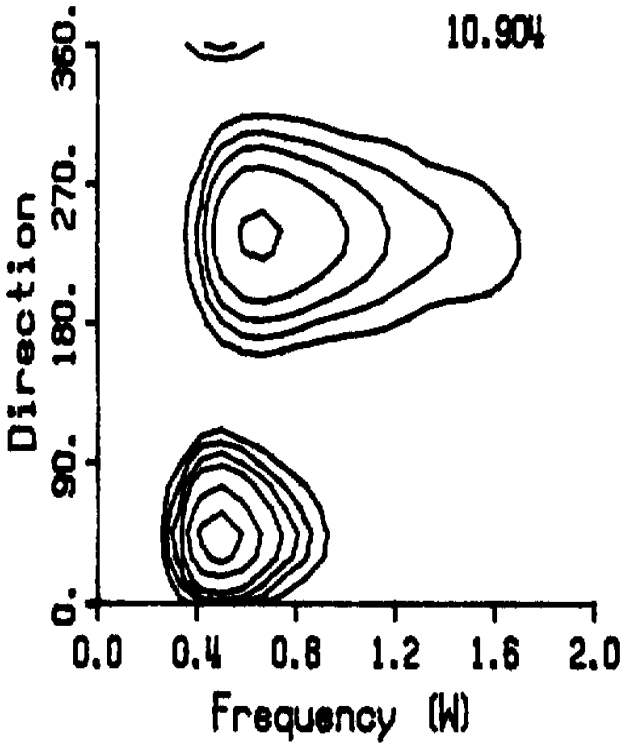
10.904
Direction
360.
270.
180.
90.
0.
0.0 0.4 0.8 1.2 1.6 2.0
Frequency (W)

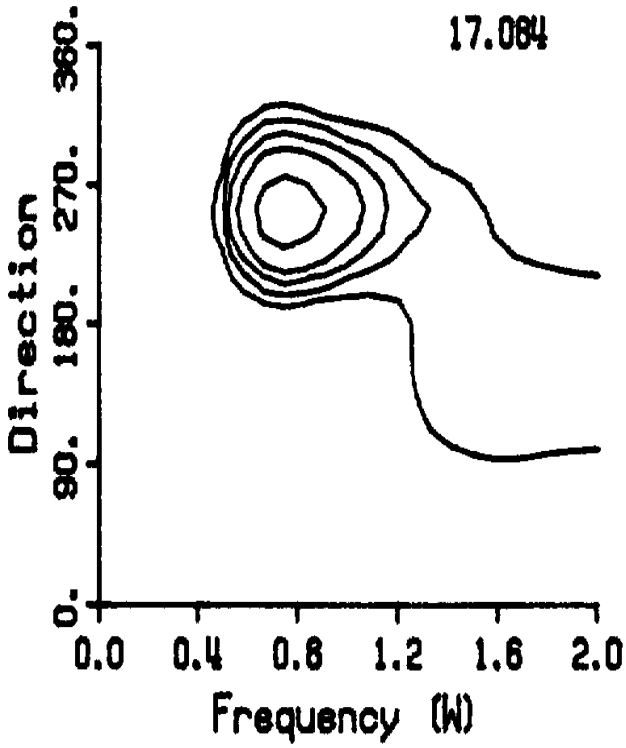
17.084
Direction
360.
270.
180.
90.
0.
0.0 0.4 0.8 1.2 1.6 2.0
Frequency (W)

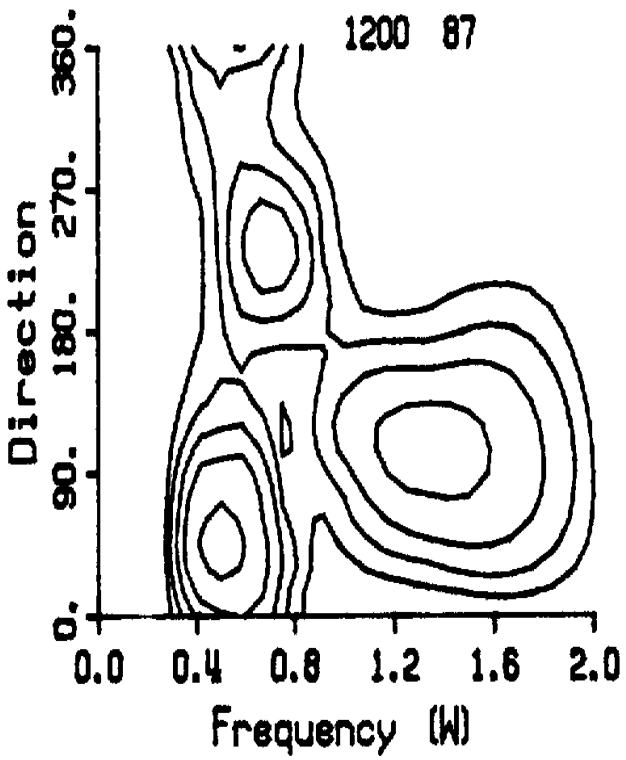
1200 87
Direction
360.
270.
180.
90.
0.
0.0 0.4 0.8 1.2 1.6 2.0
Frequency (W)

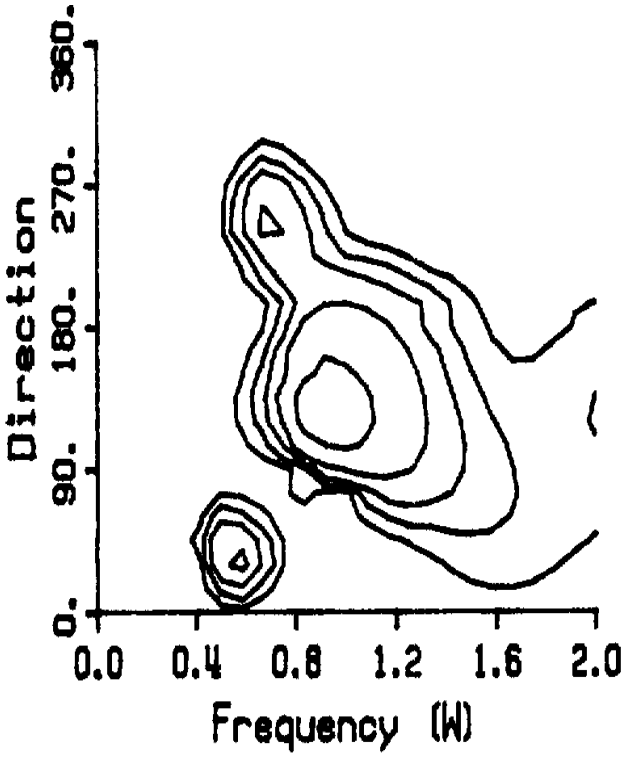
Direction
360.
270.
180.
90.
0.
0.0 0.4 0.8 1.2 1.6 2.0
Frequency (W)

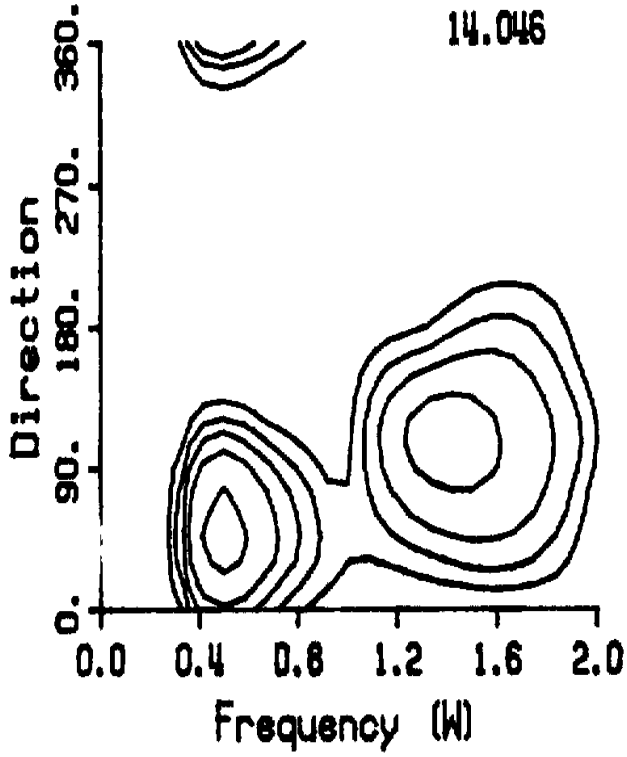
14.046
Direction
360.
270.
180.
90.
0.
0.0 0.4 0.8 1.2 1.6 2.0
Frequency (W)

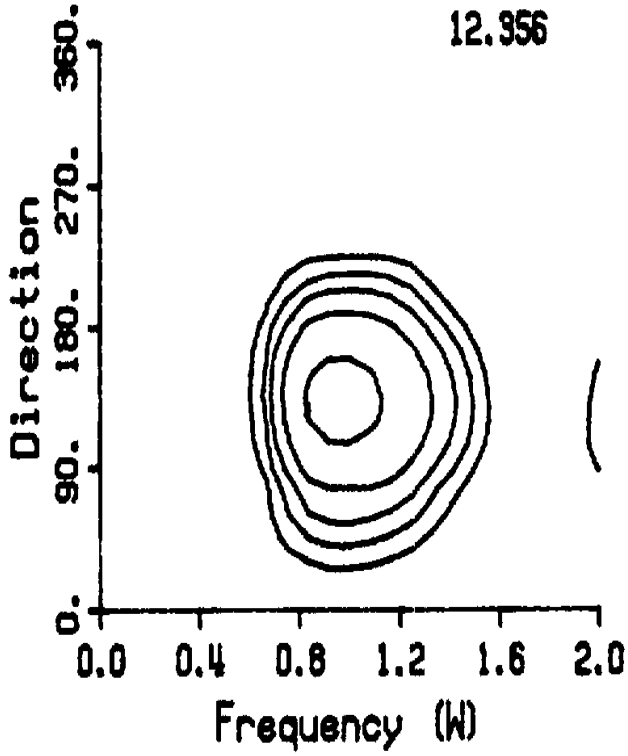
12.956
Direction
360.
270.
180.
90.
0.
0.0 0.4 0.8 1.2 1.6 2.0
Frequency (W)

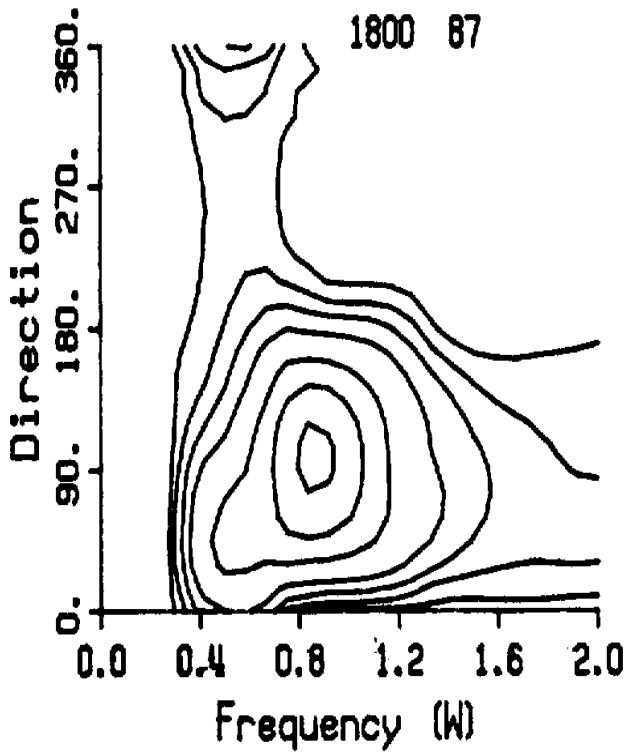
1800 87
Direction
360.
270.
180.
90.
0.
0.0 0.4 0.8 1.2 1.6 2.0
Frequency (W)

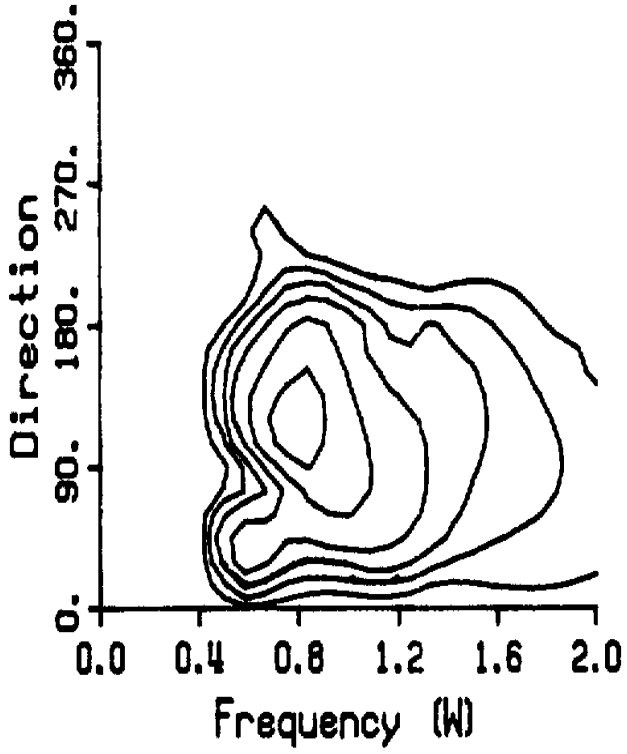
Direction
360.
270.
180.
90.
0.
0.0 0.4 0.8 1.2 1.6 2.0
Frequency (W)

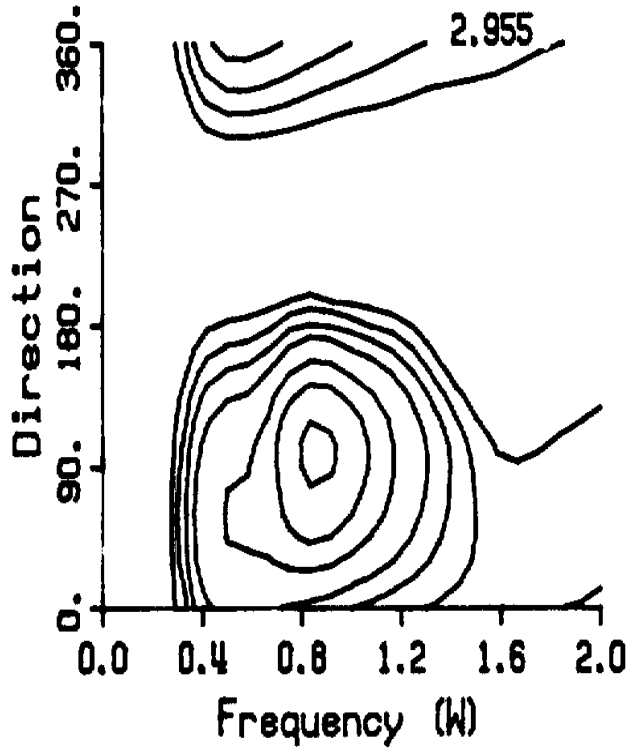
2.955
Direction
360.
270.
180.
90.
0.
0.0 0.4 0.8 1.2 1.6 2.0
Frequency (W)

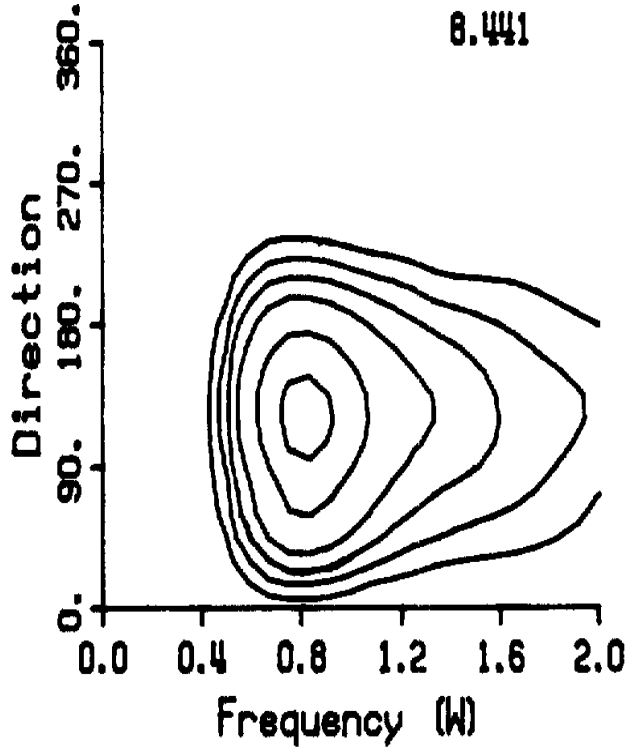
8.441
Direction
360.
270.
180.
90.
0.
0.0 0.4 0.8 1.2 1.6 2.0
Frequency (W)

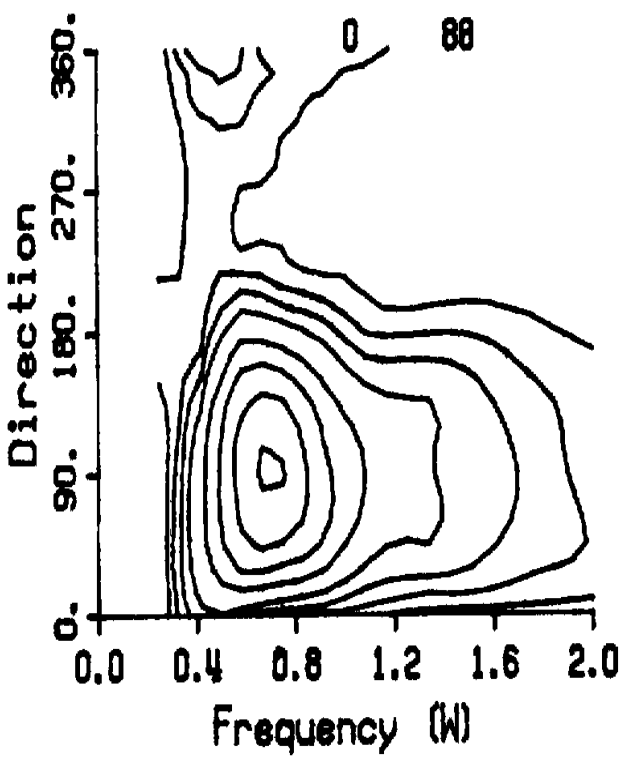
0
88
Direction
360.
270.
180.
90.
0.
0.0
0.4
0.8
1.2
1.6
2.0
Frequency (W)

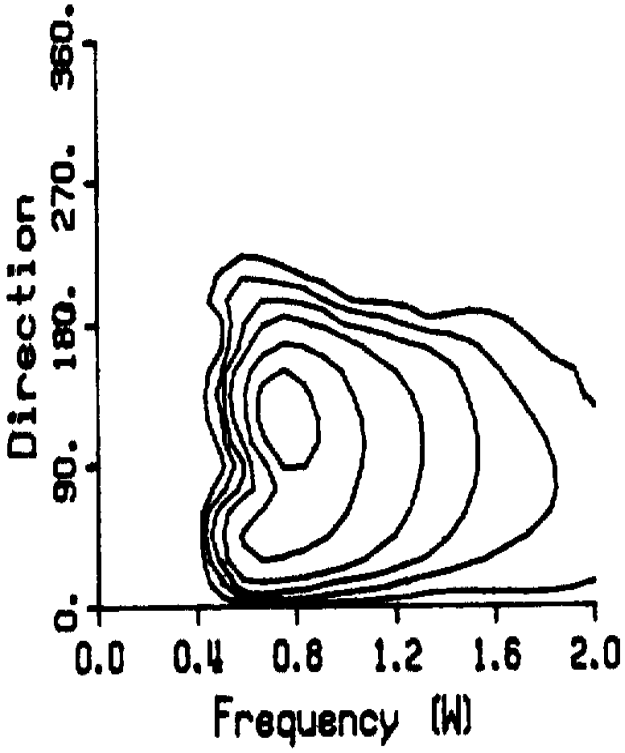
Direction
360.
270.
180.
90.
0.
0.0
0.4
0.8
1.2
1.6
2.0
Frequency (W)

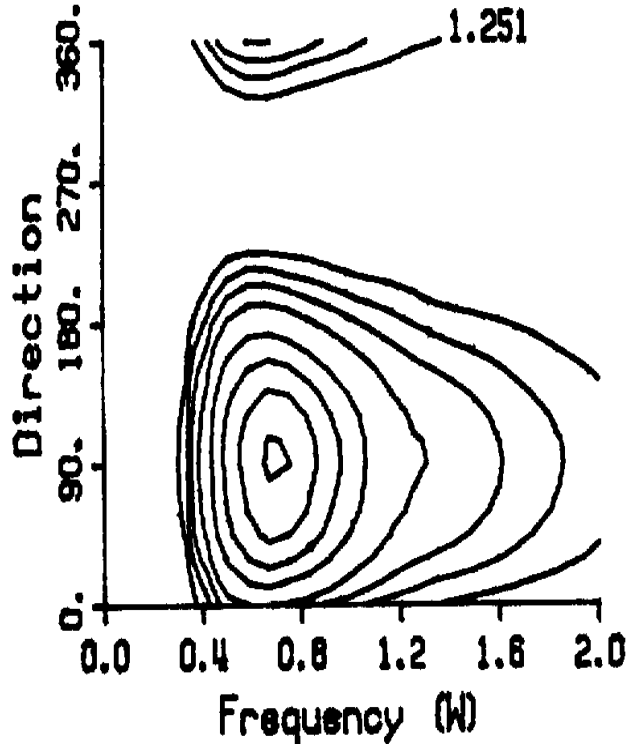
1.251
Direction
360.
270.
180.
90.
0.
0.0
0.4
0.8
1.2
1.6
2.0
Frequency (W)

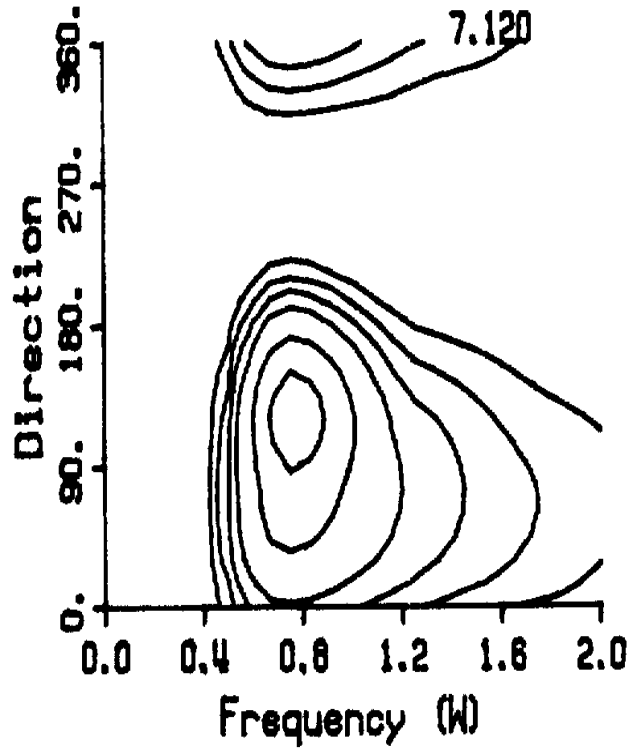
7.120
Direction
360.
270.
180.
90.
0.
0.0
0.4
0.8
1.2
1.6
2.0
Frequency (W)

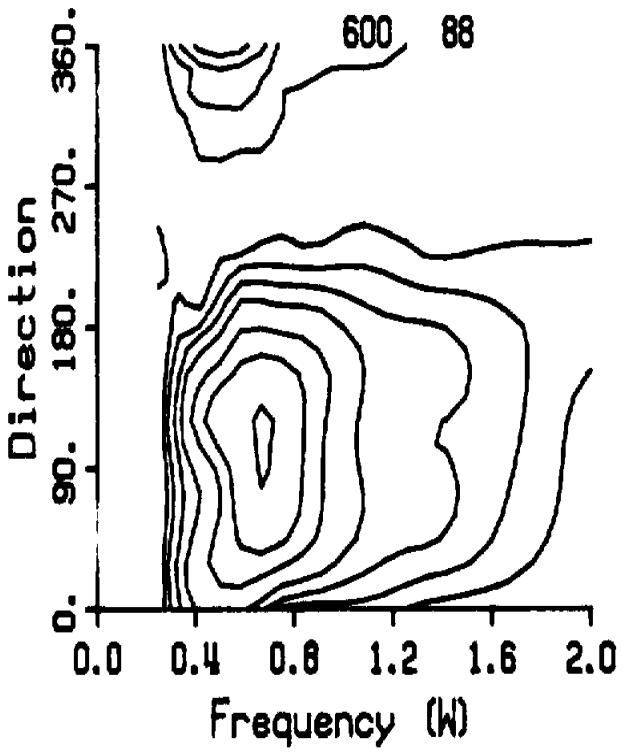
600 88
Direction
360.
270.
180.
90.
0.
0.0 0.4 0.8 1.2 1.6 2.0
Frequency (W)

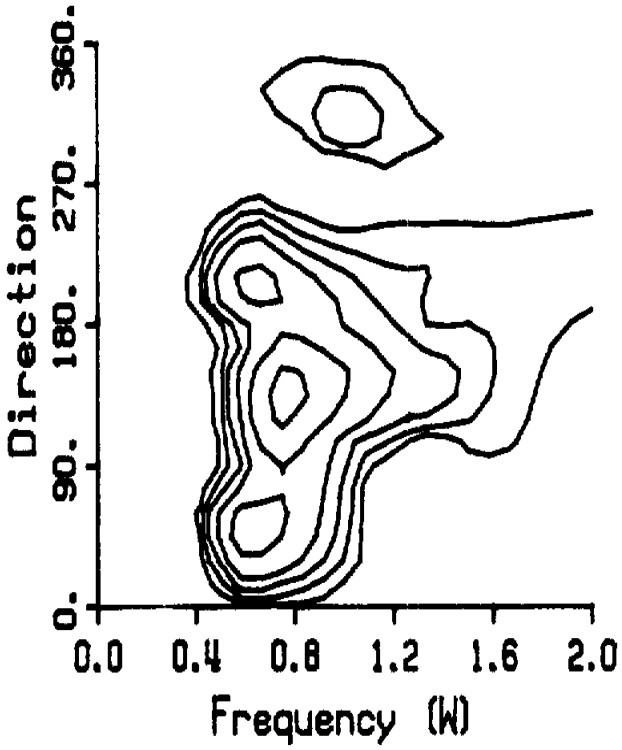
Direction
360.
270.
180.
90.
0.
0.0 0.4 0.8 1.2 1.6 2.0
Frequency (W)

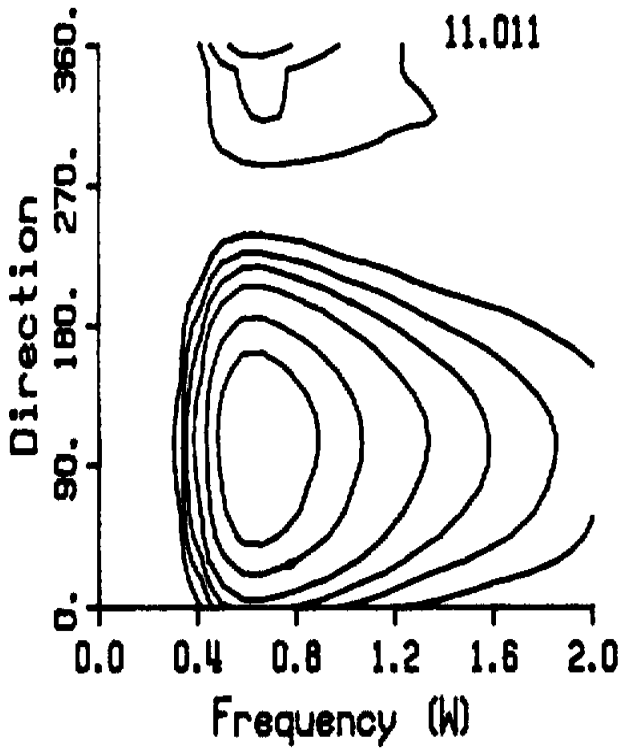
11.011
Direction
360.
270.
180.
90.
0.
0.0 0.4 0.8 1.2 1.6 2.0
Frequency (W)

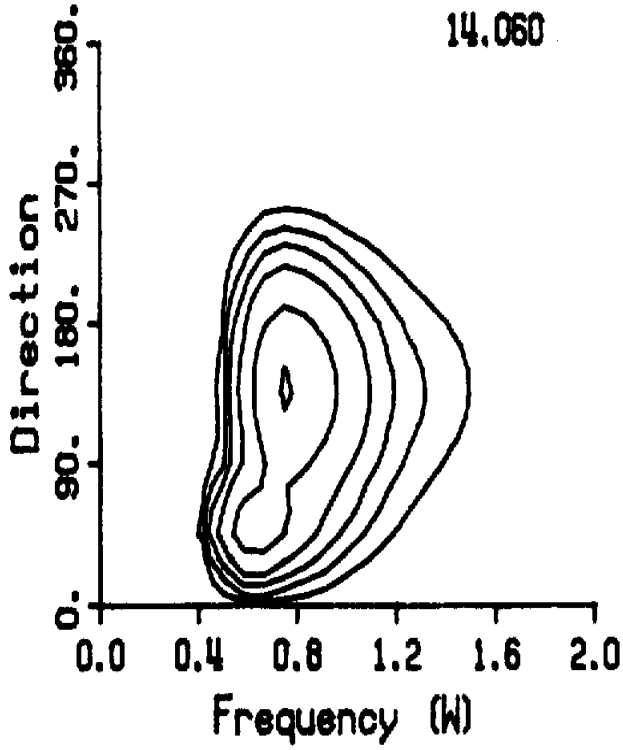
14.060
Direction
360.
270.
180.
90.
0.
0.0 0.4 0.8 1.2 1.6 2.0
Frequency (W)

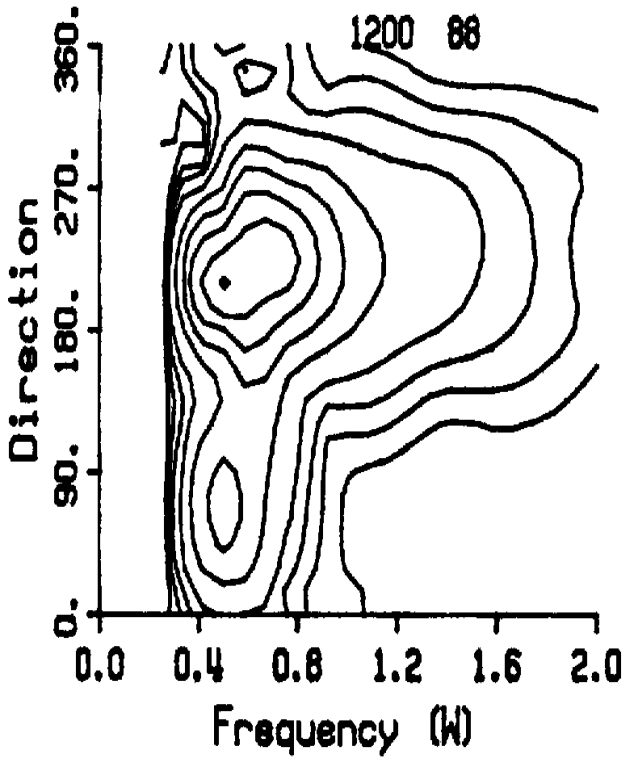
1200 88
Direction
360.
270.
180.
90.
0.
0.0
0.4
0.8
1.2
1.6
2.0
Frequency (W)

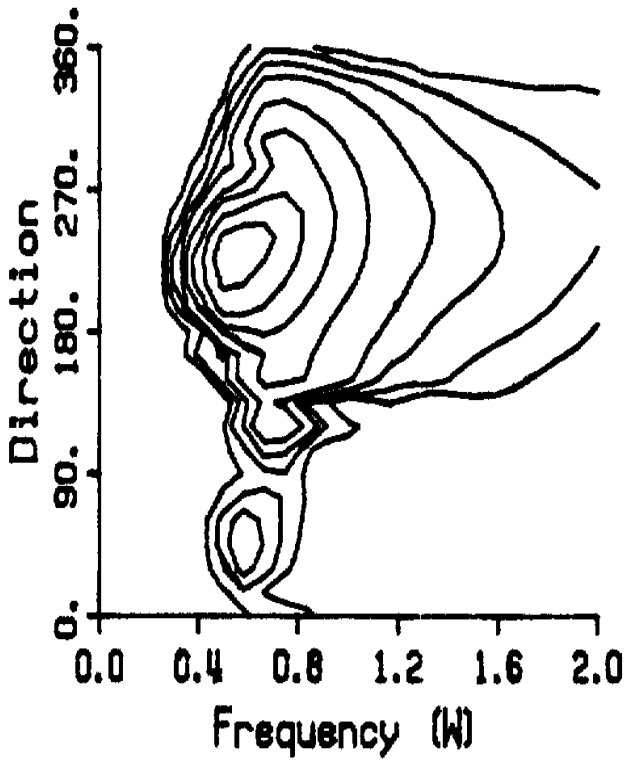
Direction
360.
270.
180.
90.
0.
0.0
0.4
0.8
1.2
1.6
2.0
Frequency (W)

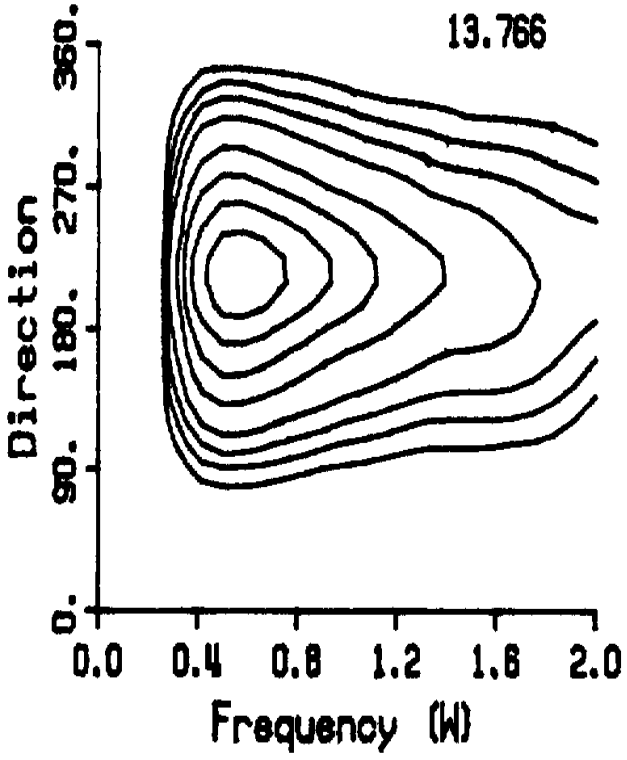
13.766
Direction
360.
270.
180.
90.
0.
0.0
0.4
0.8
1.2
1.6
2.0
Frequency (W)

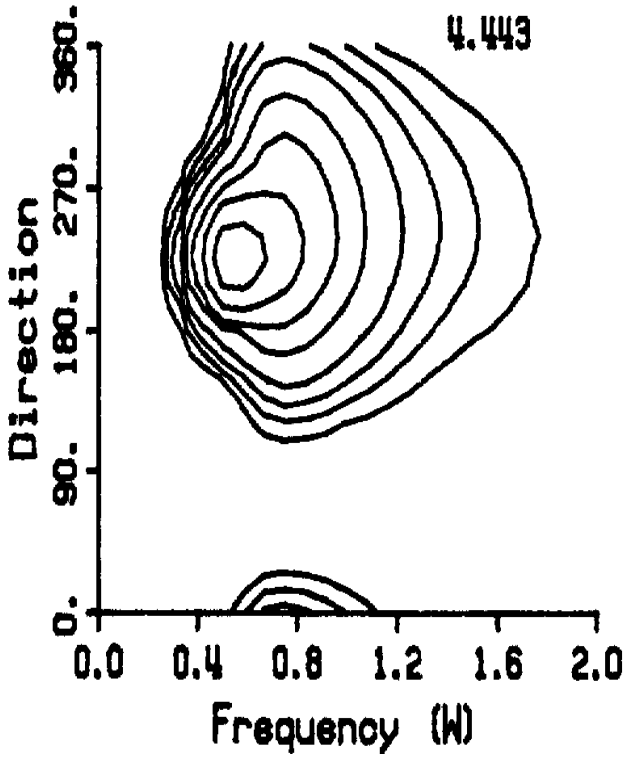
4.443
Direction
360.
270.
180.
90.
0.
0.0
0.4
0.8
1.2
1.6
2.0
Frequency (W)

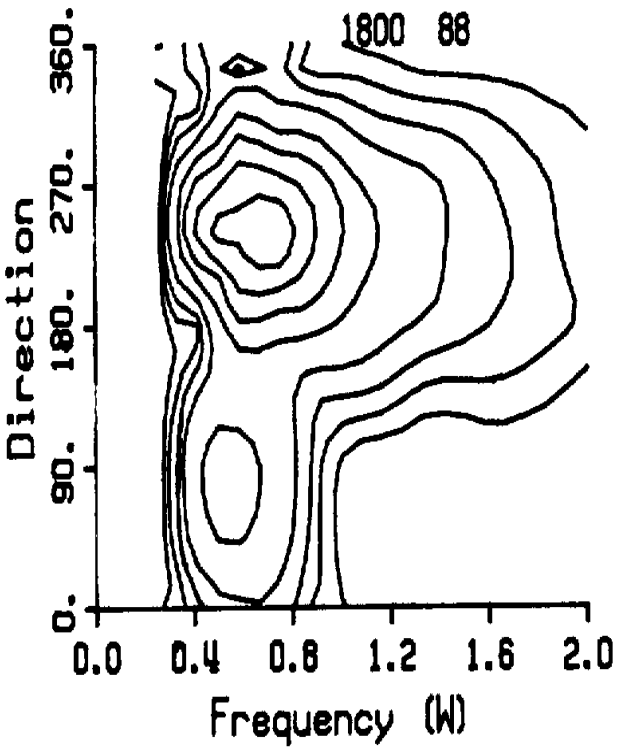
1800 88
Direction
360.
270.
180.
90.
0.
0.0 0.4 0.8 1.2 1.6 2.0
Frequency (W)

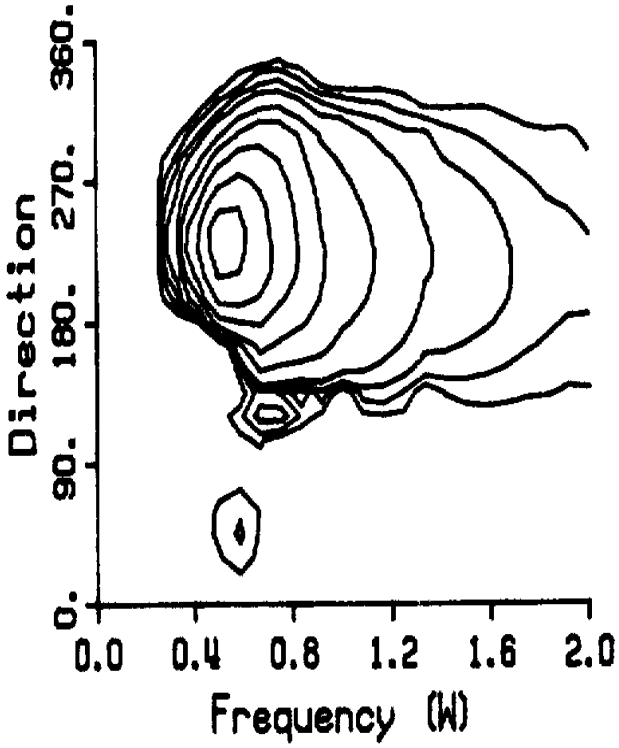
Direction
360.
270.
180.
90.
0.
0.0 0.4 0.8 1.2 1.6 2.0
Frequency (W)

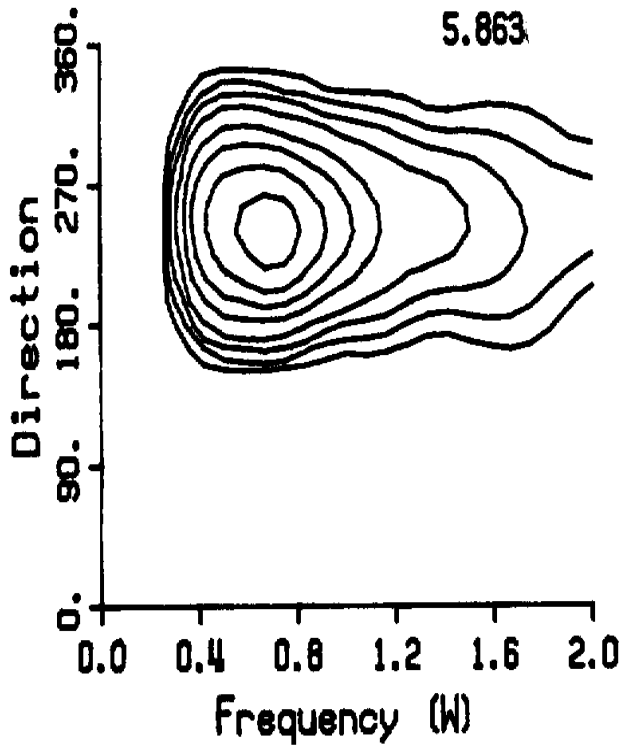
5.863
Direction
360.
270.
180.
90.
0.
0.0 0.4 0.8 1.2 1.6 2.0
Frequency (W)

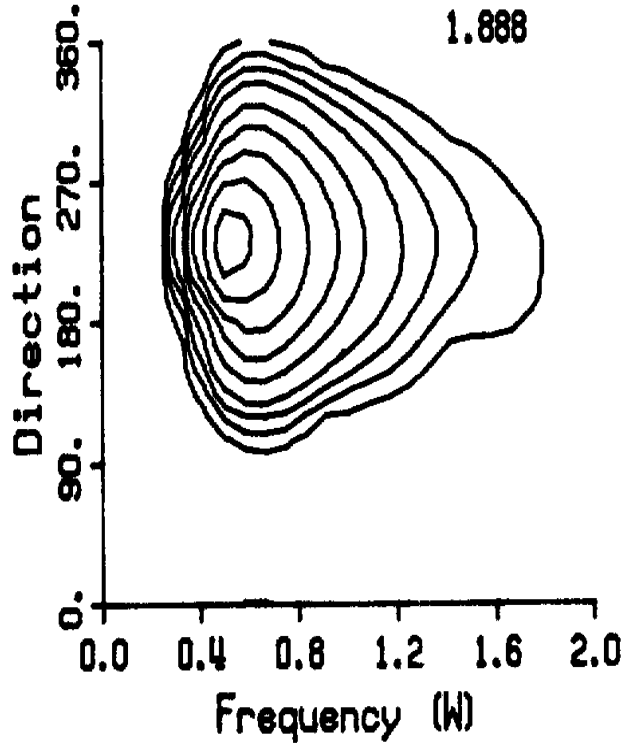
1.888
Direction
360.
270.
180.
90.
0.
0.0 0.4 0.8 1.2 1.6 2.0
Frequency (W)

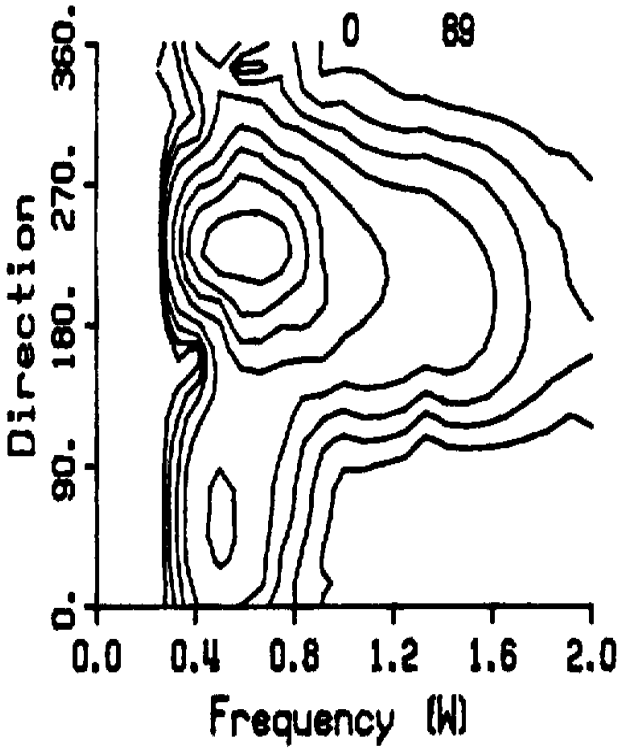
0 89
Direction
0. 90. 180. 270. 360.
0.0 0.4 0.8 1.2 1.6 2.0
Frequency (W)

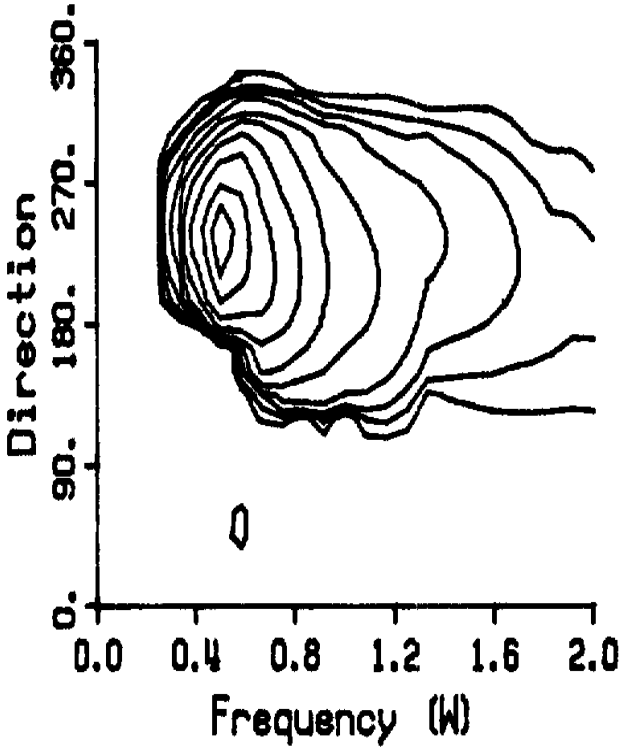
Direction
0. 90. 180. 270. 360.
0
0.0 0.4 0.8 1.2 1.6 2.0
Frequency (W)

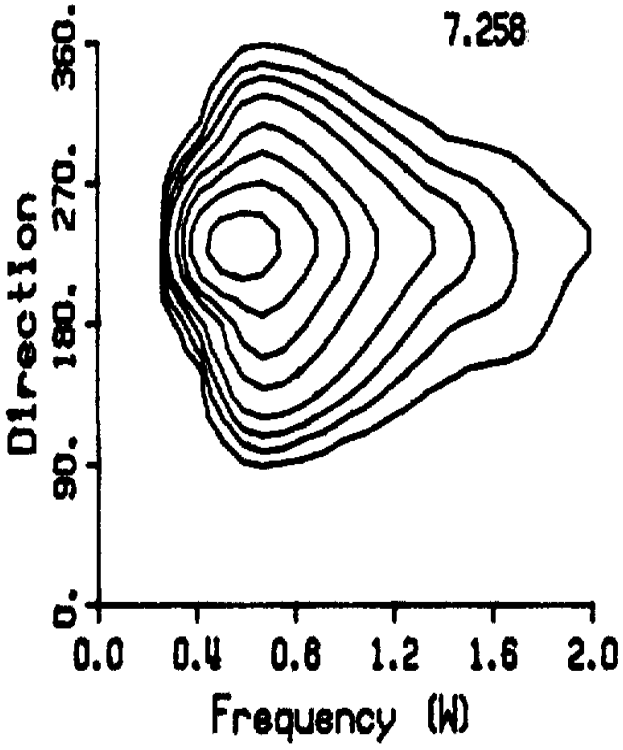
7.258
Direction
0. 90. 180. 270. 360.
0.0 0.4 0.8 1.2 1.6 2.0
Frequency (W)

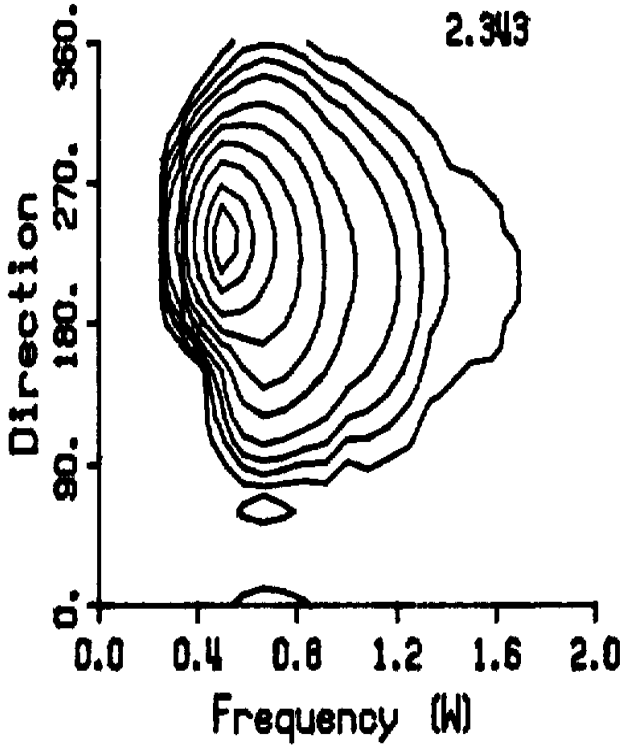
2.343
Direction
0. 90. 180. 270. 360.
0.0 0.4 0.8 1.2 1.6 2.0
Frequency (W)

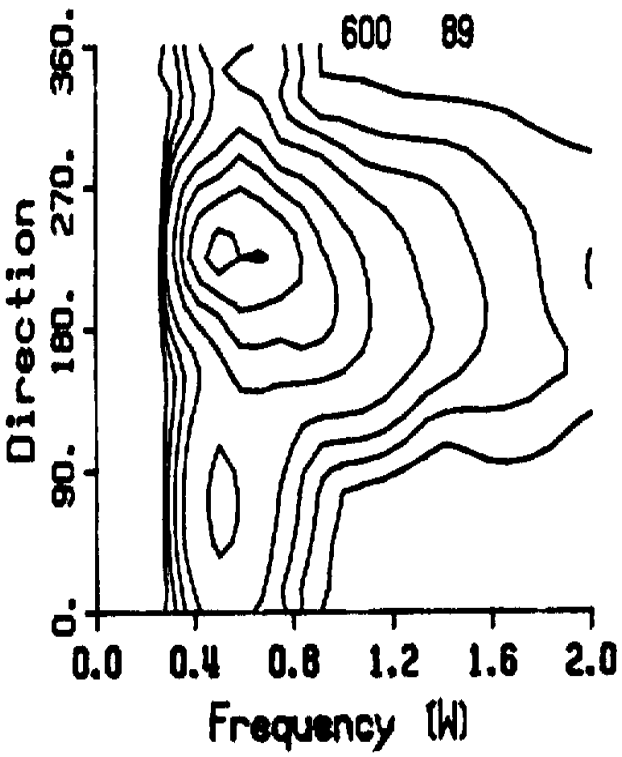
600 89
Direction
360.
270.
180.
90.
0.
0.0 0.4 0.8 1.2 1.6 2.0
Frequency (W)

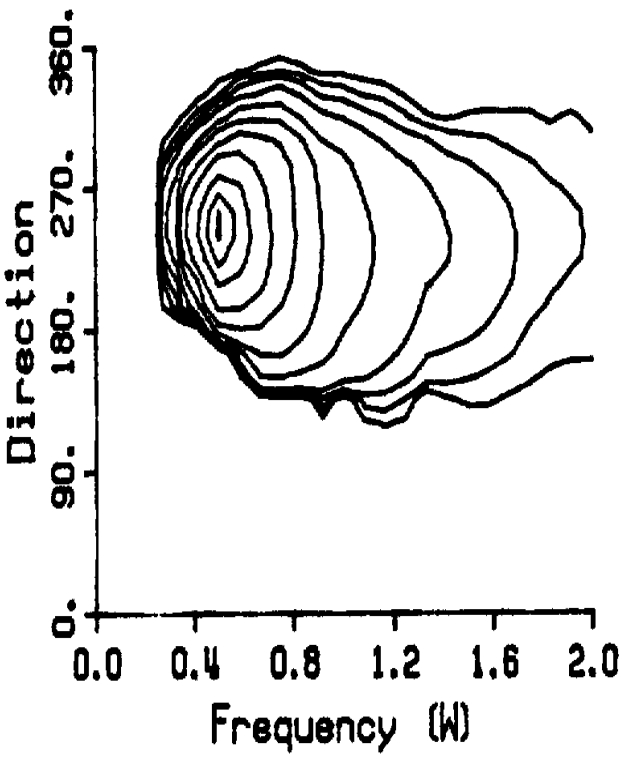
Direction
360.
270.
180.
90.
0.
0.0 0.4 0.8 1.2 1.6 2.0
Frequency (W)

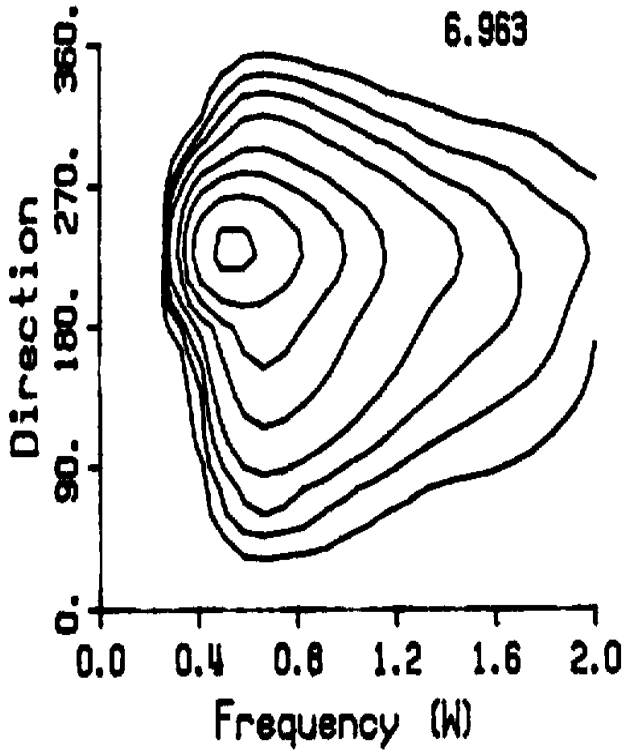
6.963
Direction
360.
270.
180.
90.
0.
0.0 0.4 0.8 1.2 1.6 2.0
Frequency (W)

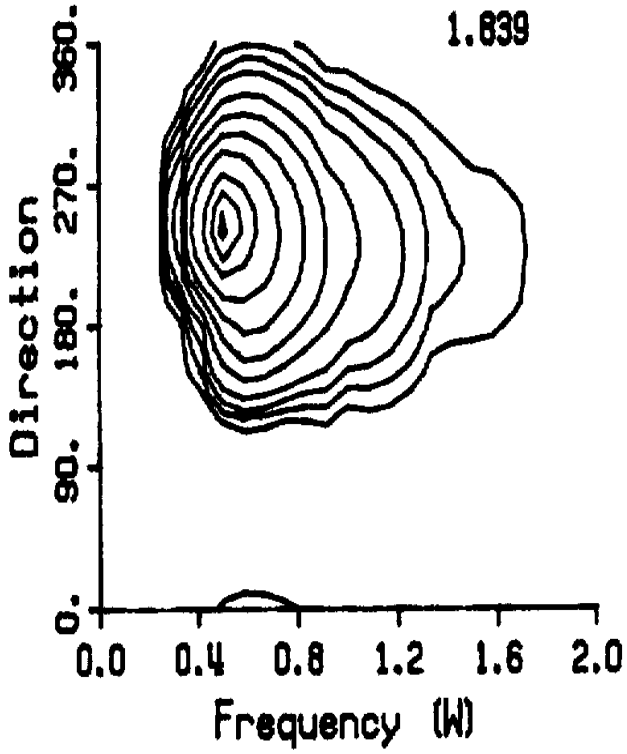
1.839
Direction
360.
270.
180.
90.
0.
0.0 0.4 0.8 1.2 1.6 2.0
Frequency (W)

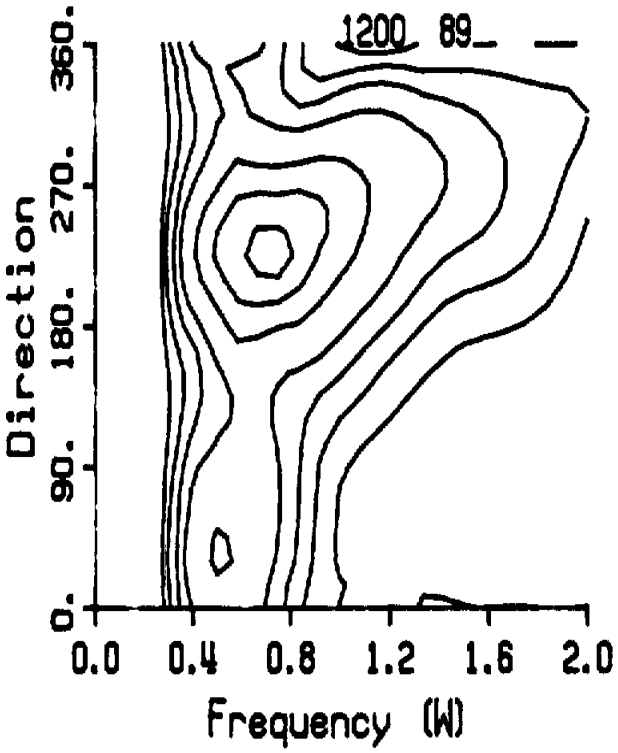
1200 89
Direction
360.
270.
180.
90.
0.
0.0 0.4 0.8 1.2 1.6 2.0
Frequency (W)

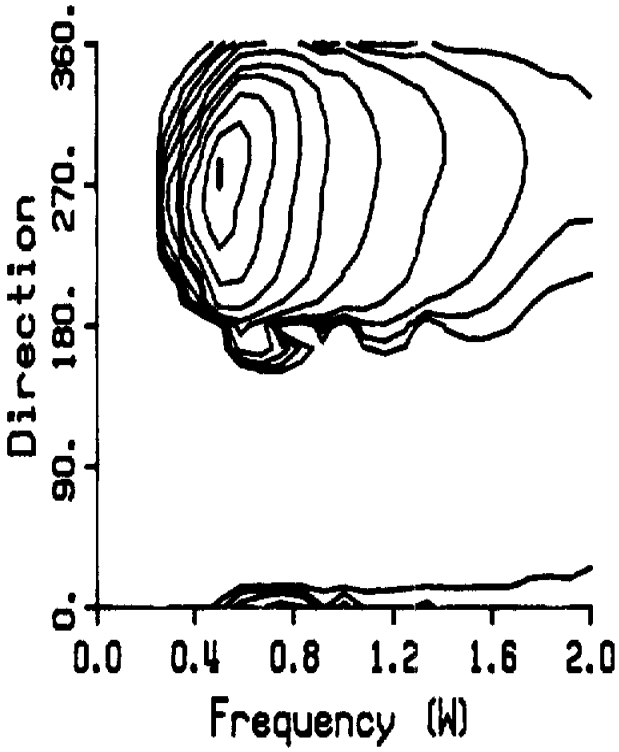
Direction
360.
270.
180.
90.
0.
0.0 0.4 0.8 1.2 1.6 2.0
Frequency (W)

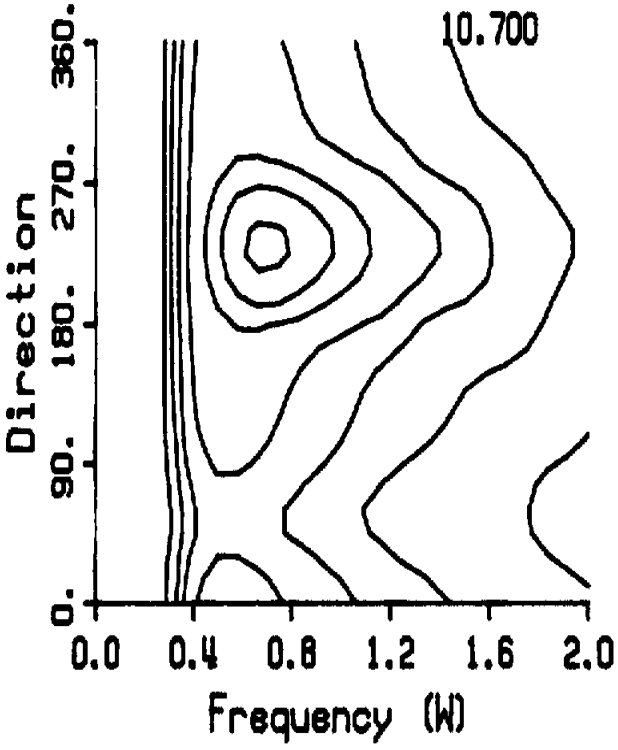
10.700
Direction
360.
270.
180.
90.
0.
0.0 0.4 0.8 1.2 1.6 2.0
Frequency (W)

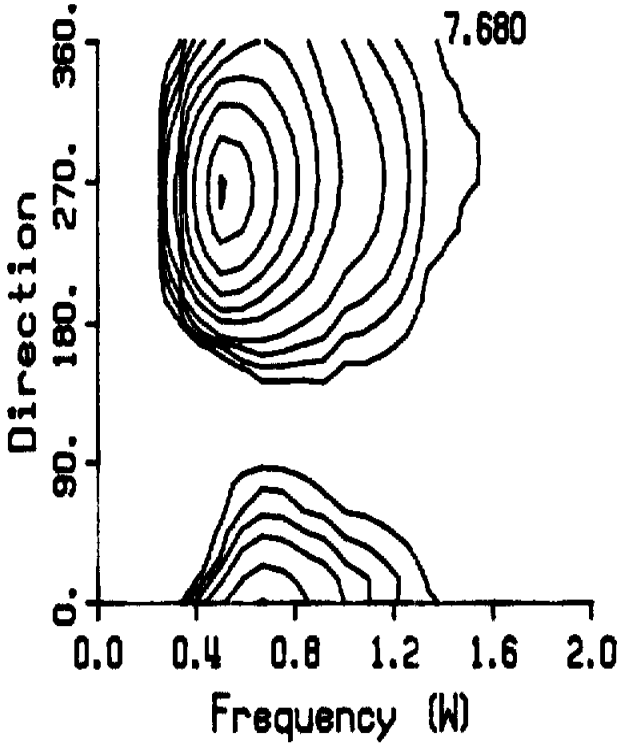
7.680
Direction
360.
270.
180.
90.
0.
0.0 0.4 0.8 1.2 1.6 2.0
Frequency (W)

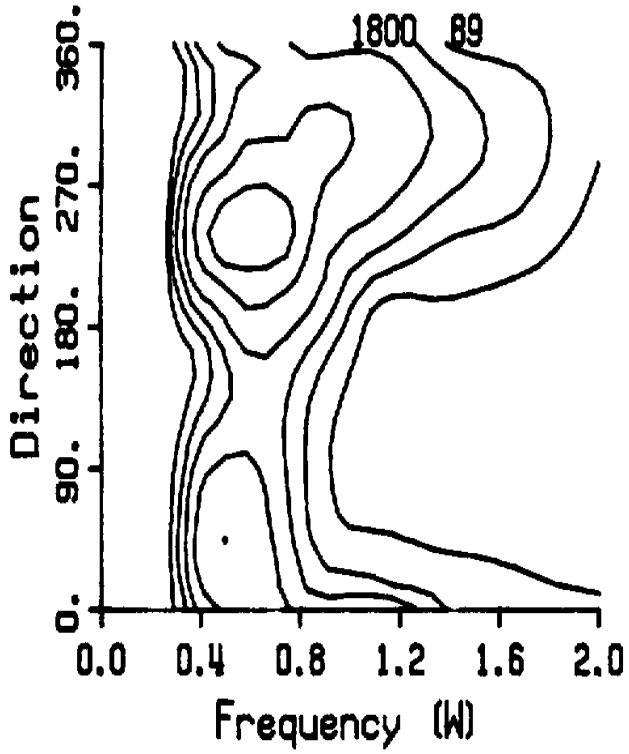
1800 89
Direction
360.
270.
180.
90.
0.
0.0 0.4 0.8 1.2 1.6 2.0
Frequency (W)

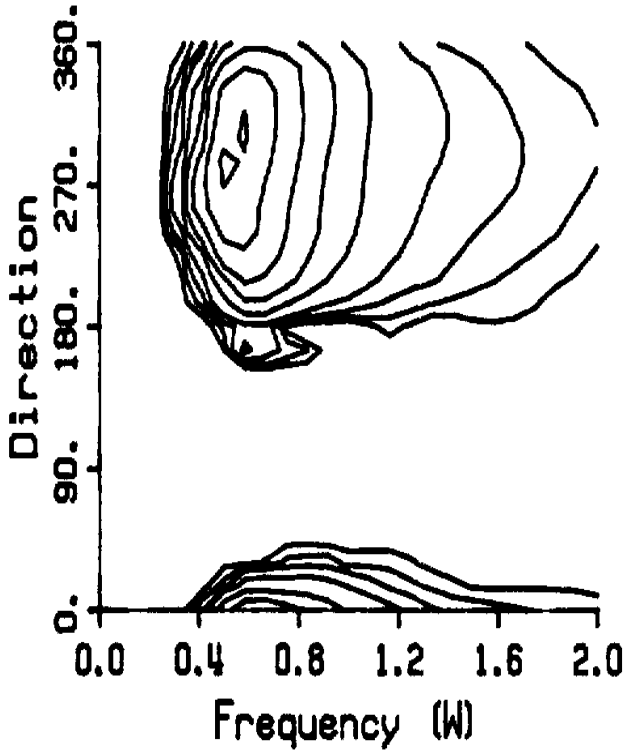
Direction
360.
270.
180.
90.
0.
0.0 0.4 0.8 1.2 1.6 2.0
Frequency (W)

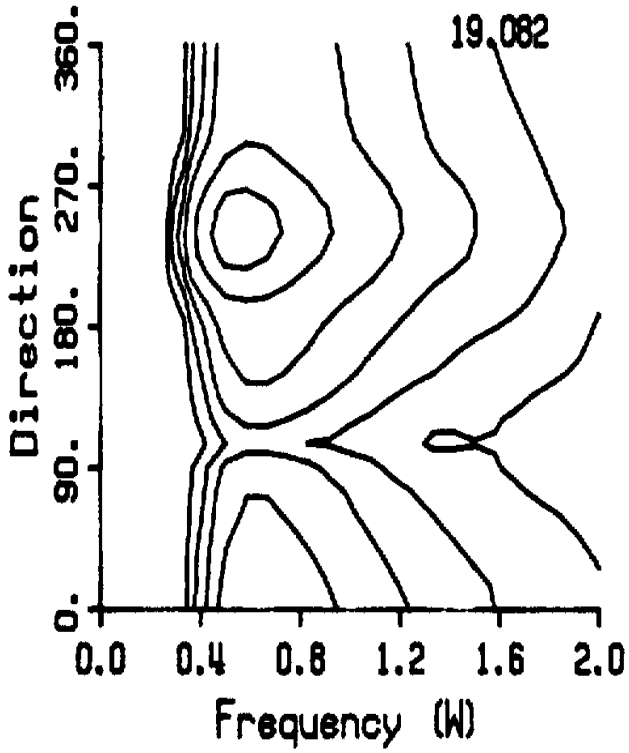
19.082
Direction
360.
270.
180.
90.
0.
0.0 0.4 0.8 1.2 1.6 2.0
Frequency (W)

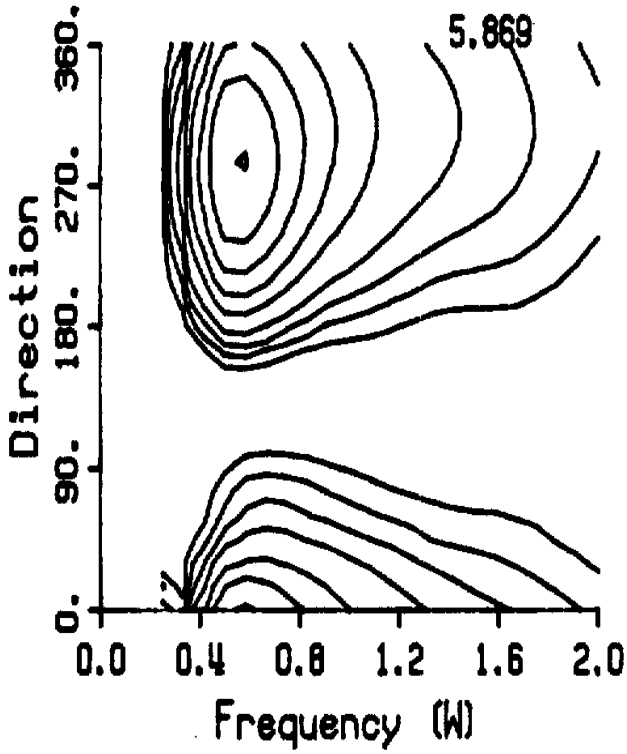
5.869
Direction
360.
270.
180.
90.
0.
0.0 0.4 0.8 1.2 1.6 2.0
Frequency (W)

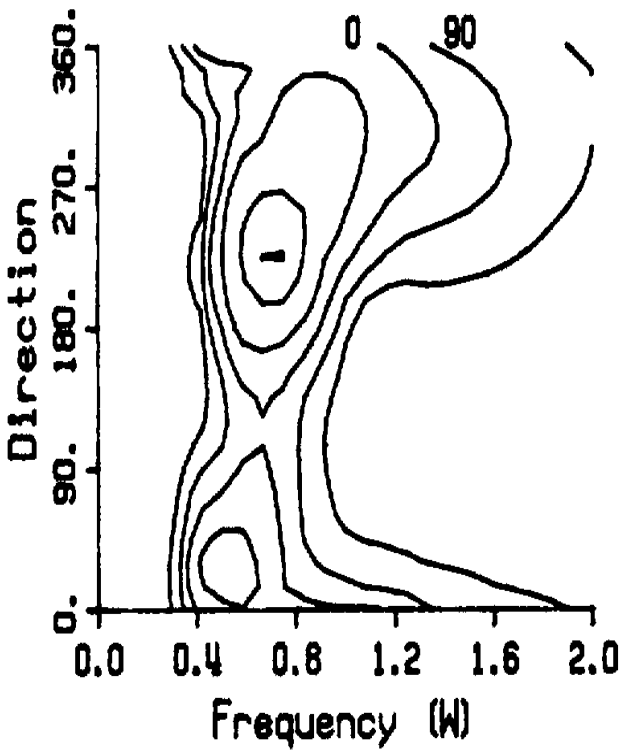
0
90
Direction
360.
270.
180.
90.
0.
0.0
0.4
0.8
1.2
1.6
2.0
Frequency (W)

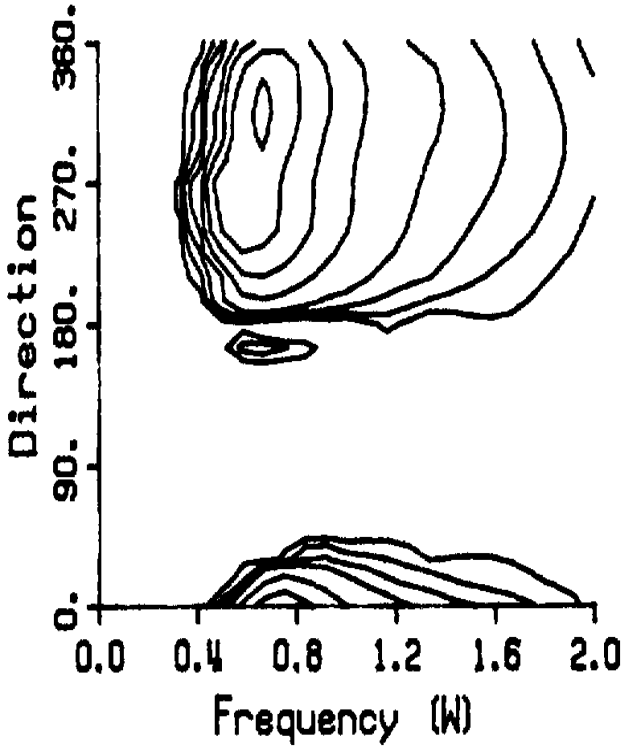
Direction
360.
270.
180.
90.
0.
0.0
0.4
0.8
1.2
1.6
2.0
Frequency (W)

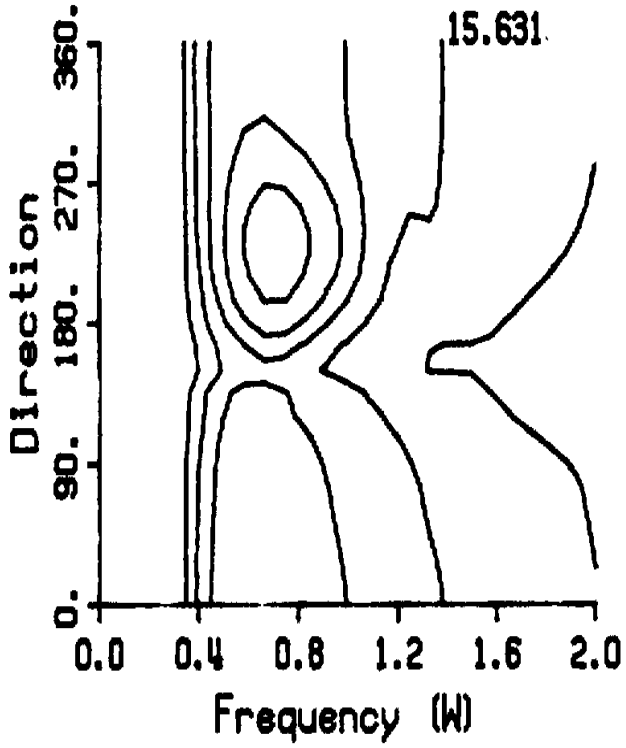
15.631
Direction
360.
270.
180.
90.
0.
0.0
0.4
0.8
1.2
1.6
2.0
Frequency (W)

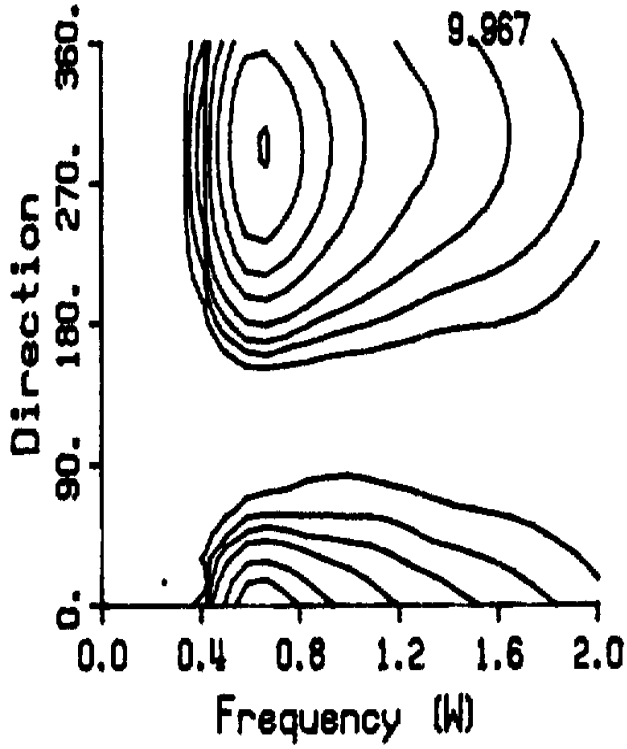
9.867
Direction
360.
270.
180.
90.
0.
0.0
0.4
0.8
1.2
1.6
2.0
Frequency (W)

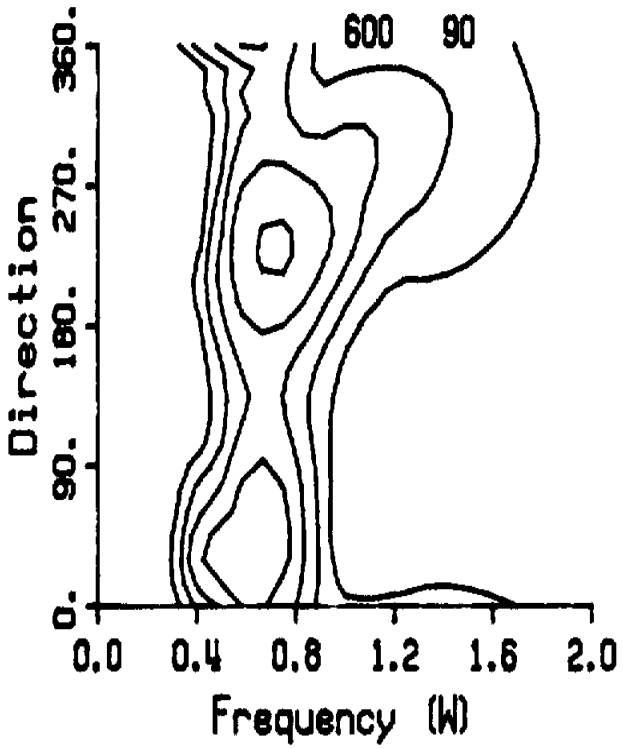
600 90
Direction
360.
270.
180.
90.
0.
0.0 0.4 0.8 1.2 1.6 2.0
Frequency (W)

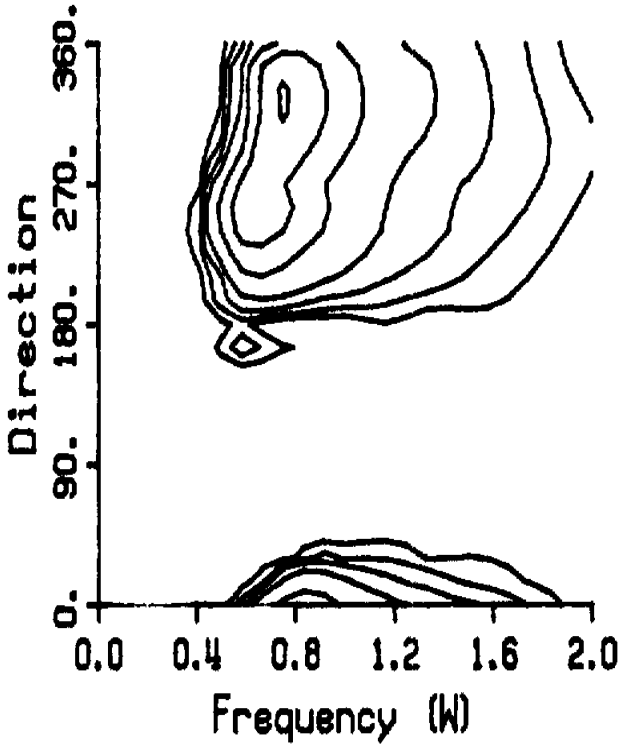
Direction
360.
270.
180.
90.
0.
0.0 0.4 0.8 1.2 1.6 2.0
Frequency (W)

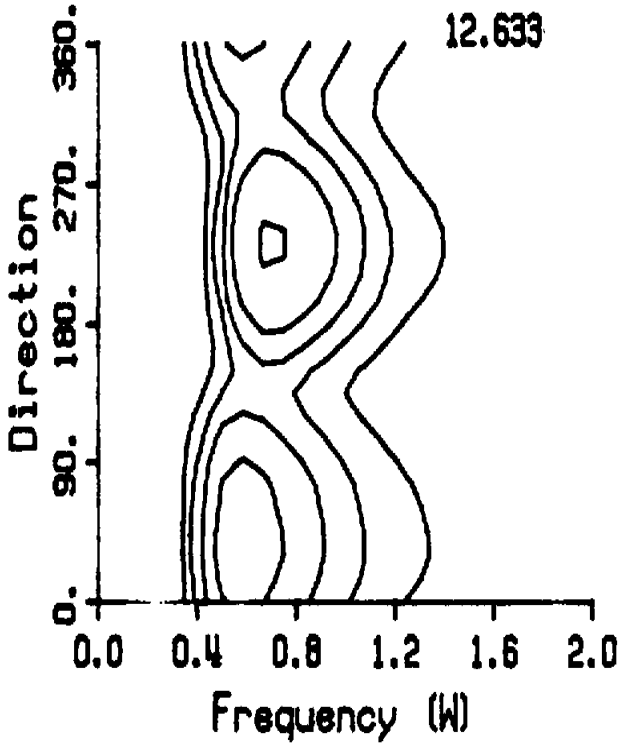
12.633
Direction
360.
270.
180.
90.
0.
0.0 0.4 0.8 1.2 1.6 2.0
Frequency (W)

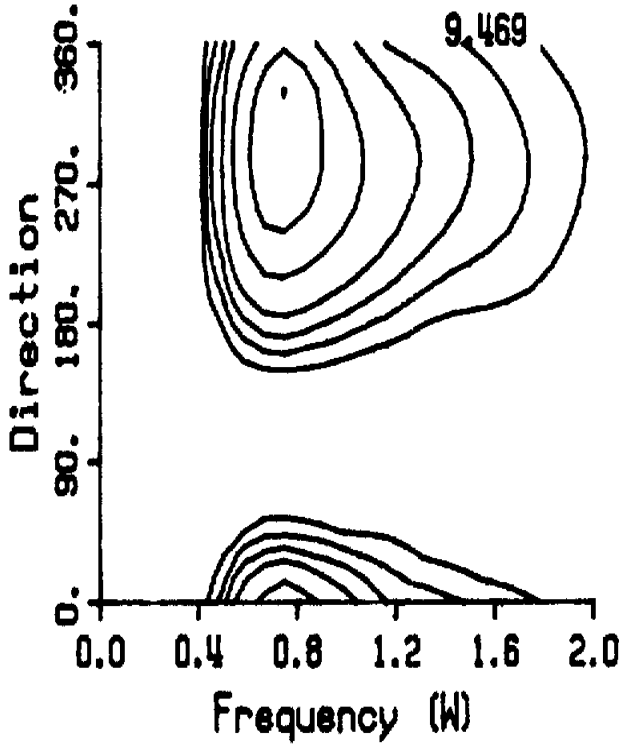
9.469
Direction
360.
270.
180.
90.
0.
0.0 0.4 0.8 1.2 1.6 2.0
Frequency (W)

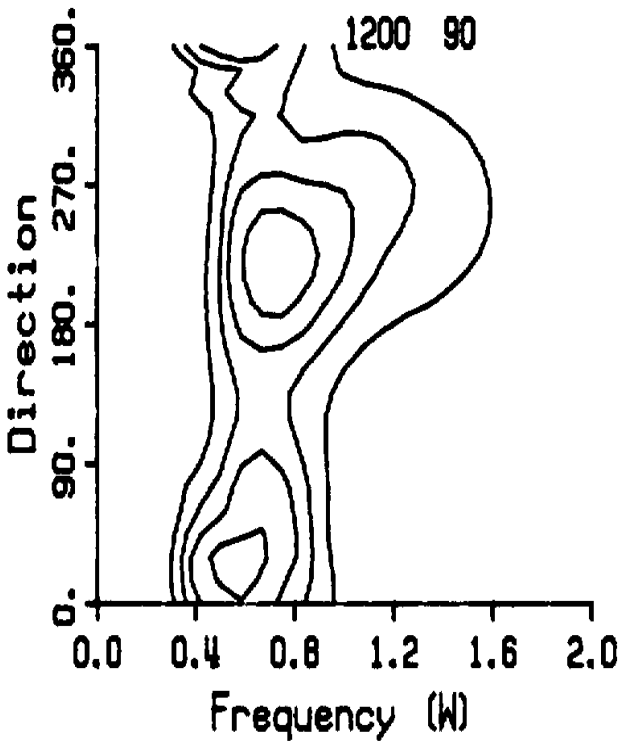
1200 90
Direction
0.
90.
180.
270.
360.
0.0
0.4
0.8
1.2
1.6
2.0
Frequency (W)

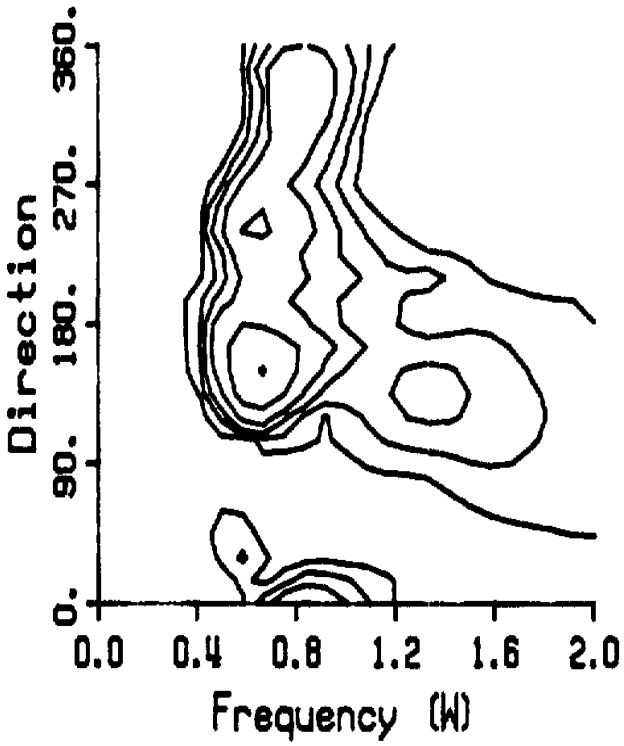
Direction
0.
90.
180.
270.
360.
0.0
0.4
0.8
1.2
1.6
2.0
Frequency (W)

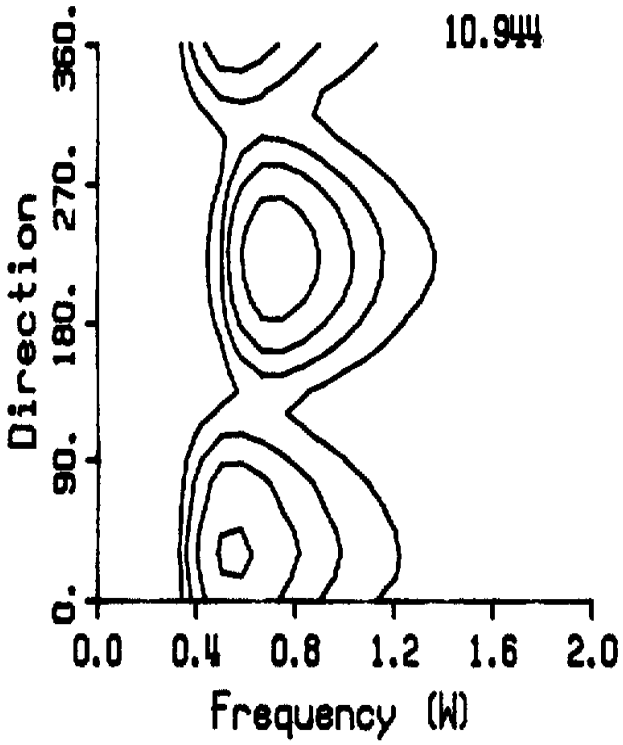
10.944
Direction
0.
90.
180.
270.
360.
0.0
0.4
0.8
1.2
1.6
2.0
Frequency (W)

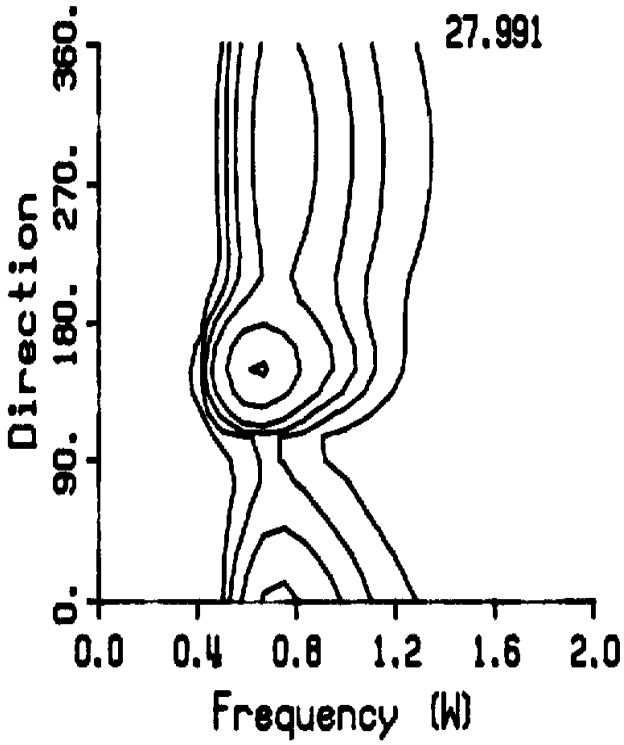
27.991
Direction
0.
90.
180.
270.
360.
0.0
0.4
0.8
1.2
1.6
2.0
Frequency (W)

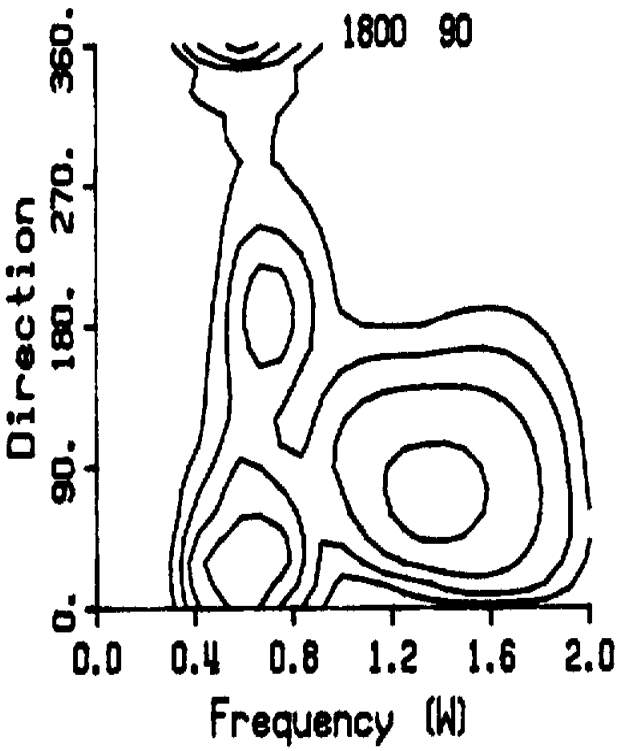
1800 90
Direction
360.
270.
180.
90.
0.
0.0
0.4
0.8
1.2
1.6
2.0
Frequency (W)

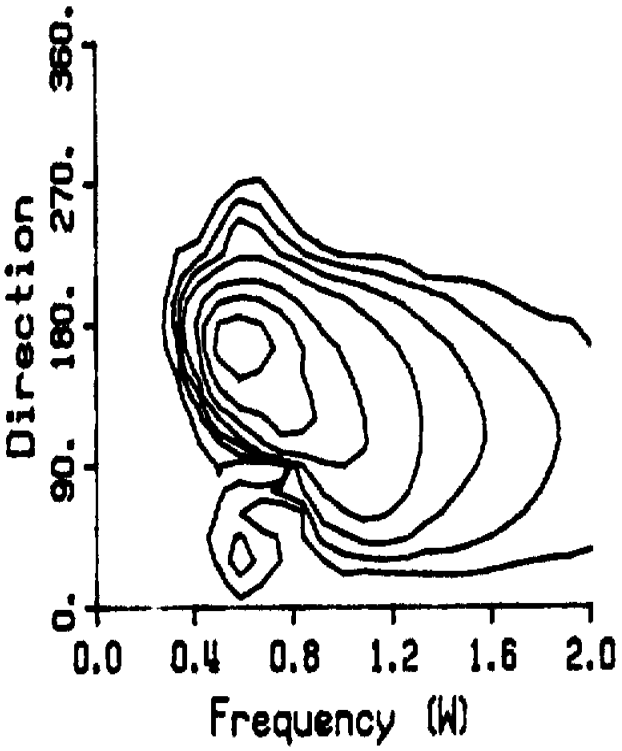
Direction
360.
270.
180.
90.
0.
0.0
0.4
0.8
1.2
1.6
2.0
Frequency (W)

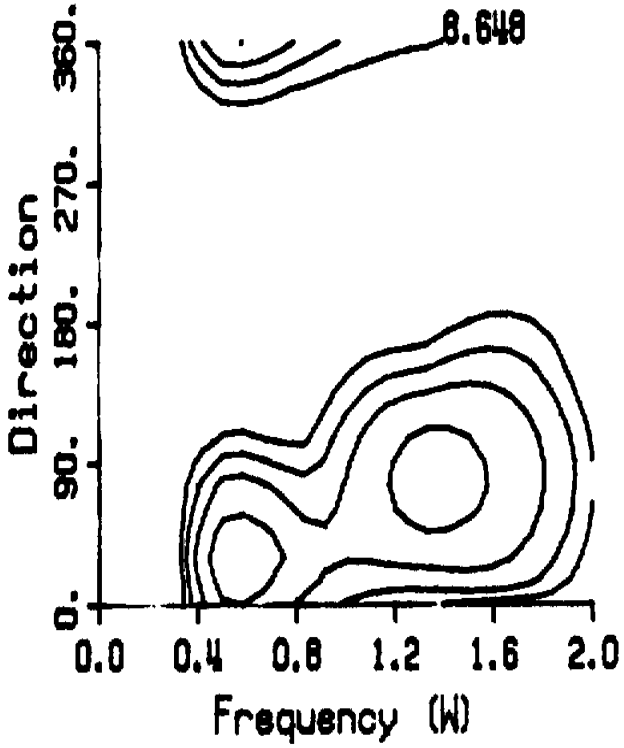
8.648
Direction
360.
270.
180.
90.
0.
0.0
0.4
0.8
1.2
1.6
2.0
Frequency (W)

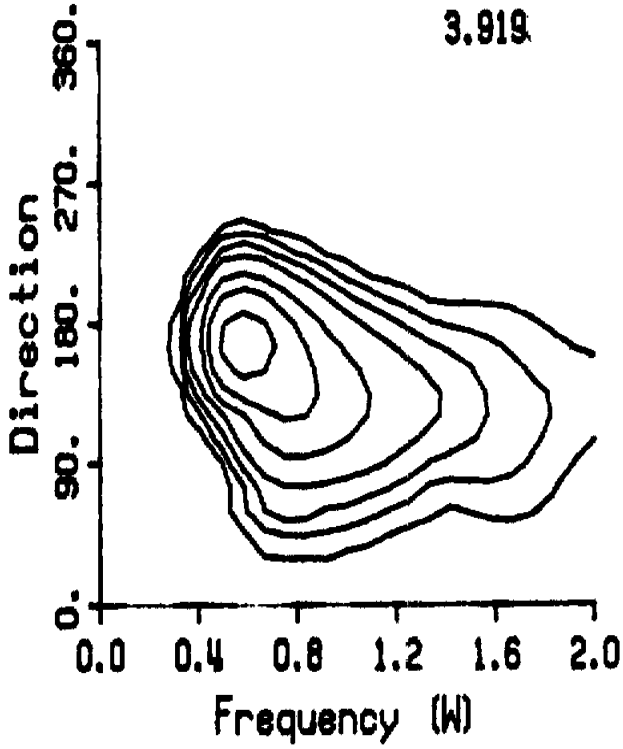
3.919
Direction
360.
270.
180.
90.
0.
0.0
0.4
0.8
1.2
1.6
2.0
Frequency (W)

DND 2

UNCLASSIFIED
SECURITY CLASSIFICATION OF FORM
(highest classification of Title, Abstract, Keywords)

DOCUMENT CONTROL DATA

(Security classification of title, body of abstract and indexing annotation must be entered when the overall document is classified)

1. ORIGINATOR (the name and address of the organization preparing the document Organizations for whom the document was prepared, e.g. Establishment sponsoring a contractor's report, or tasking agency, are entered in section 8.)

Juszko Scientific Services

2. SECURITY CLASSIFICATION (overall security classification of the document including special warning terms if applicable).

Unclassified

3. TITLE (the complete document title as indicated on the title page. Its classification should be indicated by the appropriate abbreviation (S,C,R or U) in parentheses after the title).

Parameterization of Directional Spectra - Part 2, Volume I: Final Report

4. AUTHORS (Last name, first name, middle initial. If military, show rank, e.g. Doe, Maj. John E.)

Juszko, Barbara-Ann

5. DATE OF PUBLICATION (month and year of publication of document)

December 1989

6a. NO OF PAGES (total containing information Include Annexes, Appendices, etc).

115

6b. NO. OF REFS (total cited in document)

10

6. DESCRIPTIVE NOTES (the category of the document, e.g. technical report, technical note or memorandum. If appropriate, enter the type of report, e.g. interim, progress, summary, annual or final. Give the inclusive dates when a specific reporting period is covered).

Contractor Report

8. SPONSORING ACTIVITY (the name of the department project office or laboratory sponsoring the research and development. Include the address).

Defence Research Establishment Atlantic
PO Box 1012, Dartmouth, N.S. B2Y 3Z7

9a. PROJECT OR GRANT NO. (if appropriate, the applicable research and development project or grant number under which the document was written. Please specify whether project or grant).

1AG

9b. CONTRACT NO. (if appropriate, the applicable number under which the document was written).

W7707-9-0214/01-OSC

10a. ORIGINATOR'S DOCUMENT NUMBER (the official document number by which the document is identified by the originating activity. This number must be unique to this document).

DREA/CR/89/445-Vol I

10b. OTHER DOCUMENT NOS. (Any other numbers which may be assigned this document either by the originator or by the sponsor).

11. DOCUMENT AVAILABILITY (any limitations on further dissemination of the document, other than those imposed by security classification)

(X) Unlimited distribution
( ) Distribution limited to defence departments and defence contractors; further distribution only as approved
( ) Distribution limited to defence departments and Canadian defence contractors; further distribution only as approved
( ) Distribution limited to government departments and agencies; further distribution only as approved
( ) Distribution limited to defence departments; further distribution only as approved
( ) Other (please specify):

12. DOCUMENT ANNOUNCEMENT (any limitation to the bibliographic announcement of this document. This will normally correspond to the Document Availability (11). However, where further distribution (beyond the audience specified in 11) is possible, a wider announcement audience may be selected).

UNCLASSIFIED
SECURITY CLASSIFICATION OF FORM

DCD03 2/06/87-M

UNCLASSIFIED
SECURITY CLASSIFICATION OF FORM

13. ABSTRACT (a brief and factual summary of the document. It may also appear elsewhere in the body of the document itself. It is highly desirable that the abstract of classified documents be unclassified. Each paragraph of the abstract shall begin with an indication of the security classification of the information in the paragraph (unless the document itself is unclassified) represented as (S), (C), (R), or (U). It is not necessary to include here abstracts in both official languages unless the text is bilingual).

The objectives of this work were to assess the ability of the 10-parameter model, examined in Part 1 of the study, to represent hindcast directional wave spectra and to provide an appraisal of how well the ODGP hindcast model predicted existing WAVEC observations. The parametric model acceptably reproduced the hindcast spectra over 90% of the time, with nearly 70% of the records having residual errors of less than 10%. There was little loss of information as indicated by the behavior of selected spectral statistics. A comparison of the hindcast spectra with field observations showed a significant correlation between energy levels, peak wave direction and vector mean direction. The hindcast directional peaks appeared to be generally sharper than the field data. No definite conclusions could be formed on specific frequency-direction features due to intrinsic limitations in directional spectra techniques. A coherence analysis between hindcast and measured winds indicated that the man-machine mix of hindcast input winds did provide an improvement over a purely geostrophic estimate. The coherence-squared dropped below acceptable levels at frequencies above 0.75 cycles per day (cpd). This behavior was reflected in the coherences of the vector mean wave field (i.e. significant waveheight at the vector mean direction). Limiting the analysis to selected wave frequency bands, indicated that the hindcast model did not reproduce the observed swell signature with any statistical confidence while the "sea" showed acceptable coherences to frequencies between 0.75 and 1.0 cpd.

14. KEYWORDS, DESCRIPTORS or IDENTIFIERS (technically meaningful terms or short phrases that characterize a document and could be helpful in cataloguing the document. They should be selected so that no security classification is required. Identifiers, such as equipment model designation, trade name, military project code name, geographic location may also be included. If possible keywords should be selected from a published thesaurus. e.g. Thesaurus of Engineering and Scientific Terms (TEST) and that thesaurus-identified. If it not possible to select indexing terms which are Unclassified, the classification of each should be indicated as with the title).

Waves
Ocean waves
Wave spectra
Directional wave spectra
Hindcast spectra

UNCLASSIFIED
SECURITY CLASSIFICATION OF FORM